UCSF

UC San Francisco Electronic Theses and Dissertations

Title

The control of mitotic progression by kinetochore-microtubule attachments

Permalink

https://escholarship.org/uc/item/9p9863jd

Author

Kuhn, Jonathan Alexander

Publication Date

2019

Peer reviewed|Thesis/dissertation

The control of mitotic progression by kinetochore-microtubule attachments

by
Jonathan Kuhn

DISSERTATION
Submitted in partial satisfaction of the requirements for degree of
DOCTOR OF PHILOSOPHY

in

Cell Biology

in the

GRADUATE DIVISION
of the
UNIVERSITY OF CALIFORNIA, SAN FRANCISCO

Approved:

DocuSigned by:

Sophie Dumont

——8305715E0D454DC...

Sophie Dumont
_____
Chair

DocuSigned by:

David Morgan

——DocuSigned by472...

David Morgan
_____

Wallace Marshall

——43941FCFA7C0447...

Wallace Marshall
_____

_____

_____
Committee Members

Dedication

To my parents, who are always there.

Acknowledgements

I'd like to thank my PhD mentor, Sophie Dumont, who always found time for me, encouraged me, and pushed me to be better. I'd like to thank my undergraduate mentors Daniel Starr, Joel Rothman, and Songi Han for taking a chance on me and giving me their time. I'd like to thank my thesis committee members David Morgan and Wallace Marshall for all their input and advice. I'd also like to thank Fred Chang, Diane Barber, Torsten Wittmann, Noelle L'Etoile, Andrei Goga, Geeta Narlikar, and Todd Nystul for being generous with their time and expertise.

I'd like to thank my fellow Dumont lab members Christina Hueschen, Alex Long, Mary Elting, Dylan Udy, Pooja Suresh, Andrea Serra-Marques, Eline Ter Steege, Josh Guild, Lila Naehring, Meelad Amouzhar, Manuela Richter, and Miquel Rosas.

A big thanks to all of the others at UCSF that made this journey possible and even fun, including Andreas Ettinger, Dai Horuichi, Hayley Pemble, Jeffrey Van Haren, Bree Grillo-Hill, Katherine White, Arthur Molines and Rebab Cherafaddine. I'd also like to thank my fellow Tetrad classmates, especially Rebecca Kim and Jessica Witchley. Finally, a huge thanks to all of the UCSF staff that work hard every day to make this university function, especially our administrators Jeanes Villaneuva and Tiffany Criger.

I'd like to thank my close friends outside UCSF, including Sam Crowley, Dylan Baker, Ian Donahue, Devvrat Malholtra, Kaitlyn Manighalim, Holly Christensen, and Matt Malanche. I'd like to thank close family friends and mentors Mark Sherwin and Cathy Weinberger. I'd like to thank my brother Michael, who has been my best friend for as long as I can remember, and his wife Nicolle, for being a fantastic new sister. I'd like to thank my parents Barbara and Peter; whose contributions I could never adequately describe. Finally, I want to thank Sarah Powers, who has been by my side through everything – none of this would be possible without her.

Contributions to Presented Work

Chapter 2 of this dissertation is a reprint of previously published material: Kuhn J, Dumont S. Spindle assembly checkpoint satisfaction occurs via end-on but not lateral attachments under tension. Journal of Cell Biology 216, 1533-1542 (2017)

I performed the studies described in Chapter 2 under the guidance of Sophie Dumont, PhD.

Chapter 3 of this dissertation contains unpublished material that is a work in progress: Kuhn, J. and Dumont, S. Mammalian kinetochores count attached microtubules in a sensitive and switch-like manner.

I performed the studies described in Chapter 3 under the guidance of Sophie Dumont, PhD.

Chapter 4 of this dissertation is a reprint of previously published material: Kuhn J, Dumont S. Imaging and physically probing kinetochores in live dividing cells. Methods in Cell Biology 123, 467-487 (2014).

I performed the studies described in Chapter 4 under the guidance of Sophie Dumont, PhD.

Abstract

The control of mitotic progression by kinetochore-microtubule attachments

Jonathan Kuhn

To maintain genomic integrity, the Spindle Assembly Checkpoint (SAC) prevents anaphase onset until all chromosomes attach to the mitotic spindle in a bioriented fashion. The generation of SAC signal at individual kinetochores is controlled by the amount of localization of the SAC protein Mad1. In this work, I ask how kinetochores detects and counts correct microtubule attachments to control Mad1 localization and thus prevent mitotic errors. There are two long-standing candidate signals that turn off the checkpoint – the binding interaction between kinetochores and microtubules and the tension generated on kinetochores by attached microtubule pulling forces. It has been difficult to analyze the independent contribution of these signals to Mad1 loss because they are closely associated in space and time. Using live imaging, I demonstrate that mammalian kinetochores under tension but lacking plus-end microtubule attachments remain Mad1-positive, indicating that tension is not sufficient for SAC satisfaction. I then use laser ablation to show that kinetochores that are attached to microtubules but not under tension are Mad1-negative, proving that tension is not necessary for SAC satisfaction. Finally, having shown that kinetochores detect microtubule binding to control Mad1 levels, I ask how many attachments are required to turn off the checkpoint. By limiting the number of possible kinetochore-microtubule attachments, I show that while individual kinetochores bind 15-25 microtubules at metaphase, they are capable of complete – albeit slow – Mad1 loss with four or less attachments. Taken together, my data show how kinetochores detect spindle attachments, how they process them quantitatively, and how they respond in real time.

Understanding these properties of kinetochore signaling is critical for understanding kinetochore

structure and biochemistry and how cells manage to divide in an accurate and robust manner.

Table of Contents

List of Figures

x

Chapter 1: Controlling mitotic progression

I. Principles of cellular decision-making

The process of decision-making is a fundamental part of life at all scales. We as organisms decide when to eat, where to live, and who to associate with. Individual cells must also make complex and important decisions, like where to migrate, what shape to adopt, and when to divide. Across scales, the basic concept of decision-making is identical: organisms accept inputs from the surrounding environment, process them, and output a decision. On the whole-organism level, decision-making is simple to understand: for example, if we look at a piece of fruit and see mold, we decide not to eat it. On smaller length-scales, this problem becomes more convoluted: how can a cell which possesses no brain or eyes process inputs and make choices?

In order to respond to their environments, cells have created a multitude of methods to detect and process inputs. In order to move towards a chemical cue (e.g. food or a bacterium), cell surface receptors must interact with that cue and activate actin polymerization locally (to produce force in the direction of the cue) while preventing it globally (to allow movement in a specific direction) (Devreotes et al., 2017). How the cell processes these chemical cues quantitatively is critical to cell function: an overly sensitive response could lead to constant activation in response to false positives, while an overly stringent one could lead to cells missing important cues. Like all signaling networks, the quantitative properties of this response is controlled by the structure of the biochemical network its associated with, in this case linking signal detection to actin polymerization (Devreotes et al., 2017; Lim et al., 2013). Understanding the quantitative relationship of input and output is therefore critical for understanding the biochemical network, and vice versa.

In addition to chemical cues, cells must also be able to respond to their mechanical environment. For example, developing axons use ion channels that respond to changes in force in order to detect the stiffness of their local environment and grow towards their respective

target neurons (Koser et al., 2016). The aforementioned ion channel, Piezo1, detects force by undergoing a conformational change under force that leads to channel-opening (Saotome et al., 2018; Zhao et al., 2018). Similarly, application of tensile force across cell adhesion protein Talin leads to the exposure of binding sites in the molecule which can recruit proteins important for responding to increases in substrate stiffness. How – and if – different biological structures respond to force affects nearly every aspect of cell's life, from differentiation, to growth, to birth.

One critical cellular process which presents a critical decision-making challenge is cell division. Knowing when to divide and when not to is critical for tissue development and homeostasis as well as mutation prevention. The stakes of this decision are extremely high – genome segregation is irreversible and errors can lead to cell death and disease. How cells combine chemical and mechanical cues to make this choice correctly has been a basic and long-standing question within cell biology for over a century.

II. Ensuring accurate cell division

The division of individual cells is a fundamental part of the life cycle across all organisms. Unicellular bacteria reproduce via cell division, while multicellular organisms like humans must produce trillions of cells as raw material to build and maintain complex tissue structures. While the specific details may differ, the general principles of cell division remain constant: cells must first create a copy of their genome and then separate the two genomes so that each cell gets one copy. This presents two fundamental challenges that cells must overcome in order to divide successfully: First, cells must ensure they copy their genome before completing cell division. Second, cells must partition their two genome copies such that, when they divide, each daughter cell gets exactly one copy. A mistake in either of these processes can lead to cell death or dangerous mutations. While these two processes are tightly coupled in

3

bacteria (Haeusser and Levin, 2008), chromosome replication and segregation in eukaryotes occur in distinct phases separated in time (Harashima et al., 2013). In order to divide successfully, cells must be able to choose when to enter and exit these stages – a decision-making problem that requires cells to integrate spatial, temporal, and mechanical information robustly and accurately.

After replicating their DNA, somatic cells enter into mitosis and prepare to separate their genomes. Upon mitotic entry (prophase) the individual chromosomes composed of genetically identical sister chromatids within the nucleus and (in metazoans) enter the cytoplasm and begin to move independently of one another. The mitotic spindle, the microtubule-based machine which moves chromosomes, organizes these chromosomes by moving them to the middle of the cell during metaphase and orienting them with one chromatid attached to one side of the spindle and one chromatid attached to the other – a process known as biorientation. Then, the sister chromatids split apart as the cell enters anaphase and the spindle pulls chromatids to the opposing sides of the cell which eventually become two daughter cells. Because the gain or loss of chromosomes (aneuploidy) is a serious error which leads to cell death and disease (Giam and Rancati, 2015), the cell must be able to prevent anaphase onset (sister chromatid segregation) until all chromosomes are properly bioriented.

To ensure accurate chromosome segregation, the cell has developed a system known as the Spindle Assembly checkpoint (SAC) which prevents anaphase onset until all chromosomes are correctly attached to the mitotic spindle (London and Biggins, 2014c). The first reports of the SAC date back to 1936, when it was observed that treating tissues with microtubule-depolymerizing drug colchicine leads to accumulation of cells arrested in mitosis due to spindle defects (Levan, 1938; Ludford, 1936). It was later shown that a single unaligned chromosome in a healthy spindle could delay anaphase until it was properly aligned (Zirkle, 1970). It was not until the 1990s that the mechanism of the anaphase delay became more clear:

4

when a chromosome is not correctly oriented, the SAC prevents the degradation of Cohesin, the protein that physically holds sister chromatids together (Uhlmann et al., 1999). In order for the SAC to preserve genomic integrity, the cell must somehow be able to detect chromosome biorientation. How are cells able to monitor the spatial organization of their chromosomes?

III. Detecting correct kinetochore attachment

SAC signaling is controlled by a protein machine known as the kinetochore. The kinetochore is a complex of variable size composed of >100 different proteins which connects sister chromatids to microtubules (Musacchio and Desai, 2017). In 1995, a series of key laser ablation experiments identified the kinetochores of unaligned chromosomes as the source of the "wait-anaphase" signal (Rieder et al., 1995). Concurrently, it was determined that almost all proteins involved in the SAC response localized to the kinetochores of unattached and incorrectly attached kinetochores (Chen et al., 1996; Li and Benezra, 1996; Taylor and McKeon, 1997). Later, it was shown that the kinetochore localization of one specific SAC protein, Mad1, is necessary and sufficient to generate the diffusible signal that inhibits Cohesin degredation and delays anaphase onset (De Antoni et al., 2005; Maldonado and Kapoor, 2011). Understanding how kinetochores know when to recruit and release Mad1 is therefore critical for understanding how cells prevent mitotic errors.

Historically, the kinetochore has been proposed to detect both mechanical and chemical signals to control anaphase onset. Early work using micromanipulation suggested the application of tension across the DNA between the two sister kinetochores (a region known as the centromere) of unaligned chromosomes can trigger anaphase onset (Li and Nicklas, 1995). The hypothesis that centromere tension turns off the SAC is an attractive one from first principles: because spindle microtubules exert a pulling force on kinetochores, a kinetochore pair attached to opposite poles would come under tension while a pair with only one attachment or a pair where both sisters are attached to the same pole would not. However, other evidence

5

suggests that instead of tension, kinetochores control the SAC by monitoring their own binding to spindle microtubules. For example, pharmacological treatments that depolymerize microtubules lead to Mad1 kinetochore localization, while treatments that maintain attachments but prevent centromere tension generation do not (Waters et al., 1998). The debate over which of these two inputs – tension or attachment – controls Mad1 localization and therefore mitotic progression has persisted for decades after these initial observations (London and Biggins, 2014d; Pinsky and Biggins, 2005). There are even two distinct (although not exclusive) molecular models for how kinetochores could turn off the SAC based on what signal kinetochores detect (Aravamudhan et al., 2015; Hiruma et al., 2015; Ji et al., 2015). Parsing which of these two signals are important is critical for understanding how the kinetochore functions as a signaling platform.

A variety of complications have made separating and assessing the impacts of tension and attachment on SAC signaling extremely difficult. These two potential signals are intrinsically linked – kinetochore-microtubule attachments are required to generate tension, and kinetochore pairs at low tension levels lose microtubule attachments as way of correcting erroneous attachment (Lampson and Cheeseman, 2011). Also, kinetochore pairs can experience both tension and attachment through a variety of structures and molecules: Tension can applied across the centromere (interkinetochore tension) or within the structure of one individual kinetochore (intrakinetochore tension) (Maresca and Salmon, 2009; Uchida et al., 2009). Kinetochores can attach to the plus-ends of microtubules through outer kinetochore protein Hec1/NDC80 (end-on attachments) or to the sides of microtubules through a variety of motor proteins (lateral attachments) (Foley and Kapoor, 2013). Distinguishing between these different modes of tension and attachment is critical, because they have different molecular and mechanical origins and therefore implications for kinetochore function. Finally, both of these properties are variable and highly dynamic during mitosis (Magidson et al., 2011; McEwen et al.,

1997). Tools to monitor and perturb tension and attachment types and assess their impact on Mad1 localization and checkpoint signaling are crucial for understanding the SAC response.

In chapter 2, I describe our efforts to parse the impact of tension and attachment on checkpoint signaling by imaging kinetochore pairs and SAC activation in live dividing cells. By monitoring tension, attachment, and Mad1 localization on kinetochore pairs as they biorient, we are able to quantitatively describe the loss of Mad1 on individual kinetochores for the first time and assess which physical changes cause the SAC to turn off. We show that neither tension nor lateral microtubule attachment is sufficient for Mad1 loss. It is only upon the formation on an end-on microtubule attachment the SAC is satisfied and Mad1 leaves in a rapid one-step process. These findings demonstrate that kinetochores must acquire attachment or tension through a specific kinetochore module – Hec1 and its associated proteins – to turn off the SAC. This constrains the molecular models of kinetochore error detection and Mad1 removal and provide insight into how kinetochores ensure that they are bioriented prior to SAC satisfaction.

IV. How do kinetochores count microtubules?

Identifying what input the kinetochore uses to make decisions is important, but in order to understand how the kinetochore functions as a signaling platform it is critical to understand how it processes attachment information quantitatively. How do kinetochores decide when they have enough microtubule attachments, or enough tension from end-on attachments, to turn off the SAC? In budding yeast, this problem is simple: each kinetochore only binds one microtubule (Peterson and Ris, 1976). Mammalian kinetochores are much more complex: each kinetochore binds 15-25 microtubules at metaphase with ~250 Hec1 subunits. How these kinetochores count attachment information is intimately linked to the physical structure and network architecture of the kinetochore and has important implications for how cell division functions.

The question of how biological systems count and process quantitative information is a fundamental and longstanding one. For example, human cells are able to count how many X-chromosomes they possess and transcriptionally deactivate all but one (Avner and Heard, 2001). Cells can also tune their regulatory networks to produce different behaviors, from dimmer switch (analog) responses, to switch-like (digital) responses, to more complex adaptation and timer behaviors (Lim et al., 2013). While we understand many of the molecules involved in the SAC response, we understand very little about their overall behavior as a network and its downstream consequences for cell division.

While there have been some observations, including in chapter 2, that Mad1 loss is activated on kinetochores with less than a full complement of microtubule attachments (DeLuca et al., 2003; Dudka et al., 2018; Sikirzhytski et al., 2018), the constantly fluctuating number of microtubule attachments within cells make assessing the quantitative relationship between Mad1 and attachment number difficult. In chapter 3, I describe a system we developed to control and fix the number of kinetochore-microtubule contacts on individual kinetochores at a steady state. Our findings reveal that kinetochores are able to shut off the SAC with very few – 4 or less – microtubule attachments, indicating that the relationship between attachment and Mad1 localization is switch-like and sensitive. Interestingly, we also observe that low microtubule occupancy slows the rate of Mad1 loss, suggesting a mechanism through which a highly sensitive checkpoint avoids responding to errant attachments. Finally, we show that this response is mediated solely through microtubule attachment, not the tension generated by pulling forces. Together, these findings illustrate what signals the kinetochore detects, how it's processing machinery works, and suggests mechanisms for how mitosis can be both accurate and robust.

V. Observing and perturbing kinetochores in mammalian cells.

One of the primary reasons why such fundamental questions about kinetochores remain unanswered is that their structure is extremely difficult to analyze and they functions are difficult to perturb. Imaging kinetochore structure with conventional light microscopy is impossible: mammalian kinetochores are dense, composed of 100s of proteins, and only around 200 nm along the chromosome-spindle axis. Analyzing their mechanical and chemical properties outside of the cell where manipulation is easy is also extremely difficult: to this point, a mammalian kinetochore has not been successfully purified or reconstituted. Therefore, special techniques are required in order to image the kinetochore structure *in vivo* and to perturb their function in real time during cell division. In chapter 4, we describe methods to both image and physically perturb kinetochores in mammalian cells. We discuss specific technical considerations for two techniques our laboratory specializes in: sub-pixel resolution imaging of kinetochore deformations in living cells and using cellular compression to exert forces on spindles and kinetochores. We intend this as resource for those in the field that want to gain deeper insight about the structural arrangement and mechanical abilities of the kinetochore.

Chapter 2: Spindle assembly checkpoint satisfaction occurs via end-on but not lateral attachments under tension

Abstract:

To ensure accurate chromosome segregation, the spindle assembly checkpoint (SAC) prevents anaphase until all kinetochores attach to the spindle. What signals the SAC monitors remains unclear. We do not know the contributions of different microtubule attachment features, or tension from biorientation, to SAC satisfaction in normal mitosis – or how these possible cues change during attachment. Here, we quantify concurrent Mad1 intensity, reporting on SAC silencing, and real-time attachment geometry, occupancy, and tension at individual mammalian kinetochores. We show that Mad1 loss from the kinetochore occurs in switch-like events with robust kinetics, and that metaphase-like tension across sister kinetochores is established just before Mad1 loss events at the first sister. We demonstrate that CenpE-mediated lateral attachment of the second sister can persistently generate this metaphase-like tension prior to biorientation, likely stabilizing sister end-on attachment, yet cannot induce Mad1 loss from that kinetochore. Instead, Mad1 loss begins after several end-on microtubules attach. Thus, end-on attachment provides geometry-specific molecular cues, or force on specific kinetochore linkages, that other attachment geometries cannot provide.

Introduction:

The spindle assembly checkpoint (SAC) ensures correct partitioning of the genome (London and Biggins, 2014c; Musacchio and Salmon, 2007) by preventing the onset of anaphase until all sister kinetochores are attached to the spindle (Rieder et al., 1995). The level of SAC proteins at kinetochores regulates cell cycle progression (Collin et al., 2013; Dick and Gerlich, 2013; Heinrich et al., 2013). Specifically, the removal of Mad1 from attached kinetochores controls the anaphase-inhibitory signal (Maldonado and Kapoor, 2011). Both tension from biorientation (McIntosh, 1991) and microtubule attachment have been proposed to

control Mad1 loss from kinetochores in mammalian cells (Etemad and Kops, 2016; Pinsky and Biggins, 2005). While tension across the centromere is not essential for SAC satisfaction (O'Connell et al., 2008; Rieder et al., 1995), tension within (and across) a single kinetochore may be (Maresca and Salmon, 2009; Uchida et al., 2009). Across which linkages tension could be monitored, and whether that tension would be necessary, sufficient, or neither, remains unclear (Etemad et al., 2015; Magidson et al., 2016; Smith et al., 2016; Tauchman et al., 2015). Instead, or in addition, the SAC may monitor the presence of microtubules or of a specific attachment feature such as whether the kinetochore binds to the end (end-on) or side (lateral) of microtubules (i.e. geometry), how many microtubules it binds (occupancy), and the timescale over which it remains attached to any – or a given –microtubule (lifetime).

We do not know what physical changes ultimately trigger Mad1 loss and, critically, we do not know how changes in tension and attachment features map to those of Mad1 at individual kinetochores during mammalian spindle assembly. One barrier is that to this point we have only visualized tension, attachment and SAC signaling together in fixed cells. Challenges to live imaging these dynamics include concurrently visualizing individual kinetochores moving in 3D, dim microtubule structures, and dim Mad1 – and doing so at high resolution over long periods. Since tension and attachment candidate cues both evolve during mitosis (Magidson et al., 2011; McEwen et al., 1997), and often co-vary and go through short-lived intermediates, uncoupling their contributions has been difficult. In particular, it is not yet clear if lateral attachments, which utilize motors rather than Ndc80 for binding microtubules, are able to trigger SAC silencing (Cheeseman and Desai, 2008; Kops and Shah, 2012; Nezi and Musacchio, 2009), and whether the answer to this is based on the specificity of their molecular interface, or to a different stability or force-generating ability. Determining which kinetochore interfaces can and cannot trigger SAC silencing upon binding to, or being pulled on by, microtubules is essential to understanding what the kinetochore monitors to control cell cycle progression.

12

Here, we develop an approach to quantitatively map in real-time the structural dynamics of centromere tension, attachment geometry, and attachment occupancy onto those of Mad1 signaling at individual mammalian kinetochores during spindle assembly. Together, our work reveals the space-time trajectory of a sister pair to SAC silencing, and indicates that engagement of microtubule ends is the trigger for SAC silencing. We demonstrate that CenpE-based lateral attachments can generate long-lived force, and are thus well-suited to stabilize end-on attachments before biorientation, but they cannot satisfy the SAC. Thus, end-on attachment must provide specific molecular cues – or force on a specific linkage – to control the SAC that other persistent, force-generating attachments cannot provide.

Results and discussion:

To measure the real-time kinetics of Mad1 depletion once initiated at individual kinetochores, we used a two-color reporter consisting of EYFP-Mad1 and CenpC-mCherry (Fig. 2.1A). Mad1 localization is necessary and sufficient for SAC activation (Maldonado and Kapoor, 2011), its N- or C-terminal EYFP fusions behave similarly (Shah et al., 2004), and Mad1 binding and dissociation kinetics are well understood on unattached – but not attached – kinetochores (Dick and Gerlich, 2013; Howell et al., 2004; Shah et al., 2004). In turn, CenpC is a stable kinetochore component (Shah et al., 2004). The ratio of Mad1 to CenpC intensities controls for variation in kinetochore size and for out of focal plane movements. We imaged this reporter live over four focal planes with ~10 s resolution in mammalian PtK2 cells. These cells are ideal to track kinetochores and map physical attachment and tension changes as they are large, flat, and have few chromosomes. We tracked individual kinetochores from prophase or prometaphase to metaphase using CenpC-mCherry, and quantified reporter intensities (Fig. 2.1A).

13

We found that Mad1 levels at individual kinetochores are stable during spindle assembly (Mad1-ON state), until they drop sharply to background (Mad1-OFF state) while CenpC levels stay constant (Fig. 2.1A, B, Video 1). While there may be short-lived fluctuations in Mad1 levels that we cannot detect, we did not find intermediate steady-states with intensities between those of Mad1-ON and -OFF states, and did not observe any significant re-recruitment of Mad1 upon the completion of Mad1 loss. To determine the distribution of Mad1 loss rates, we aligned all Mad1 loss events in time at the start of Mad1 loss (t=0). This revealed that Mad1 loss kinetics are switch-like and strikingly similar over kinetochores and cells (n=46 kinetochores in 17 cells; Fig. 2.1C). The kinetics of Mad1 loss are well fit by a single exponential (t1/2=79 s, R2=0.97; Fig. 2.1C), with only a marginal fit improvement with a double exponential (R2=0.99). This suggests that the process of removing Mad1 from kinetochores has one rate-limiting step. This single event could, for example, be the turnover of phosphorylation marks involved in recruiting Mad1 (Nijenhuis et al., 2014), or Mad1 removal by dynein (Howell et al., 2001).

To probe the events that govern Mad1 loss, we examined Mad1 removal at individual kinetochore pairs and in different conditions. Mad1 loss events at each sister were broadly distributed in time (10.6±9.5 min apart; Fig. S2.1A), and thus pairs with a single SAC-satisfying sister exist (Gorbsky and Ricketts, 1993), and were broadly distributed in in space (Fig. 2.1D, S1B). While this distribution in space does not have a large effect on the distribution in time (Fig. S2.1C), it follows a particular pattern: the first sister in a pair to satisfy the SAC began losing Mad1 close to its spindle pole, often as it transitioned from poleward to away-from-pole movement; meanwhile, the second sister began losing Mad1 at a different location (p=0.0009), close to the metaphase plate, and typically after a sharp movement towards the plate that also aligned (Magidson et al., 2015) sisters along the pole-to-pole axis (Fig. S2.1D). Despite these differences, Mad1 loss events at the first and second kinetochores had indistinguishable kinetics after the onset of Mad1 loss (Fig. 2.1E). We then asked what physical properties of the

14

kinetochore, if any, regulated this rate-limiting step in Mad1 loss. We hypothesized that tension

or attachment, both proposed to be required for Mad1 loss, tune kinetics of Mad1 removal after

its onset. To test this hypothesis, we imaged Mad1 in cells with monopolar spindles (Fig. S2.2A-

B) which have lower tension (Fig. S2.2D), and in cells expressing Hec1-9A-mRuby2 (Fig.

S2.2C) which have higher tension (Fig. S2D) and microtubule occupancy (Zaytsev et al., 2014).

We use centromere stretch (interkinetochore (K-K) distance) as a reporter of tension: while

centromere stretch is not itself necessary for SAC satisfaction, changes in centromere stretch

imply changes in load on the k-fiber and across at least some kinetochore linkages. Despite

these tension differences, Mad1 loss kinetics remained unchanged in monopoles (p=0.15, n=20

kinetochores, Fig. 2.1E; Video 2) and Hec1-9A cells (p=0.95, n=18 kinetochores; Fig. 2.1E).

This suggests that after the onset of Mad1 loss, the rate of loss is insensitive to tension and

attachment occupancy levels; once the SAC satisfaction decision is made, the kinetochore

silences the SAC in a stereotypical event.

To gain insight into what events initiate Mad1 loss, we quantified how tension and

attachment change before and around these stereotypical Mad1 loss events. We began by

measuring the K-K distance of a sister pair before and during Mad1 loss (Fig. 2.2A-C, Video 3).

In all cases mapped, the K-K distance of a single chromosome increased just before the first

sister lost Mad1 (Fig. 2.2B-C): it started at 1.06 ± 0.06 µm for t<-2 min, indistinguishable

(p=0.46) from that in nocodazole (n=10 pairs), and increased (p=0.008) to 2.14±0.32 µm by t=0,

the start of Mad1 loss (Fig. 2.2D). The K-K distance as Mad1 leaves the first kinetochore is

higher in bipoles than in monopoles (2.14±0.32 µm versus 1.20±0.03, p=0.02; Fig. 2.2D and

S2C), suggesting that an opposing force other than polar ejection force acts prior to silencing

the first kinetochore in normal, bipolar mammalian mitosis. The K-K distance increase just

before Mad1 loss, in all cases measured (Fig. 2.2E), is consistent with – but does not imply –

tension across the kinetochore being necessary to initiate Mad1 loss. However, kinetochore

pairs persist at a metaphase-level of tension (p=0.55) for minutes without Mad1 loss at the second sister (1.89±0.19 µm for t<-2 min, n=19 pairs; Fig. 2.2D) with no significant tension increase (p=0.96) at t=0 (1.89±0.14 µm). Thus, neither microtubule attachment nor the transmission of force (i.e. load-bearing) across the kinetochore, from chromosome to microtubule, is sufficient to satisfy the SAC in normal dividing cells.

To uncover how kinetochores form persistent force-generating attachments without satisfying the SAC, we concurrently quantified Mad1 intensity and the position and intensity of microtubules at kinetochores in live cells. We expressed EYFP-Mad1 and mCherry-tubulin (Fig. 2.3A, Video 4). On pairs with one Mad1-ON sister (K2, orange), the Mad1-ON sister was associated with a microtubule bundle whose intensity continued past the kinetochore rather than terminating at it (Fig. 2.3A, Video 4). This is consistent with motor-driven lateral kinetochore-microtubule attachments, which we identified as cases where i) the tubulin intensity is equal on both sides of a kinetochore (Fig. 2.3B) and where ii) there is centromere tension (Kapoor et al., 2006) confirming productive microtubule engagement. We detected the same intermediates (pairs under tension with one lateral, Mad1-ON kinetochore, and one Mad1-OFF kinetochore) in fixed PtK2 cells stained for endogenous Mad2 (Fig. S2.3A-C, n=17 pairs), validating EYFP-Mad1 as a live-cell reporter. Despite interactions with lateral microtubules (Fig. 2.3A-C) and high tension for long periods (Fig. 2.3D), the levels of Mad1 on these kinetochores did not change (n=8 kinetochores; Fig. 2.3E).

Consistent with the lateral attachments imaged being powered by CenpE, a plus-end-directed kinesin, rigor inhibition of this motor with GSK-923295 (Wood et al., 2010) (Fig. 2.3F) generated kinetochore pairs stuck near a pole that failed to congress (Fig. 2.3G). These pairs remained with one laterally attached, Mad1-positive sister (Magidson et al., 2015) (n=10 kinetochores; Fig. 2.3H, Video 5), under some, albeit reduced, centromere tension (Fig. 2.3I). Thus, stable lateral microtubule-kinetochore attachments that generate long-lived metaphase

16

centromere tension levels exist during normal mitosis, are mediated by CenpE, and are not sufficient to (even partially) satisfy the SAC. If the SAC monitors tension across the kinetochore, it must do so across a kinetochore linkage that is not put under sufficient load in these lateral attachments.

Finally, to probe how microtubule attachment geometry and occupancy changed before and around Mad1 loss, we imaged three-color cells expressing EYFP-Mad1 and CenpC-mCherry, and stained with the far-red microtubule dye SiR-Tubulin (Lukinavičius et al., 2014) (Fig. 2.4A, Video 6). We captured Mad1 loss events for the second kinetochore in a pair, and concurrently quantified (Fig. 2.4A, B) the dynamics of Mad1 intensity (Fig. 2.4C), microtubule attachment geometry and occupancy (Fig. 2.4D) and centromere tension (Fig. 2.4E) at single kinetochores. Strikingly, signature Mad1 loss events (Fig. 2.4C) always coincided with a sharp increase in end-on microtubule occupancy levels (n=21 kinetochores; Fig. 2.4B, D). As the first several microtubule ends bind from t=-100 s to t=0 (p=0.003; Fig. 2.4D), there is no corresponding decrease in Mad1 levels (Fig. 2.4C). After several end-on microtubules have bound, which we estimate to be half a mature kinetochore-fiber (thus about 10-12 microtubules in PtK cells (McEwen et al., 1997)), Mad1 loss then initiates (t=0), before end-on attachment levels reach their mature kinetochore-fiber levels at around t=100 s (p=0.001). Over this same time period, there was no change in centromere tension on these kinetochores (Fig. 2.4E).

Consistent with end-on attachments maturing during Mad1 loss, SKAP-ΔEB-tdTomato – which specifically binds kinetochores with mature attachments (Schmidt et al., 2010) – began to localize at kinetochores as EFYP-Mad1 left and apparent end-on attachments (SiR-tubulin) formed (Fig. S2.3D, n=13 pairs). Together, our work indicates that the trigger for Mad1 loss is kinetochore engagement to microtubule ends, and that this engagement provides a unique, geometry-specific cue – whether molecular or physical – that other persistent force-generating attachments cannot provide.

Many elegant studies have used genetic and chemical perturbations to change tension and kinetochore-microtubule attachments, and thereby probe the events triggering Mad1 depletion. Here, our approach was to image naturally occurring centromere tension and attachment changes during spindle assembly – and to map those to the real-time kinetochore SAC silencing response. This allowed us to map a trajectory of events, that is likely one of a few, leading to SAC satisfaction in unperturbed cells (Fig. 2.5).

The contributions of tension and attachment (lifetime, geometry, occupancy) have been hard to decouple. Here, we identify a long-lived state with high centromere tension and no detectable end-on attachment. Consistently, Mad1 had been found at some laterally-attached kinetochores in fixed cells (Dick and Gerlich, 2013; Drpic et al., 2015; Magidson et al., 2015; Shrestha and Draviam, 2013); however, whether the captured attachments were stable and generated sustained force – and therefore if end-on geometry was the only missing element of a correct attachment – was not known. While lateral attachments have been proposed to help SAC protein stripping (Howell et al., 2000) and lateral attachments satisfy the SAC in budding yeast (Krefman et al., 2015; Shimogawa et al., 2010), end-on attachment is necessary for SAC satisfaction in mammalian cells. The pathways that control dynein-dependent SAC protein stripping may also help confer end-on geometric specificity (Gassmann et al., 2010; Matson and Stukenberg, 2014) in mammals. Mammalian cells are thought to use both dynein-dependent and -independent pathways for Mad1 removal (Gassmann et al., 2010) and their individual contributions to this process are not yet clear. Finally, what are the minimal attachment events sufficient for SAC satisfaction? We find that Mad1 loss begins without a full complement of microtubules; further, the different kinetics of k-fiber formation and Mad1 loss suggest that there is not simply a linear relationship between them. Mapping the precise relationship between microtubule occupancy and SAC signaling will require tools to disrupt the rapid k-fiber formation (McEwen et al., 1997) we observe.

18

In unperturbed mitosis, we never observed Mad1 loss prior to tension generation. Our data strongly suggests that lateral attachments, which may be differently sensitive (Kalantzaki et al., 2015) to destabilization at low tension, facilitate end-on attachment formation by generating tension (Foley and Kapoor, 2013; Khodjakov and Pines, 2010; King and Nicklas, 2000; Nezi and Musacchio, 2009; Nicklas et al., 2001) prior to biorientation. While polar ejection forces may generate tension across these kinetochores (Cane et al., 2013; Drpic et al., 2015), higher tension levels may be needed for stabilization. Methods to decouple attachment and tension across the kinetochore will be needed to determine if the latter is necessary for SAC satisfaction. Critically, the inability of persistent force-generating lateral attachments to satisfy the SAC ensures that only bioriented attachments both stabilize kinetochore-microtubule interactions and satisfy the SAC to control cell cycle progression. The imaging approach we developed, employed in different molecular backgrounds and with different fluorescent SAC reporters, should help uncover the cascade of events linking end-on microtubule engagement to SAC satisfaction.

Upon attachment, several mechanisms may confer plus-end specificity. For example, the plus-end may engage a geometry-specific kinetochore interface because of its unique structure and dynamics, or plus-end geometry may allow kinetochore components to engage with more microtubules. Intriguingly, Mps1, a kinase upstream of Mad1 localization (London and Biggins, 2014a), is regulated in an end-on specific manner. Lateral attachments through CenpE may not compete with Mps1 for Ndc80 binding (Hiruma et al., 2015; Ji et al., 2015), or may not access the proper kinetochore interface to pull Mps1 away from its substrates (Aravamudhan et al., 2015). The dynamics of SKAP localization we observe (Fig. S2.3D) suggest a decrease in Aurora B and/or an increase in PP1 activity (Schmidt et al., 2010) once end-on attachments form, consistent with a model where end-on attachment specifically triggers a shift in the phosphorylation state of outer kinetochore substrates.

19

If tension-based deformations within a kinetochore are important for SAC signaling, our findings suggest that these deformations must be highly specific to end-on microtubule attachments. Further, our work suggests that if tension is sensed, it would likely be sensed at a linkage outside of the junction where CenpE- and Ndc80-based attachments both transmit force (i.e. bear load) to the centromere (Fig. 2.5, Boxes 1-2). Looking forward, it will be important to determine what kinetochore structural and biochemical changes take place when lateral and end-on attachments form.
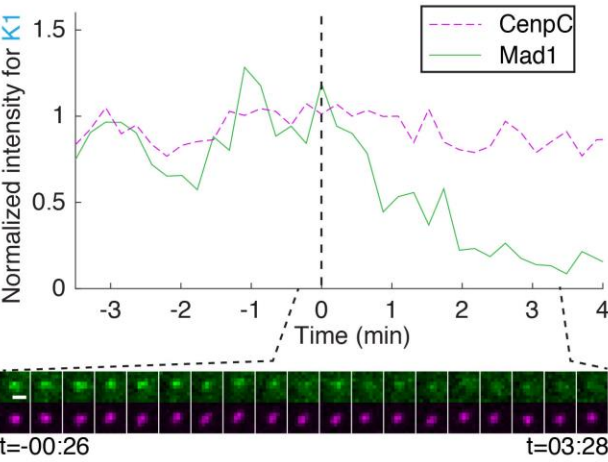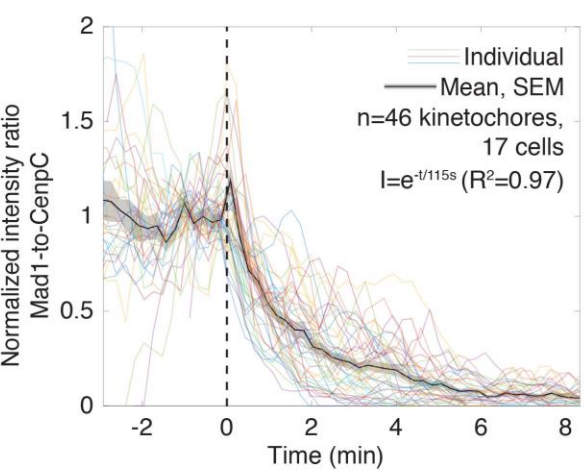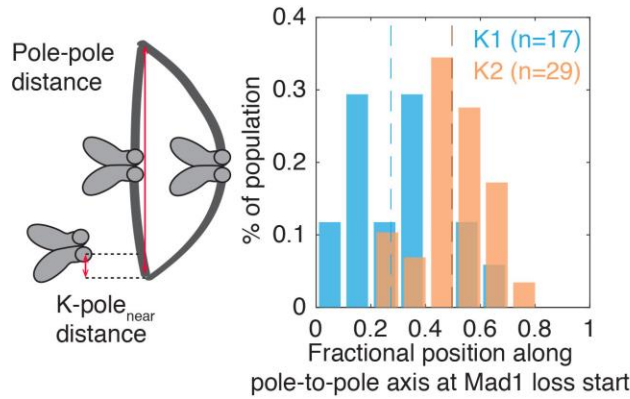
Figures and figure legends:
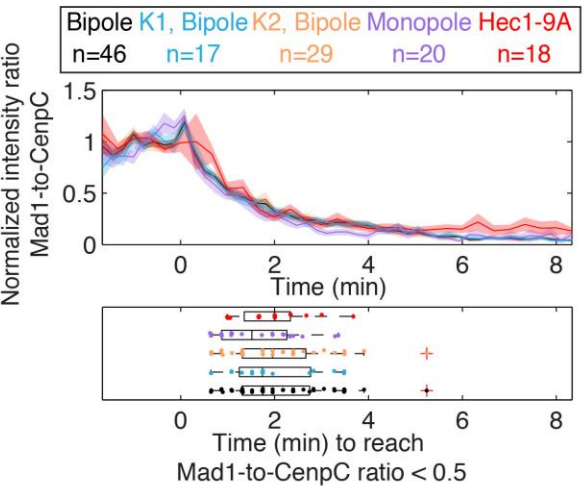
Figure 1

A
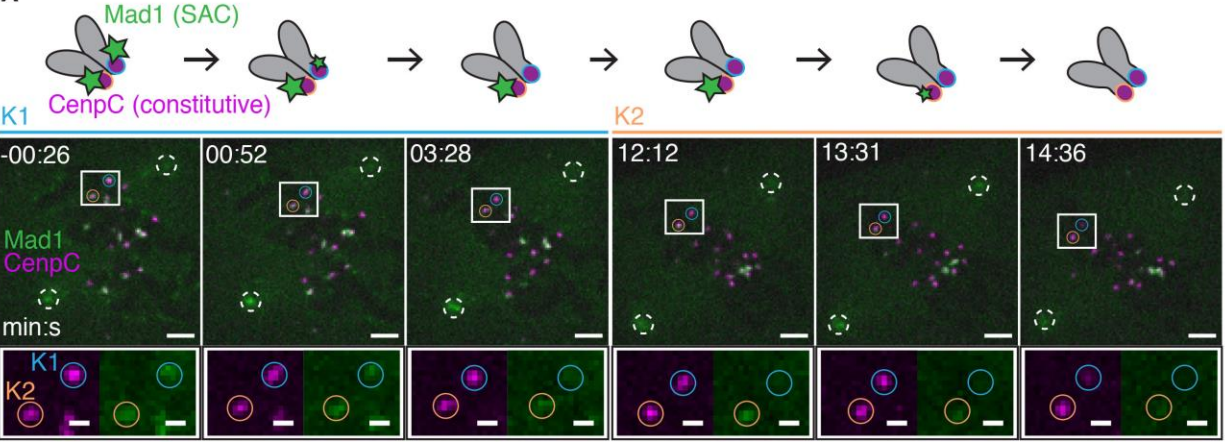
B

C

D

E

Figure 2.1: Mad1 loss at individual mammalian kinetochores is a switch-like process with robust, stereotypical single exponential kinetics.

(A) Timelapse imaging (maximum intensity projection) of representative SAC satisfaction kinetics (EYFP-Mad1, green) at individual kinetochores (CenpC-mCherry, magenta) during spindle assembly in a PtK2 cell. Full circles identify first (K1, blue) and second (K2, orange) sisters in a pair to lose Mad1, and white dashed circles identify spindle poles. Scale bars=3 μm (large) and 1 μm (zoom), and t=0 indicates the start of Mad1 loss on K1.

(B) Mad1 (solid green) and CenpC (dashed magenta) intensities for K1 in (A) around SAC satisfaction. Timelapse (bottom) of K1 at 13 s intervals. Scale bar=1 μm.

(C) Individual traces, mean and SEM of the Mad1-to-CenpC intensity ratio (I) over time (t) around SAC satisfaction, with traces synchronized at t=0.

(D) Distribution of the fractional position along the pole-to-pole axis ((k-polenear)/(pole-pole)) where kinetochores start to lose Mad1. Dashed lines indicate the mean position for each sister. The first sister (K1) loses Mad1 close to its pole and the second sister (K2) near the metaphase plate.

(E) Mean and SEM (top) of the Mad1-to-CenpC intensity ratio with t=0 Mad1 loss start, and distribution (bottom) of times to reach a threshold intensity ratio, in bipolar cells, different kinetochores (K1 and K2) in these cells, in monopolar spindles (STLC-treated) which have lower tension, and Hec1-9A-expressing cells which have higher tension and attachment levels. In all cases, Mad1 loss kinetics are indistinguishable from control (n.s. is for p>0.05).

Figure 2
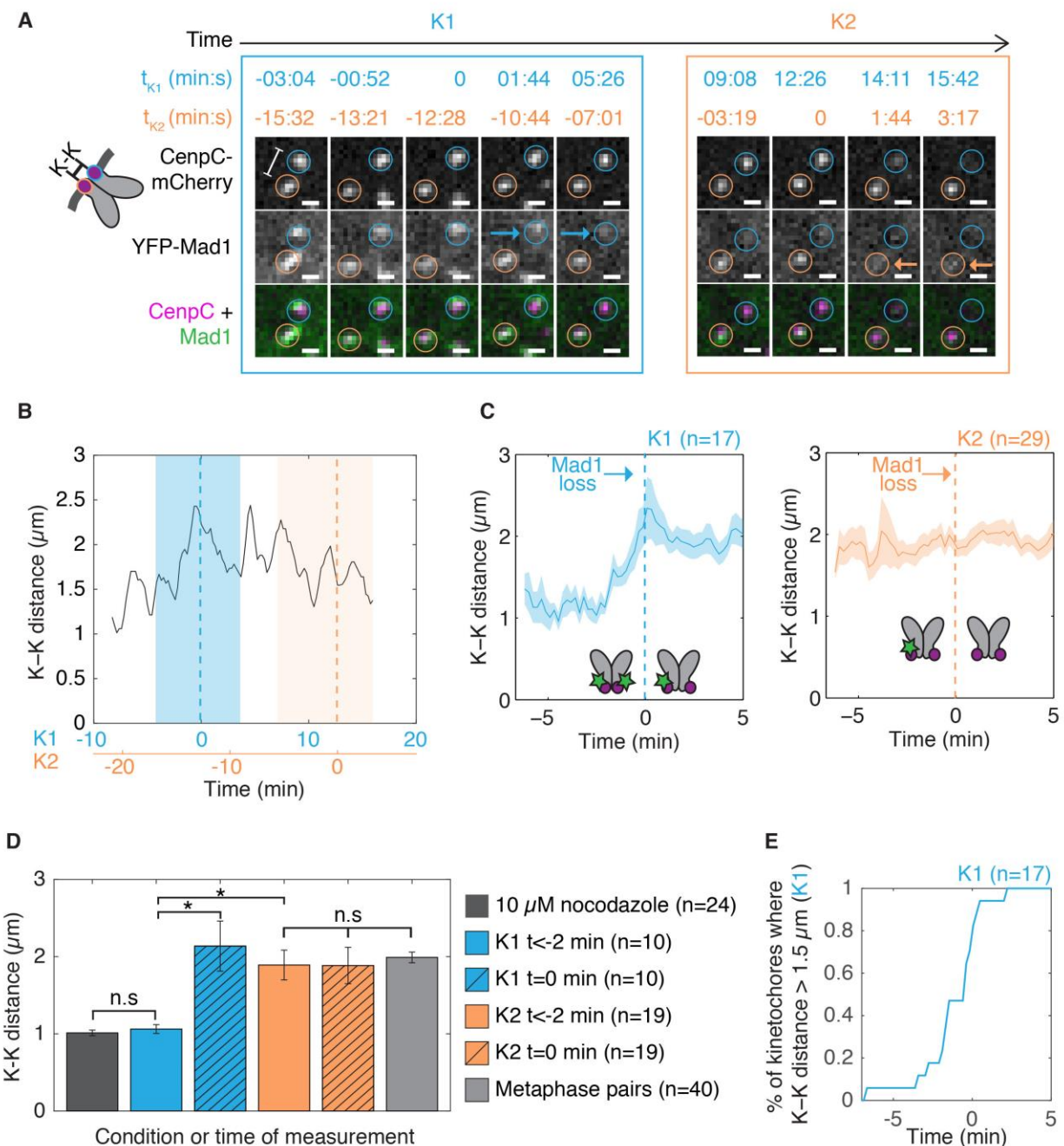
Figure 2.2: Kinetochores are under metaphase-level tension prior to Mad1 loss, but tension across the kinetochore is insufficient to initiate Mad1 loss.

(A) Timelapse imaging (maximum intensity projection) of SAC satisfaction kinetics (EYFP-Mad1) concurrently with K-K distance (CenpC-mCherry) showing representative changes in centromere tension relative to Mad1 loss (start at t=0, followed by arrows) on K1 (blue) and K2 (orange) from PtK2 cell in Fig. 2.1A.

(B) K-K distance over time for the pair in (A), with smoothing over a 3-timepoint window, and t=0 (dashed lines) indicating the start of Mad1 loss for K1 (blue) and K2 (orange).

(C) Mean and SEM of K-K distance over time plotted relative to Mad1 loss start (t=0) for each of K1 (left) and K2 (right).

(D) K-K distance at all timepoints before t=-2 min for K1 and K2, at t=0 for K1 and K2, and at reference points in separate experiments (metaphase kinetochores and 10 µM nocodazole). Measurements for K2's t=-2 min do not include any data before K1's t=0.

(E) Fraction of pairs with a K-K distance crossing > 1.5 µm as time evolves relative to Mad1 loss start at K1 (t=0).

Figure 3

A

B

C

D

E

F

G

H

I

Figure 2.3: Lateral attachments generating long-lived metaphase-level centromere tension do not satisfy the SAC.

(A) Timelapse imaging (maximum intensity projection) of representative SAC satisfaction kinetics (EYFP-Mad1) and microtubule attachment (mCherry-Tubulin) in a PtK2 cell. K2 (orange circle) sits along the side of a neighboring kinetochore-fiber, suggesting a 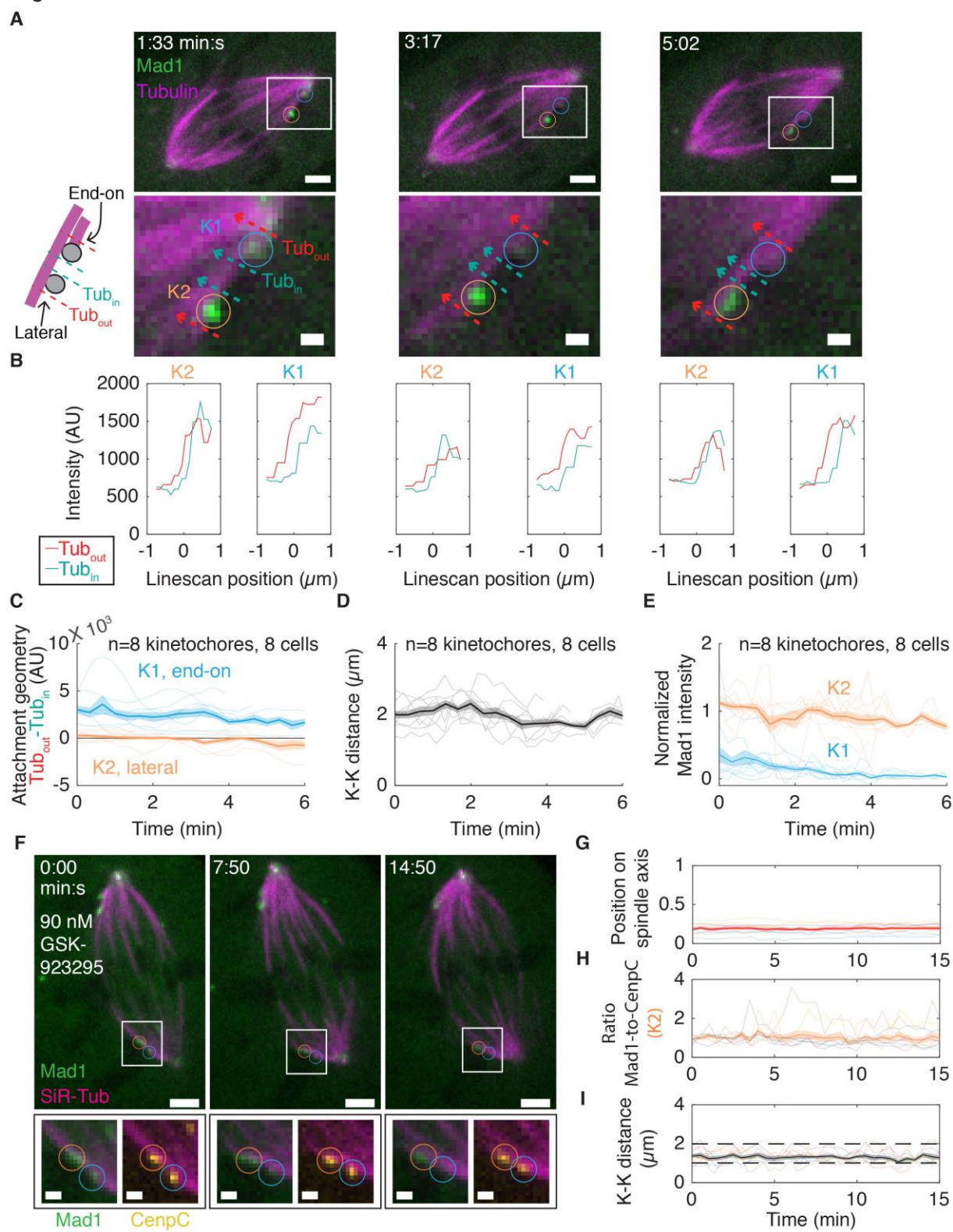lateral attachment, but remains Mad1-positive while its sister K1 (blue circle) loses Mad1. Bottom images display the analysis depicted in (B). Scale bars=3 µm (large) and 1 µm (zoom), and t=0 indicates movie start.

(B) Analysis of microtubule geometry comparing the tubulin intensity (integrated linescans) inside (Tubin) and outside (Tubout) the pair in (A). The intensity difference is high on K1, indicating an end-on attachment, and is near zero on K2, indicating a lateral attachment.

(C) Individual, mean and SEM of Tubout-Tubin for K1 (blue) and K2 (orange) in pairs where K2 begins Mad1-positive.

(D) Individual, mean and SEM of K-K distances for the traces in (C).

(E) Individual, mean and Mad1 intensity for K1 (end-on, blue) and K2 (lateral, orange) in (C-D).

(F) Timelapse imaging (maximum intensity projection) of representative SAC inactivation kinetics (EYFP-Mad1) and microtubule attachment (SiR-Tubulin) at a kinetochore pair (CenpC-mCherry) in a PtK2 cell where some kinetochores are locked in a CenpE-mediated lateral attachment (90nM GSK-923295 CenpE inhibitor) for >15 min. Scale bars=3 µm (large) and 1 µm (zoom), t=0 indicates movie start.

(G-H) Analysis (individual, mean and SEM) of **(G)** fractional position along the pole-to-pole axis (see Fig. 2.1D), **(H)** Mad1-to-CenpC intensity ratio and **(I)** K-K distance for such K2 kinetochores highlighted in (F), where t=0 indicates movie start. Dashed black lines in (I) indicate reference average K-K distances (same data as Fig. 2D) for pairs in nocodazole (lower) and at metaphase (upper).
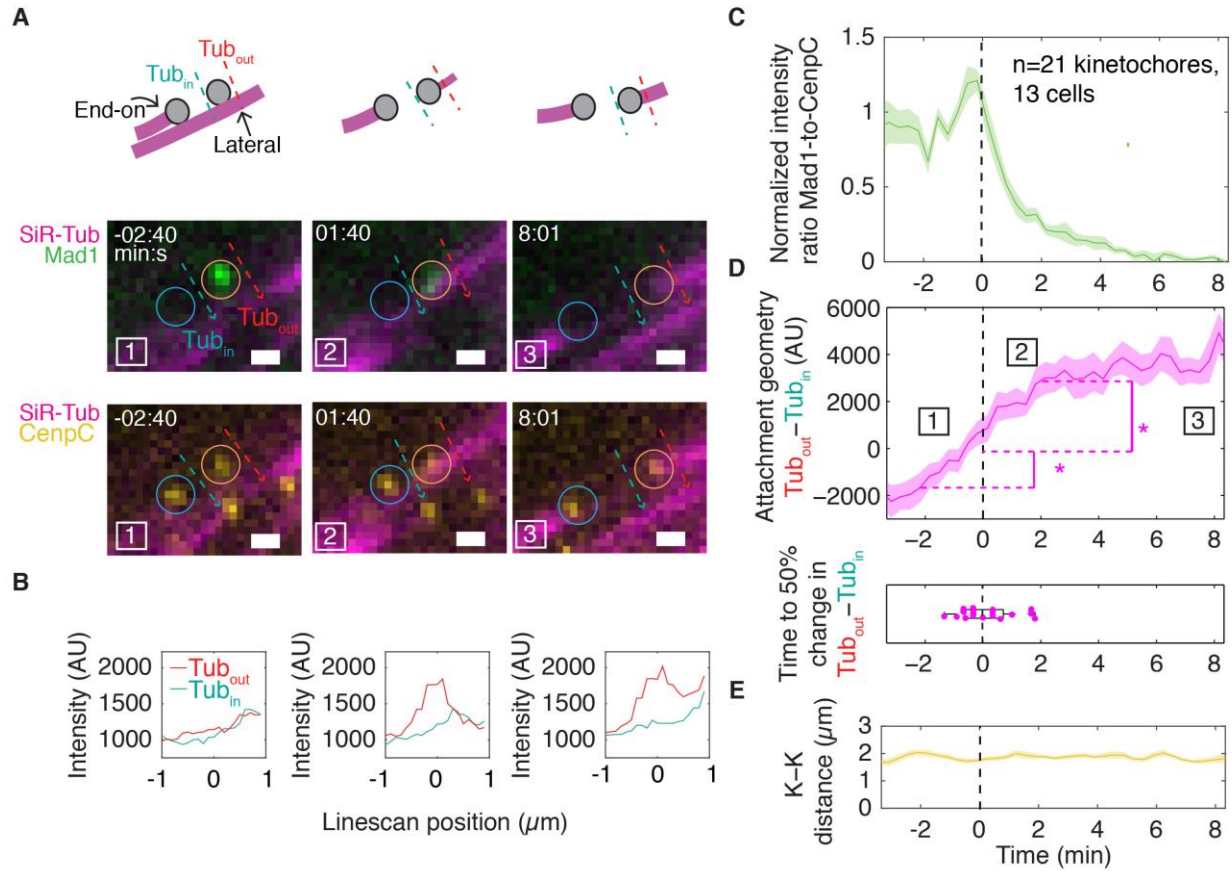
Figure 2.4: Mad1 loss begins rapidly after end-on attachment initiation and before a full kinetochore-fiber forms.

(A) Timelapse imaging (maximum intensity projection) of a representative kinetochore pair's SAC satisfaction kinetics (EYFP-Mad1; Mad1 loss start at t=0), attached microtubules' geometry and intensity (SiR-Tubulin) and centromere tension (CenpC-mCherry) in a PtK2 cell. Dotted lines illustrate analysis shown in (B). Scale bars=1 μm.

(B) Microtubule attachment geometry (and occupancy) analysis as an end-on attachment forms, corresponding to images in (A). A negative value indicates that the kinetochore is near the end of its lateral microtubule track.

(C-E) Concurrent quantification (mean, SEM) of **(C)** Mad1-to-CenpC intensity ratio, **(D)** microtubule attachment geometry (Tubout- Tubin), and **(E)** tension (K-K distance) around SAC satisfaction, with t=0 indicating the start of Mad1 loss on K2. Boxed numbers map to images in (A). Mad1 loss starts rapidly after end-on attachment initiation, when less than (* p<0.01, pairwise t-test) a full complement of microtubules are bound.

27
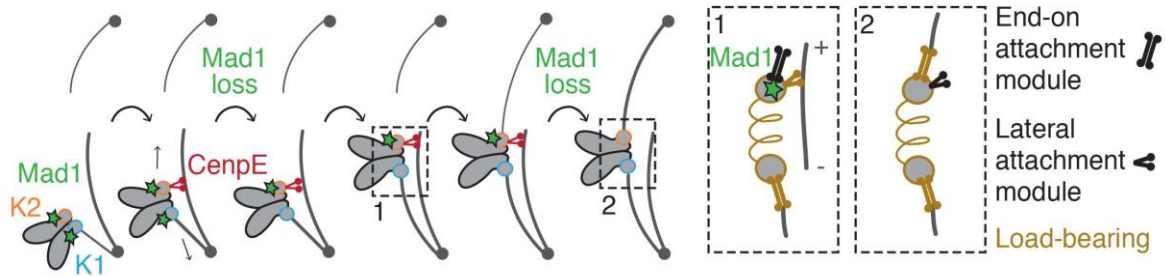
Figure 5

Figure 2.5: Model for attachment trajectory and triggering cue leading to SAC silencing of sister kinetochores.

In the trajectory we map, the first kinetochore (K1, blue circle) loses Mad1 (green star) and satisfies the SAC near its pole, The second kinetochore (K2) laterally attaches through CenpE (red motor), generating tension that can stabilize end-on attachment of K1 – helping K1 bypass tension-based inhibition of initial end-on attachments. Despite being able to transmit force and bear load from the outer to inner kinetochore (Box 1, gold), this attachment does not induce Mad1 loss at K2. CenpE pulls the pair towards the metaphase plate, where K2 forms end-on microtubule attachments and rapidly loses Mad1. SAC satisfaction must be triggered by a geometry-specific cue unique to end-on attachment that CenpE-based attachments (even persistent force-generating ones) cannot supply. This cue could, for example, be binding interactions specific to end-on attachments, or deformation of a linkage that only bears sufficient load in an end-on attachment (Box 2, gold).

28

Supplemental figures and legends:

Figure S1

A

B

C

D
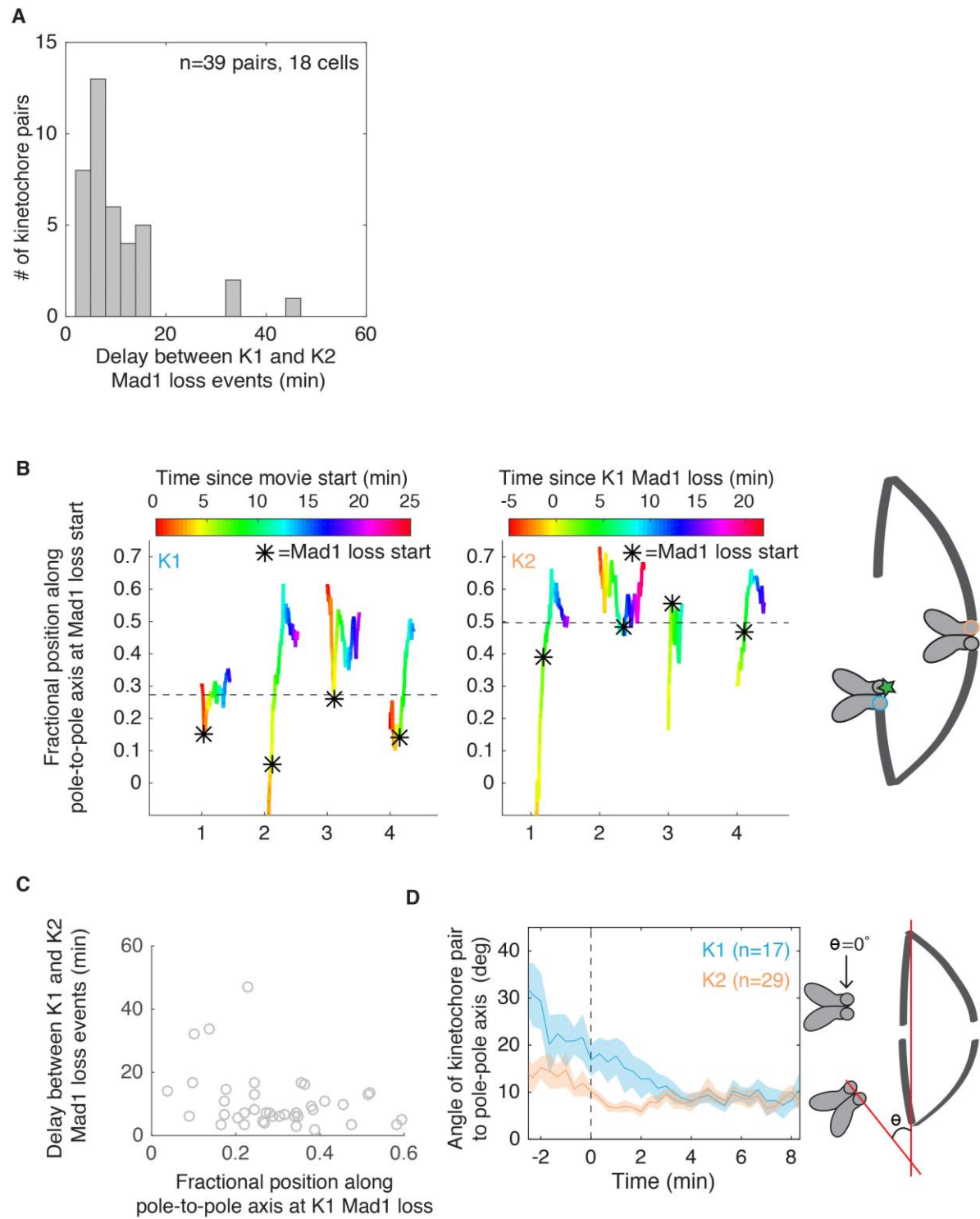
Figure S2.1: Characterization of Mad1 loss trajectories on sister kinetochores, related to Figure 2.1.

(A) Distribution of time delays between first (K1) and second (K2) sisters in a pair to lose Mad1, from events such as Fig. 2.1A. Sisters satisfy the SAC at different times, with variable delays.

(B) Representative kinetochore position trajectories (K1, left; K2, right) around Mad1 loss start (*), with dashed line indicating the average position at the start of Mad1 loss (from (Fig. 2.1D)), and color-coding depicting the time since movie start (K1) or time since K1's Mad1 loss start (K2).

(C) Distribution of time delays in (A) relative to pair position on the pole-to-pole axis when K1 loses Mad1. While there is a small negative correlation ($\rho = -0.309$, Pearson correlation coefficient), it is not significant ($p = 0.056$).

(D) Mean and SEM of the angle of kinetochore pairs relative to the pole-pole axis relative to Mad1 loss start (t=0) for K1 (blue) and K2 (orange).

Figure S2

A

Monopolar cells: Lower tension levels

B

C

Hec1-9A cells: Higher attachment, tension levels

D
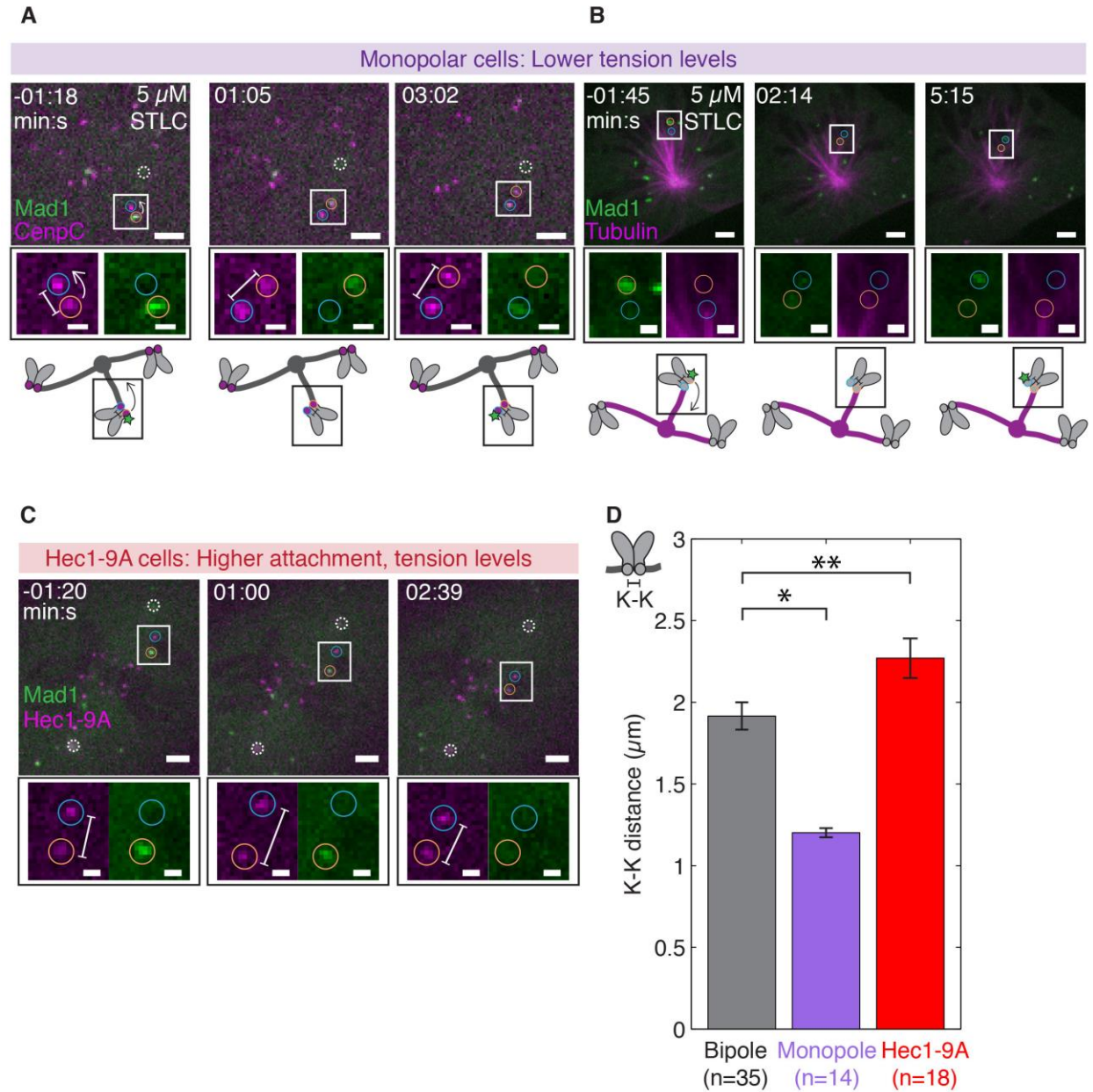
Figure S2.2: Observing Mad1 loss kinetics in in different tension and attachment scenarios, related to Figure 2.1.

(A) Timelapse imaging (maximum intensity projection) of representative SAC satisfaction kinetics (EYFP-Mad1) in a PtK2 monopolar cell with reduced kinetochore tension (CenpC-mCherry, 5 μM STLC). One kinetochore (orange circle) pivots towards the pole (dashed white circle) and loses Mad1, while the other (blue circle) pivots away and recruits Mad1. Scale bars=3 μm (large) and 1 μm (zoom), and t=0 indicates the start of Mad1 loss.

(B) Timelapse imaging (maximum intensity projection) of representative SAC satisfaction kinetics (EYFP-Mad1) and attachment status in a PtK2 monopolar cell (5 μM STLC). One kinetochore, either detached or laterally attached (orange circle), pivots towards the pole, forms

an end-on attachment, and loses Mad1, while the other (blue circle) begins end-on attached, pivots away from the pole, and recruits Mad1. Scale bars=3 µm (large) and 1 µm (zoom), and t=0 indicates the approximate start of Mad1 loss.

(C) Timelapse imaging (maximum intensity projection) of representative SAC satisfaction kinetics (EYFP-Mad1) in a PtK2 cell with increased kinetochore tension and attachment levels (Hec1-9A-mRuby2 expression). Scale bars=3 µm (large) and 1 µm (zoom), and t=0 indicates the start of Mad1 loss on the orange kinetochore. SiR-Tubulin was used to visualize microtubules (not displayed).

(D) K-K distance (white bars in (A) and (B)) in pairs with at least one Mad1-negative kinetochore in bipolar (Fig. 2.1A), monopolar (A) and Hec1-9A-mRuby2 (B) spindles (* $p<0.01$, ** $p<0.05$).

Figure S3
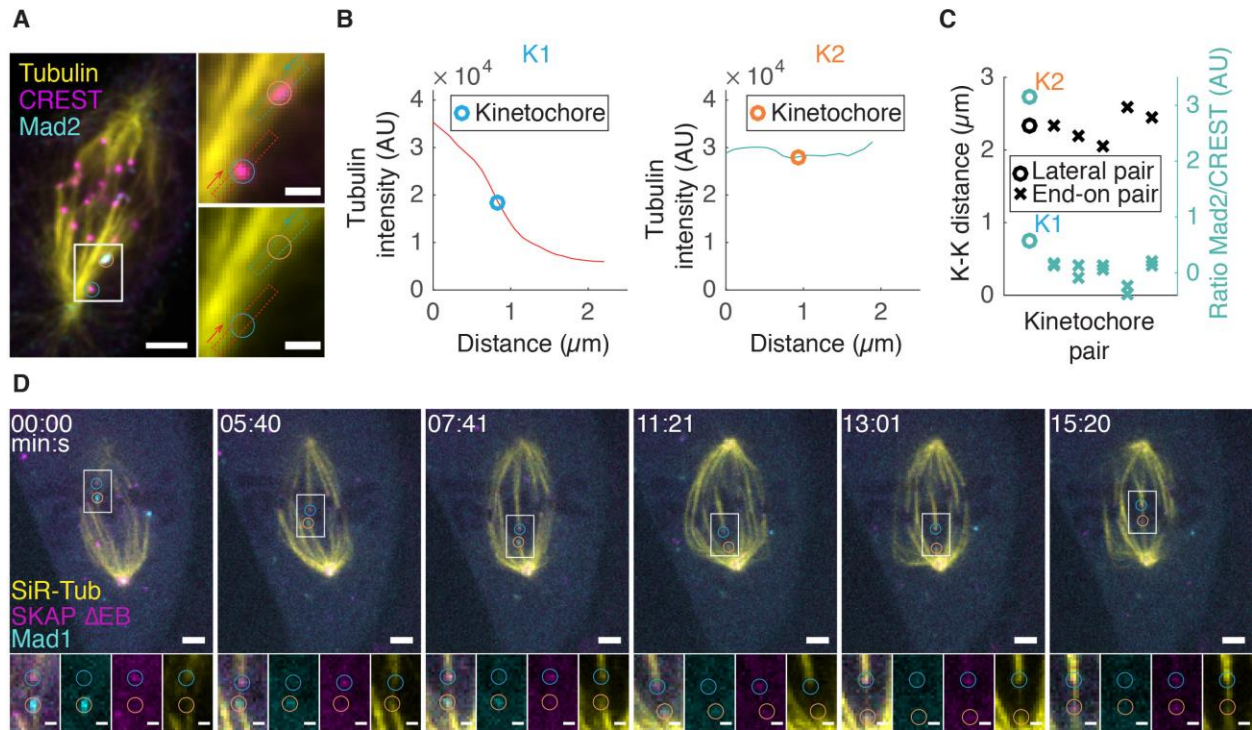
Figure S2.3: Characterizing Mad1-OFF and Mad1-ON attachments with an endogenous SAC reporter and with SKAP recruitment, related to Figures 3 and 4.

(A) Immunofluorescence imaging (sum intensity projection) of endogenous Mad2 together with kinetochores (CREST) and microtubules in a wild type PtK2 cell. Sister kinetochores are under tension, with one (blue circle) end-on attached and Mad2-OFF, and the other (orange circle) laterally attached and Mad2-ON. Bars indicate linescan areas and arrows indicate linescan direction. Scale bars=3 µm (large) and 1 µm (zoom). **(B)** Microtubule attachment geometry analysis across the two highlighted kinetochores in (A). Circles indicate the maximum CREST intensity in the same linescan. **(C)** Comparison of the K-K distance and Mad2/CREST intensity ratio of the highlighted kinetochore pair and of end-on, Mad2-OFF kinetochore pairs in the same cell. **(D)** Timelapse imaging (maximum intensity projection) of a representative kinetochore pair's SAC satisfaction kinetics (EYFP-Mad1; movie start at t=0), attached microtubules' geometry and intensity (SiR-Tubulin) and attachment status (SKAP-ΔEB-tdTomato; (Kern et al., 2016)) in a PtK2 cell. SKAP does not localize to Mad1-positive kinetochores under tension, suggesting a lateral attachment, and kinetochores recruit SKAP, reporting on mature, end-on attachments, as they lose Mad1.

Materials and methods

Cell culture and transfection: PtK2 EYFP-Mad1 cells (Shah et al., 2004) (gift from Jagesh

Shah, Harvard Medical School) and wild type PtK2 cells were cultured as previously described

(Elting et al., 2014). For imaging, cells were plated on 35 mm dishes with #1.5 poly-d-lysine

coated coverslips (MatTek) and media was switched to identical media without phenol red 24 h

prior to imaging. Cells were transfected using Fugene6 or Viafect (Promega) and imaged 36-48

h after transfection with mCherry-α-tubulin (gift from Michael Davidson, Florida State University),

mCherry-CenpC (gift from Aaron Straight, Stanford University), SKAP-ΔEB-tdTomato (gift from

Iain Cheeseman, Massachusetts Institute of Technology and the Whitehead institute), or Hec1-

9A-mRuby2 (mRuby2 (gift from Michael Davidson) was swapped for EGFP in Hec1-9A-EGFP

(Guimaraes et al., 2008)(gift from Jennifer DeLuca, Colorado State University).

Drug and dye treatments: To make monopolar spindles, 5 µM STLC (Sigma-Aldrich) was

added 15 min before imaging (10 mM stock). To rigor CenpE to microtubules, 90 nM GSK-

923295 (MedChem Express) was added 15 minutes before imaging (30 µM stock) (Magidson et

al., 2015). To visualize tubulin as a third color, 100 nM SiR-Tubulin dye (Cytoskeleton, Inc.) was

added 1 h prior to imaging (1 mM stock), along with 10 µM verapamil (Cytoskeleton, Inc.; 10

mM stock) to prevent dye efflux.

Immunofluorescence: For Immunofluorescence, cells were fixed in 95% methanol with 5 mM

EGTA for 1 min. The following antibodies were used: mouse anti-α-tubulin DM1 (1:1,000;

Sigma-Aldrich), human anti-centromere (CREST; 1:25; Antibodies, Inc.), rabbit anti-rat

kangaroo-Mad2 (1:100), mouse and rabbit secondary antibodies conjugated to Alexa 488 and

647 respectively (1:500; Invitrogen), and a human secondary antibody conjugated to DyLight

405 (1:100, Jackson ImmunoResearch Laboratories).

Imaging: Live imaging was performed on an inverted (Eclipse Ti-E; Nikon), spinning disk

confocal (CSU-X1; Yokogawa Electric Corporation) microscope as previously described (Elting

et al., 2014) for two-color imaging. For three- and four-color imaging, a Di01-T405/488/568/647

34

head dichroic (Semrock) was used, along with 405 nm (100mW) and 642 nm (100 mW) diode lasers, and ET455/50M and ET690/50M emission filters (Chroma Technology Corp). Cells were imaged by phase contrast (200-400 ms exposures) and fluorescence (40-75ms exposures) in four z-planes spaced 350 nm apart every 13-30 s, with a 100× 1.45 Ph3 oil objective through a 1.5× lens (Metamorph 7.7.8.0; Molecular Devices). All live images were collected at bin=2 (to improve imaging contrast for dim Mad1 and microtubule structures), 5x pre-amplifier gain, and no EM gain (210 nm/pixel). Cells were imaged at 30 °C, 5% CO_2 in a closed, humidity-controlled Tokai Hit PLAM chamber. The only image processing done prior to display were maximum intensity projections at each timepoint and (for videos only) linear scaling up of the image size in ImageJ. Fixed cell images (Fig. S2.3A-C) were acquired 200 nm apart with bin=1, and images are displayed as sum intensity projections of all frames where the highlighted pair was visible.

Data Analysis:

Tracking: Kinetochore pairs were visually identified by coordinated motion and selected for analysis if they stayed away from other kinetochores and if at least one sister lost Mad1 during the movie. All further analysis was done within Matlab (Mathworks). If mCherry-CenpC was present, kinetochores were tracked using SpeckleTracker (Wan et al., 2012a); if it was not present (Fig. 2.3), kinetochore tracking was done manually using Mad1, tubulin, and phase contrast images and custom software. Spindle poles were tracked manually.

Intensity measurements: To measure EYFP-Mad1 and mCherry-CenpC intensities at each time point, movies were thresholded by setting to zero all pixels <2 standard deviations above image background at the first frame. For each time point, the intensities of all pixels in a 5x5 pixel (1.05x1.05 μm) box around the kinetochore were summed together over all planes. The same

35

operation was performed at areas outside the spindle and subtracted from the kinetochore intensity. Time points with no detectable CenpC were not analyzed.

To calculate tubulin intensity around a given kinetochore (Figs. 2.3 and 2.4), two intensity linescans (1.5 µm long) were taken perpendicular to the sister kinetochore axis: one positioned 0.7 µm towards the centromere (Tub_{in}) and one 0.7 µm away from the centromere (Tub_{out}). To synchronize traces to the beginning of Mad1 loss, traces were examined visually to locate the time where Mad1 levels dropped while CenpC levels stayed constant, and t=0 was set for the time point immediately before such Mad1 loss began. The Mad1-to-CenpC ratio was then normalized to the average ratio from -100 s to 0 s. In Figs. 2.3E and 2.3H (no Mad1 loss), intensities were normalized to K2's Mad1 intensity in the first 100 s and 300 s of the trace, respectively. Immunofluorescence intensities were measured on sum intensity projections using a 3 pixel (0.315 µm) wide linescan for tubulin and a 10x10 pixel (1.05x1.05 µm) box for Mad2 and CREST.

Other measurements: Kinetochore-to-pole distances (Fig. 2.1D) were calculated by projecting where an individual kinetochore fell on the pole-to-pole axis. The "near" pole was designated as the pole closest to K1 at the time of K1's Mad1 loss start.

Statistics: Data are expressed as mean ± SEM. Calculations of p-values (Student's t-test) were done in StatPlus.

Chapter 3: Mammalian kinetochores count attached microtubules in a sensitive and switch-like manner

Abstract:

The Spindle Assembly Checkpoint (SAC) prevents anaphase until all kinetochores attach to the spindle. Each mammalian kinetochore binds many microtubules, but how many attached microtubules are required to turn off the checkpoint, and how the kinetochore monitors microtubule numbers, are not known – and central to understanding SAC mechanisms and function. To address these questions, here we systematically tune and fix the fraction of Hec1 molecules capable of microtubule binding. We show that Hec1 molecules independently bind microtubules within single kinetochores, but that the kinetochore does not independently process attachment information from different molecules. Few attached microtubules (20% occupancy) can trigger complete Mad1 loss, and Mad1 loss is slower in this case. Finally, we show using laser ablation that individual kinetochores detect changes in microtubule binding, not in spindle forces that accompany attachment. Thus, the mammalian kinetochore responds specifically to the binding of each microtubule, and counts microtubules as a single unit in a sensitive and switch-like manner. This may allow kinetochores to rapidly react to early attachments and maintain a robust SAC response despite dynamic microtubule numbers.

Introduction:

The Spindle Assembly Checkpoint (SAC) protects genomic integrity by preventing anaphase until all kinetochores stably attach to the spindle (Rieder et al., 1995). Unattached kinetochores, and certain improperly attached ones, recruit Mad1 and Mad2, which generate an anaphase-inhibitory signal (De Antoni et al., 2005; Chen et al., 1998; Maldonado and Kapoor, 2011). The attachment of microtubule plus-ends ("end-on" attachments) is required for removing Mad1/Mad2 from kinetochores, and consequently for cell cycle progression (Chen et al., 1998; Waters et al., 1998). About 15-25 end-on microtubules bind mammalian kinetochores at metaphase (McEwen et al., 1997; Wendell et al., 1993), but how many microtubules are

39

necessary for Mad1/2 loss, and how the kinetochore measures microtubule number, are not known. Yet, determining how the kinetochore detects and responds to varying microtubule numbers is critical to understanding the mechanisms and function of this signaling platform.

While we have a growing understanding of the individual molecules that give rise to the mammalian kinetochore, how they function together, as an ensemble *in vivo*, remains poorly understood. Kinetochores bind microtubule plus-ends through a dynamic subset of Hec1 molecules (of the Ndc80 complex) (Cheeseman et al., 2006; DeLuca et al., 2006; Yoo et al., 2018), and in metazoans kinetochore-microtubule binding triggers dynein to "strip" Mad1/2 away from kinetochores (Howell et al., 2001; Wojcik et al., 2001). In budding yeast kinetochores, which only bind one microtubule (Peterson and Ris, 1976), attachments may trigger and be detected by Mps1 kinase being displaced or blocked from its substrates (Aravamudhan et al., 2015). Loss of Mps1 activity prevents Mad1/2 kinetochore recruitment and is required for SAC satisfaction (Hewitt et al., 2010; Jelluma et al., 2010; London and Biggins, 2014b; Maciejowski et al., 2010; Santaguida et al., 2010). In mammalian kinetochores, mechanisms to reduce Mps1 activity and thereby permit and potentially activate Mad1/2 loss (Hiruma et al., 2015; Jelluma et al., 2010; Ji et al., 2015) must operate over a disordered kinetochore "lawn" binding many microtubules (Zaytsev et al., 2014). The necessary and sufficient microtubule occupancy levels needed for Mad1/2 loss will drive kinetochore function: triggering anaphase with too few bound microtubules could increase mitotic errors (Dudka et al., 2018), and waiting for too many microtubules could cause mitotic delays, and thereby DNA damage and cell death (Orth et al., 2012; Uetake and Sluder, 2010). Previous work indicates that kinetochores bound to few microtubules can have low Mad2 levels at early prometaphase (Sikirzhytski et al., 2018), and that Mad1/2 can leave kinetochores with reduced (DeLuca et al., 2003) microtubule occupancy (50% (Dudka et al., 2018; Etemad et al., 2018; Kuhn and Dumont, 2017)). Accessing SAC signaling at lower steady-state microtubule occupancies is challenging without perturbing proteins involved in the SAC (DeLuca et al., 2003; Martin-Lluesma et al., 2002), and capturing

40

attachment intermediates is difficult since microtubules rapidly attach during kinetochore-fiber (k-fiber) formation (David et al., 2018; Kuhn and Dumont, 2017; Sikirzhytski et al., 2018). To understand how the kinetochore counts microtubules, we need to externally tune and fix the normally dynamic number of attached microtubules. Finally, understanding how microtubule occupancy regulates SAC signaling requires defining what element of microtubule attachment is detected by the SAC at individual kinetochores. Both kinetochore-microtubule binding (Etemad et al., 2015; O'Connell et al., 2008; Rieder et al., 1995; Tauchman et al., 2015; Waters et al., 1998) and attachment-generated tension (Janssen et al., 2018; Maresca and Salmon, 2009; McIntosh, 1991; Uchida et al., 2009) have been proposed to be detected by the SAC, and decoupling their closely-linked contributions (Akiyoshi et al., 2010; Sarangapani and Asbury, 2014) is needed to identify how kinetochores count microtubules.

Here, we develop a "mixed kinetochore" system to tune and fix the fraction of Hec1 kinetochore molecules within the kinetochore lawn that are capable of microtubule binding. We demonstrate that the number of bound microtubules scales linearly with the number of functional binders, indicating a lack of binding cooperativity between the hundreds of Hec1 molecules (Johnston et al., 2010a; Suzuki et al., 2015) within the native kinetochore. We then show that kinetochores with as low as 20% of metaphase microtubule occupancy can trigger complete Mad1 loss, indicating that the kinetochore makes its decision as a single unit, not through independent subunits. However, Mad1 loss under low occupancy occurs more slowly, which may give early attachments time to mature before complete Mad1 loss. Finally, by acutely removing spindle forces we show that individual kinetochores detect changes in microtubule binding, not in pulling forces that occur with attachment. Together, our data demonstrate that microtubule binding itself activates Mad1 loss, and that it does so in an all-or-none decision with a temporally tuned response. These findings provide a quantitative framework for understanding SAC signaling: they constrain mechanisms for how the kinetochore monitors and responds to microtubule occupancy, and suggest how it can rapidly

41

react to new attachments and yet maintain a robust SAC response despite dynamic microtubule occupancy.

Results:

To vary the number of steady-state microtubule attachments at kinetochores, we designed a system to vary, fix and quantify the fraction of Hec1 molecules at kinetochores capable of strong microtubule binding (Fig. 3.1A). To this end, we depleted endogenous Hec1 in HeLa cells using an inducible CRISPR-based system (Fig. S3.1 A-C)(McKinley and Cheeseman, 2017), and co-expressed weak-affinity Hec1-9D-FusionRed and metaphase-like affinity Hec1-1D8A-EGFP (Hec1-1D) (Fig. 3.1A) (Zaytsev et al., 2014). In contrast to changing Hec1-microtubule interactions over the entire lawn, this "mixed kinetochore" system preserves a fraction of Hec1-microtubule interactions with native affinity (Zaytsev et al., 2014) and native SAC signaling (Hiruma et al., 2015; Ji et al., 2015). In this "mixed kinetochore" assay, the fraction of EGFP (Hec1-1D) vs FusionRed (Hec1-9D) at each kinetochore sets microtubule affinity (Fig. 3.1A). Notably, EGFP and FusionRed intensities varied far more between cells than within a given cell (Fig. S3.1D, F = 175, p = 10^{-220} for EGFP, F = 59, p = 10^{-139} for Fusion Red, One-Way ANOVA), suggesting that variability in protein expression more than kinetochore assembly gives rise to the spread of kinetochore compositions we observe.

We first used this "mixed kinetochore" assay to map how microtubule occupancy scales with the number of binding-competent Hec1 molecules. If microtubule binding were highly cooperative, creating broadly tunable microtubule occupancy steady-states would be difficult (Fig. 3.1A). To map the relationship between functional Hec1 numbers and microtubule occupancy, we prepared "mixed kinetochore" cells as above, and added the proteasome inhibitor MG132 for 1 hr to increase the fraction of kinetochores that reach steady-state occupancies. We then fixed and stained cells for microtubules, EGFP (Hec1-1D), and FusionRed (Hec1-9D). As expected, cells highly expressing Hec1-1D (and 'Hec1-1D alone'

42

cells) formed robust microtubule attachments and cells highly expressing Hec1-9D (and 'Hec1-9D alone' cells) did not (Fig. 3.1B, Fig. S3.1E). As the fraction of Hec1-1D increased, attachments produced more force as measured by the inter-kinetochore (K-K) distance (Fig. 3.1C, Spearman's rho=0.35 p=10^{-21}), and the intensity of end-on microtubule attachments rose in a smooth, graded way well fit by a linear relationship (Fig. 3.1D, r^2 = 0.57, p=10^{-8}) mixed kinetochores having microtubule occupancies between those of 'Hec1-9D alone' and 'Hec1-1D alone' cells. This suggests that Hec1 subunits bind microtubules independently of each other, with weak or no cooperativity in the *in vivo* native kinetochore, similar to some (but not all (Alushin et al., 2010)) *in vitro* measurements despite different binding geometries and molecular contexts (Cheeseman et al., 2006; Ciferri et al., 2008; Volkov et al., 2018; Zaytsev et al., 2015). Thus, this "mixed kinetochore" system can tune and fix kinetochore-microtubule numbers in a graded and quantifiable way.

We then used this "mixed kinetochore" system to map how kinetochores with different fractions of strong microtubule-binding Hec1s coordinate a SAC response, and how many microtubules attachments are needed for complete Mad1 loss (Fig. 3.2A). If Hec1 molecules in the outer kinetochore "lawn" (Zaytsev et al., 2014) function as independent subunits for SAC processing, we expect Mad1 levels to gradually go down as more Hec1s bind microtubules (Fig. 3.2A, top). Alternatively, if the kinetochore integrates information from all Hec1 binding sites as a single unit, Mad1 levels could suddenly drop to zero (undetectable) as more Hec1s bind microtubules and a threshold occupancy level is crossed (Fig. 3.2A, middle and bottom). To distinguish between these scenarios and others, we treated Hec1-depleted cells expressing Hec1-9D or Hec-1D or varying mixtures of both with MG132 for 1 hr and then fixed and stained cells for Mad1, GFP (Hec1-1D), and FusionRed (Hec1-9D) (Fig. 3.2B). In the "mixed kinetochore" system, cells with high Hec1-9D had many more Mad1-positive kinetochores than cells with high Hec1-1D (Fig. 3.2B-C, Fig. S3.2A). While Hec1-9D cells have no or delayed anaphase entry (Sundin et al., 2011), individual kinetochores can lose Mad1; indeed, ~60% of

43

kinetochores in high Hec1-9D cells had no detectable Mad1 (Fig. 3.2C). This same trend applies in cells expressing 'Hec1-1D alone' or 'Hec1-9D alone' (Fig. 3.2C, S2A). This distribution of kinetochore intensities is consistent with a single unit, switch-like decision to lose Mad1 in response to microtubule attachment (Fig. 3.2A, bottom). While some kinetochores remain unattached (Fig. 3.2A, purple) or in the process of Mad1 loss (Fig. 3.2A, orange), Mad1 reaches undetectable levels even at the lowest microtubule occupancy levels we can reach with "mixed kinetochores" (Fig. 3.2C). Consistently, we detected kinetochores that are capable of reaching undetectable Mad1 levels even in cells expressing 'Hec1-9D alone' (Fig. 3.2C, S2A). In contrast, in an independent subunit model we would expect the minimum Mad1 intensity at low occupancy to be high, and to then decrease gradually as occupancy increases (Fig. 3.2A, top). Thus, the decision to trigger Mad1 loss is made at the level of the whole kinetochore by a single unit, rather than at the level of kinetochore subunits (Fig. 3.2A).

To estimate how many microtubules were attached at the lowest Hec1-1D levels sampled in the "mixed kinetochores", we used the relationship between microtubule attachments we obtained in parallel (Fig. 3.1, Fig 2D). Assuming that an EGFP fraction of 1 corresponds to Hec1-1D only expression, and thus a wild type affinity kinetochore (Zaytsev et al., 2014), we estimate that the attached microtubule number in the lowest Hec1-1D fraction reached in mixed cells is about 23% of normal metaphase levels, corresponding to about 4 out of 17 microtubules (Fig. 3.2D) (Wendell et al., 1993). Using different assumptions in this estimation yields values between 2 and 4 microtubules (Fig. S3.2B), significantly lower than previous estimates (Dudka et al., 2018; Etemad et al., 2018; Kuhn and Dumont, 2017), likely because we can now generate lower steady-state microtubule occupancy levels. The sensitivity of the checkpoint to microtubule attachment – fully turning off at a small fraction of a full metaphase complement – indicates that the kinetochore must not only respond as single unit, but amplify small changes in microtubule occupancy across its entire structure. Thus, while

Hec1 molecules independently bind microtubules (Fig. 3.1), they do not independently process microtubule attachment cues to regulate the SAC (Fig. 3.2).

Previous work indicates that once the kinetochore triggers the start of Mad1 loss, Mad1 leaves with stereotyped single exponential kinetics (Kuhn and Dumont, 2017). These kinetics are likely governed by one rate-limiting step, but the nature of this step and if it is regulated are not known. Above, we show that kinetochores with lower microtubule occupancy can trigger complete Mad1 loss, and here we use live imaging to ask whether microtubule occupancy levels regulate the rate of Mad1 loss (Fig. 3.3A). Determining whether microtubule occupancy only regulates the Mad1 loss trigger or also its rate can have implications for both the SAC's molecular underpinnings and cellular role. To test how lowering steady-state microtubule occupancy affects Mad1 loss rates, we expressed Hec1-9D-FusionRed in PtK2 cells where endogenous Hec1 was depleted by RNAi (Guimaraes et al., 2008; Long et al., 2017), and monitored EYFP-Mad1 loss dynamics during attachment formation (visualized using SiR-Tubulin (Lukinavičius et al., 2014)) (Fig. 3.3B). A decrease in K-K distance versus wild type cells (Fig. 3.3C, 1.49±0.03 vs 1.87±0.04 µm, p = 10^{-8}) and in kinetochore-microtubule attachment intensity (Fig. 3.3D, p = 10^{-15}) confirms the expected reduction in kinetochore-microtubule affinity. While the Mad1 loss rate does not increase with higher microtubule occupancy (Kuhn and Dumont, 2017), we find that it decreases with decreased occupancy (Fig. 3.3E-F, $t_{1/2}$ = 190 s in Hec1-9D vs 62 s in wild type, Video 1), and yet decreased occupancy kinetochores are still capable of losing Mad1 to undetectable levels (Fig. 3.3 B, E). Together, our data indicate that low microtubule occupancy regulates the rate at which Mad1 is lost from kinetochores and the SAC is thereby satisfied (Fig. 3.3), but not the decision to satisfy the SAC (Fig. 3.2).

To understand how microtubule occupancy regulates Mad1 localization, it is necessary to define what element of microtubule attachment the SAC detects. Hec1-microtubule binding (Etemad et al., 2015; O'Connell et al., 2008; Rieder et al., 1995; Tauchman et al., 2015; Waters et al., 1998) and the tension generated by spindle pulling forces (Janssen et al., 2018; Maresca

45

and Salmon, 2009; Uchida et al., 2009) have been proposed to be the cues detected by the SAC. Tension across the centromere is not required for Mad1 removal (Fig. 3.4A) (Etemad et al., 2015; O'Connell et al., 2008; Rieder et al., 1995; Tauchman et al., 2015; Waters et al., 1998), but tension within an individual kinetochore, which is harder to remove, may be necessary. For example, unpaired kinetochores in cells undergoing Mitosis with an Unreplicated Genome (MUG) and kinetochores in monopolar spindles can still be under tension given spindle pulling forces on kinetochores and pushing forces on chromosome arms (Fig. 3.4A) (Cane et al., 2013; Maresca and Salmon, 2009; Rieder et al., 1986; Uchida et al., 2009). To determine whether the SAC responds to force across an individual kinetochore, we used laser ablation to acutely and persistently remove spindle pulling forces without detectably perturbing microtubule occupancy. By cutting the k-fiber close to its kinetochore, we minimized spindle connections and forces (Elting et al., 2017; Kajtez et al., 2016), and without these the ablated k-fiber (stub) cannot pull to move kinetochores. We expressed EGFP-tubulin and Hec1-EGFP in PtK2 cells (in a Hec1 RNAi background) to assist ablation and response tracking. If Mad1/2 loss requires spindle pulling forces, acutely removing them on attached kinetochores should re-recruit Mad1/2. To allow time for recruitment (~1.5 min) (Dick and Gerlich, 2013; Pines and Clute, 1999), we persistently prevented force generation from k-fiber-spindle reincorporation (Elting et al., 2014; Sikirzhytski et al., 2014) by repeatedly ablating the k-fiber and partially knocking down NuMA (Elting et al., 2014), essential for reincorporation (Hueschen et al., 2017). As predicted, during ablation the K-K distance dropped to nocodazole-like values (1.11±0.04 µm) (Fig. 3.4B-C), the disconnected kinetochore persistently moved away from its pole (Fig. 3.4D) (Khodjakov and Rieder, 1996a), and we could not detect significant microtubule intensity between the k-fiber stub and spindle body (Fig. 3.4B, Video 2). Thus, the above approach removes productive force generation at individual kinetochores.

    To assess SAC signaling after prolonged loss of force, we fixed each ablated cell 3-5 min after the initial cut, stained for Mad2, kinetochores, and tubulin (Fig. 3.4E, top) and re-

46

imaged each ablated cell. Consistent with force removal, ablating k-fibers led to a decrease in K-K distance compared to control pairs in the same cell (Fig. 3.4F, 1.12±0.04 vs 2.09±0.05 μm, p=10^{-4}), but had indistinguishable K-K distance from pairs in nocodazole-treated cells (1.12±0.04 vs 1.11±0.04 μm, p=0.40). K-fiber microtubule intensity appeared unchanged after ablation (Fig. 3.4G, p=0.42), implying that the timescale of any force-based microtubule destabilization is longer than the time we allow. There was no detectable increase in Mad2 intensity at kinetochores bound to the ablated k-fiber versus controls with no ablation in the same cell (Fig. 3.4E, top, and 4H, p=0.45), while unattached kinetochores in nearby cells had higher Mad2 intensity (Fig. 3.4E, bottom, and 4H, p=10^{-4}). In contrast, kinetochores in nocodazole-treated cells rapidly re-recruit Mad1 after k-fibers begin to depolymerize (Fig. S3.3A-B). We conclude that the SAC does not detect changes in spindle pulling forces and that microtubule binding itself controls Mad1 localization. Thus, microtubule binding is specifically detected, binding events are independent of each other, and yet the kinetochore monitors microtubule occupancy as a single unit.

The kinetochore processes input microtubule attachment signals to produce an output SAC signal controlling cell cycle progression. While we can now better define attachment input signals (Waters et al., 1998), the output signal (Mad1 localization (Chen et al., 1998; Maldonado and Kapoor, 2011)), and kinetochore structure and biochemistry underlying the SAC, how inputs are detected and how inputs and outputs are quantitatively related remain poorly understood. By developing an approach to tune and fix attachment inputs, here we quantitatively map inputs to SAC outputs (Fig. 3.5): the kinetochore detects as input the binding (Fig. 3.4) of microtubules which independently attach to its subunits (Fig. 3.1), and processes these inputs as a single unit to 'compute' an output response (Fig. 3.2) and response rate (Fig. 3.3). Together, our findings provide a quantitative framework for understanding SAC signaling, and have implications for both the mechanisms driving the SAC and their cellular function.

Using "mixed kinetochores", we asked how the disordered kinetochore "lawn" works as an ensemble to control k-fiber formation and kinetochore decision-making. We find that the number of k-fiber microtubules scales linearly with functional Hec1 numbers (Fig. 3.1), indicating a lack of binding cooperativity. In contrast, the relationship between microtubule binding and SAC decision-making is switch-like and sensitive (Fig. 3.2): many kinetochores in our assay cannot reach metaphase levels of microtubule occupancy, and yet still lose Mad1, as full occupancy kinetochores do. Because kinetochore subunits do not bind microtubules cooperatively (Fig. 3.1), this sensitive behavior must be created downstream of microtubule attachment. Feedback between SAC kinases and phosphatases could, for example, amplify small decreases in kinase activity upon the binding of a few microtubules, creating a switch-like Mad1 loss initiation response which communicates attachment information over the whole kinetochore (Funabiki and Wynne, 2013; Nijenhuis et al., 2014; Saurin et al., 2011).

There are two recent models for how microtubule binding could reduce Mps1 kinase activity: a competition model where microtubules occupy Mps1 binding sites (Hiruma et al., 2015; Ji et al., 2015) and a displacement model where binding distances kinases from substrates (Aravamudhan et al., 2015; Hengeveld et al., 2017). Consistent with both models, microtubule attachment may also increase the kinetochore recruitment of phosphatases which oppose Mps1 (Sivakumar et al., 2016) and are required for SAC satisfaction (Pinsky et al., 2009; Vanoosthuyse and Hardwick, 2009). The signal amplification we observe can explain how, in a binding competition model, metaphase kinetochores with highly variable microtubule occupancy (McEwen et al., 1997) and residual Mps1 localization (Howell et al., 2004) lose Mad1. The observation that Mad1 is not re-recruited to tensionless kinetochores (Fig. 3.4) indicates biochemical (e.g. binding or conformational change) rather than force-based structural signal detection – and supports the idea that signal integration is also biochemical. In a displacement model, our data suggest that displacement does not reflect relevant changes in

48

spindle forces across an individual kinetochore, consistent with observations that changes in intra-kinetochore deformations are not themselves force-dependent (Magidson et al., 2016).

While the decision to complete Mad1 loss is switch-like (Fig. 3.2), we find that the kinetics of Mad1 removal can be tuned by the number of attached microtubules (Fig. 3.3). The Mad1 loss process, dependent on dynein stripping of its binding partner Spindly in mammals (Barisic et al., 2010; Gassmann et al., 2010; Howell et al., 2001), is likely controlled by one rate-limiting step (Kuhn and Dumont, 2017). Mad1 loss may for example slow down at weakly attached kinetochores because there are fewer dynein tracks available for stripping Mad1. While we know that dynein stripping is regulated by kinetochore protein Cenp-I (Matson and Stukenberg, 2014), how microtubule attachment controls this process is not clear. The discrepancy between the effect of kinetochore-microtubule occupancy on steady-state Mad1 localization (on-off relationship) and on Mad1 loss kinetics (gradual relationship) suggests that different signaling nodes downstream of Mps1 regulate Mad1 steady-state levels and loss kinetics. Previously, neither changing centromere tension nor increasing microtubule occupancy affected Mad1 loss rates (Kuhn and Dumont, 2017), suggesting that with more microtubules wild type kinetics are limited by dynein concentration or kinetochore biochemistry, rather than the number of microtubule tracks.

In addition to their mechanistic implications, our findings suggest how kinetochore signal arrival and processing can contribute to accurate and robust chromosome segregation. First, independent binding of kinetochore subunits to microtubules (Fig. 3.1) may help prevent reinforcement of incorrect attachments. Second, by having a low threshold occupancy for Mad1 loss (Fig. 3.2), cells may ensure that attachments rapidly and robustly turn off the kinetochore's SAC response. Because metaphase microtubule occupancy is highly variable (McEwen et al., 1997), a high microtubule threshold occupancy for Mad1 loss could lead to transient reactivation at individual bioriented kinetochores; this could result in metaphase delays and consequent DNA damage and cell death (Orth et al., 2012; Uetake and Sluder, 2010). However, low

49

occupancy at anaphase leads to increased segregation errors (Dudka et al., 2018) and a higher

probability that unstable, incorrect attachments could lose Mad1 and allow anaphase entry.

Thus, and third, slowing Mad1 loss on kinetochores with low microtubule occupancy (Fig. 3.3)

may prevent rapid Mad1 loss on transient, incorrect attachments and provide time for error

correction mechanisms to act (Tanaka et al., 2002). Looking forward, uncovering the

mechanisms determining the rate of Mad1 loss and the number of required kinetochore-

microtubules for Mad1 loss will not only reveal the basis for kinetochore signal processing, but

enable us to probe its impact on accurate and timely chromosome segregation.
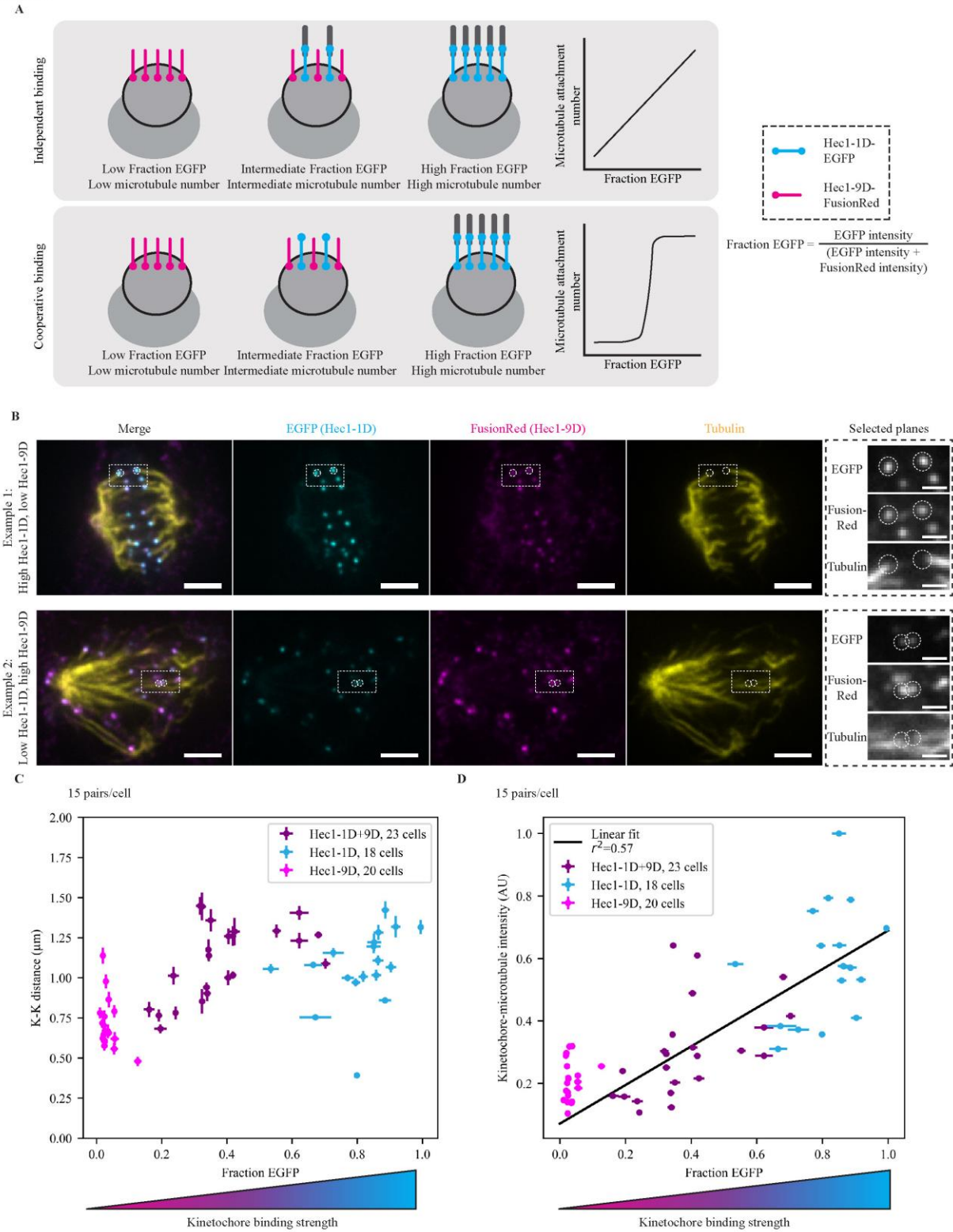
Figures and figure legends:

Figure 1

51

Figure 3.1: Kinetochore-microtubule occupancy scales linearly with the number of functional Hec1 subunits.

(A) Schematic depicting experimental design and expected outcomes. After deleting endogenous Hec1, strong (Hec1-1D, blue) and weak (Hec1-9D, pink) microtubule-binding mutants are expressed. Cells randomly receive different fractions of functional binders, and therefore have different microtubule occupancies. Depending on whether Hec1 subunits bind microtubules cooperatively or independently, microtubule attachment may change rapidly or gradually.

(B) Immunofluorescence imaging (maximum intensity projection) of microtubule attachments (tubulin), Hec1-1D intensity (anti-EGFP), and Hec1-9D intensity (anti-mKate, binds to FusionRed) in Hec1 knockout cells expressing Hec1-1D-EGFP and Hec1-9D-FusionRed. Cells were treated with 5 µM MG132 to accumulate them at a metaphase spindle steady-state. The two highlighted examples were taken from the same coverslip, where the top has a high Hec1-1D to -9D ratio and the bottom a low ratio. Scale bars=3 µm (large) and 1 µm (zoom).

(C-D) Mean of cellular EGFP fraction for each cells vs mean cellular K-K distance **(C)** and mean cellular kinetochore microtubule intensity **(D)** from Hec1 knockout cells in (B) with "mixed kinetochores" (n=345 pairs, 690 kinetochores, 23 cells; purple) and cells with control 1D-alone (n=270, 540, 18; blue) and 9D-alone coverslips (n=300, 600, 20; pink) (Fig. S3.1D). Error bars=SEM. All data displayed was acquired at the same time for all conditions and with the data in Fig. 3.2.
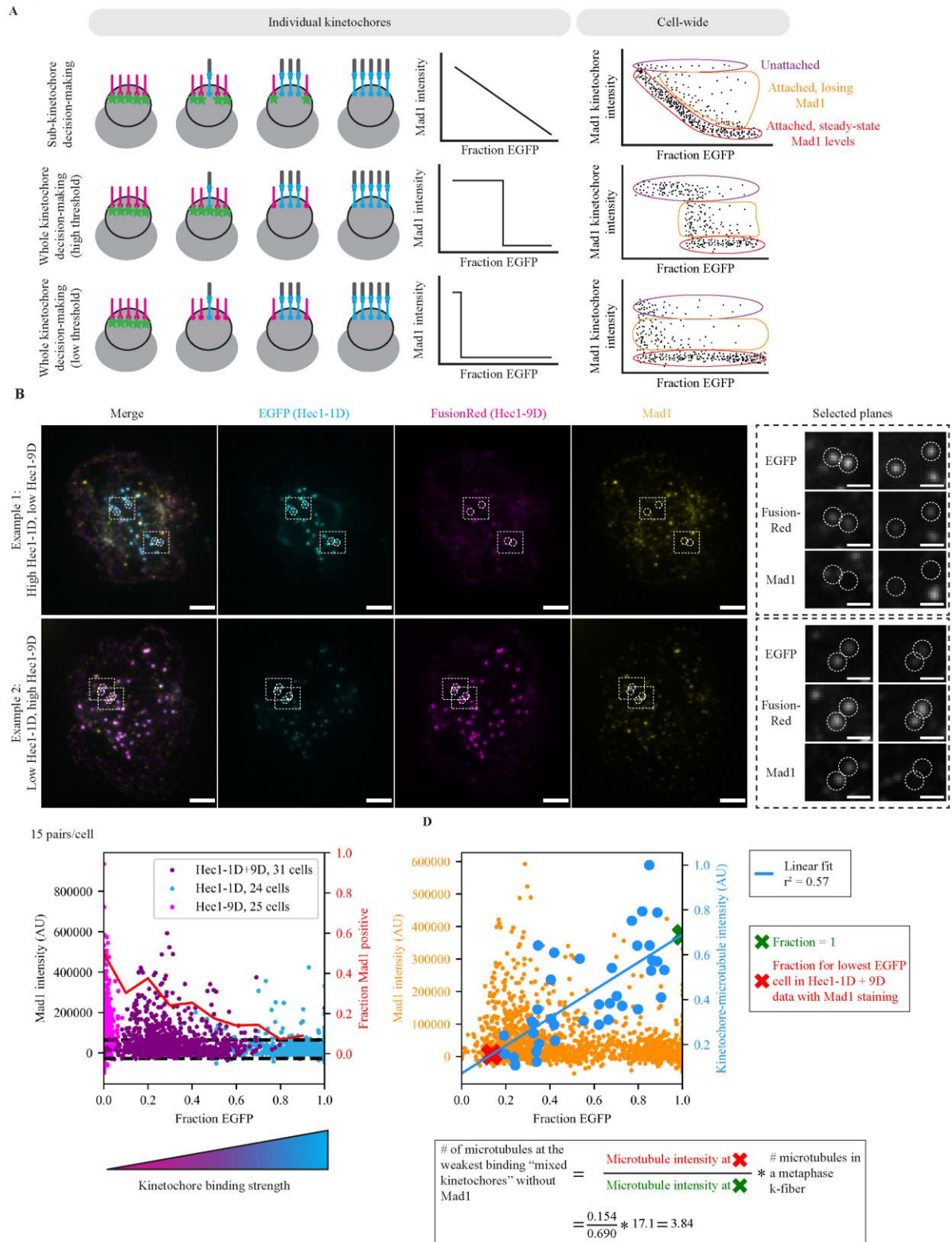
Figure 2

A

B

C 15 pairs/cell

D

$$= \frac{0.154}{0.690} * 17.1 = 3.84$$

53

Figure 3.2: The number of attached microtubules regulates steady-state Mad1 localization in a switch-like, highly sensitive manner.

(A) Schematic depicting models for kinetochore signal integration and expected outcomes. The kinetochore either processes microtubule attachments as many individual units (top) or as one single unit (switch-like) with a high (middle) or low (bottom) threshold. On the cellular scale, we expect three kinetochore populations: completely unattached (purple), attached and in the process of losing Mad1 (orange), and at attached steady-state Mad1 levels (red).
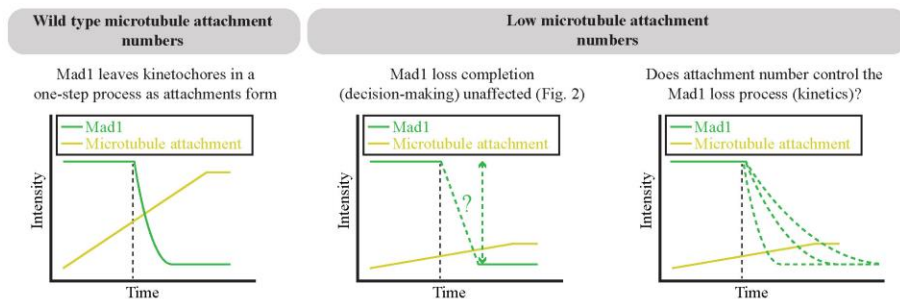
(B) Immunofluorescence imaging (maximum intensity projection) of SAC activation (Mad1), Hec1-1D intensity (anti-EGFP), and Hec1-9D intensity (anti-mKate, binds to FusionRed) in Hec1 knockout cells expressing both Hec1-1D-EGFP and Hec1-9D-FusionRed. Cells were treated with 5 μM MG132 to accumulate them at a metaphase spindle steady-state. The two examples are cells on the same coverslip where the top has a high Hec1-1D to -9D ratio and the bottom a low ratio. Kinetochores in both conditions are capable of recruiting (left zoom) and losing (right zoom) Mad1. Scale bars=3 μm (large) and 1 μm (zoom).

(C) Fraction EGFP vs Mad1 intensity from "mixed kinetochore" cells in (B) (n=930 kinetochores, 31 cells; purple) and cells with control 1D- (n=720, 24; blue) and 9D- (n=750, 25; pink) alone (Fig. S3.2C). Red line indicates the fraction of kinetochores with Mad1 intensities one standard deviation (dashed black lines) greater than average Mad1 intensity on Hec1-1D kinetochores.

(D) Fraction EGFP vs Mad1 intensity (B-C) or average end-on attached microtubule numbers (Fig. 3.1B-D) for Hec1-1D, and Hec1-1D + Hec1-9D conditions. Blue line indicates linear fit for fraction EGFP vs kinetochore-microtubule intensity (r^2=0.57, p=10^{-8}). X's indicate the points along the fit used for the calculation of attached microtubule number (red = average fraction EGFP for the lowest fraction EGFP cell in "mixed kinetochores" in which some kinetochores are Mad1-negative, green = fraction EGFP of 1). Calculation of the number of microtubules at the weakest binding "mixed kinetochores" without Mad1 uses the average number of microtubules in a metaphase k-fiber from Wendell et al., 1993 (see methods). All data displayed was acquired at the same time for all conditions and with the data in Fig. 3.1. Alternative estimation methods lead to similar estimates (Fig. S3.2B).

54

Figure 3

A

| Wild type microtubule attachment numbers | Low microtubule attachment numbers | |

Mad1 leaves kinetochores in a one-step process as attachments form

Mad1 loss completion (decision-making) unaffected (Fig. 2)

Does attachment number control the Mad1 loss process (kinetics)?

B

C

D

E

From (B)
Hec1-9D (n=46 kinetochores, 22 cells)
$I=I_o*2^{-4/79s}$ ($R^2=0.87$)
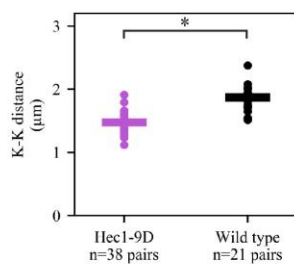Wild type (n=21 kinetochores, 14 cells)
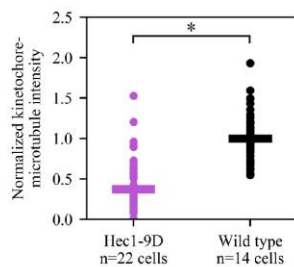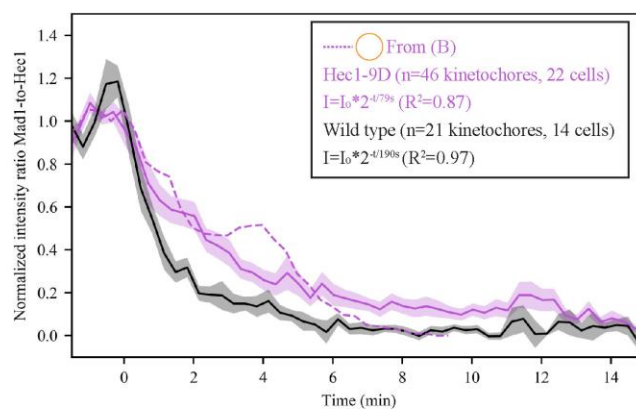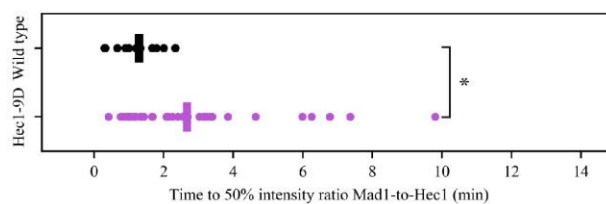$I=I_o*2^{-4/190s}$ ($R^2=0.97$)

F

55

Figure 3.3: Lowering microtubule occupancy at a kinetochore slows down the process of Mad1 loss.

(A) Schematic of how the number of attached microtubules could influence two different properties of Mad1 loss: the decision to complete loss and the speed of loss.

(B) Timelapse imaging (maximum intensity projection) of representative Mad1 loss kinetics (EYFP-Mad1) and microtubule attachment (SiR-Tubulin) in a Hec1-RNAi PtK2 cell with decreased kinetochore-microtubule affinity (Hec1-9D-FusionRed). Scale bars=3 μm (large) and 1 μm (zoom), and t=0 indicates the start of Mad1 loss on the orange-circled kinetochore.

(C) Individual (circles) and average (lines) K-K distance in wild type (n=21 pairs) and Hec1-9D (n=38) cells. K-K distance is reduced in Hec1-9D vs wild type cells.

(D) Individual (circles) and average (lines) kinetochore-microtubule intensity normalized to cellular astral microtubule intensity in Hec1-9D (n=22 cells) and wild type cells (n=14 cells). Kinetochore microtubule intensity is reduced in Hec1-9D cells vs wild type cells.

(E-F) Mean, SEM, and individual trace **(E)** of the orange-circled kinetochore in (B) of the Mad1-to-Hec1 intensity ratio with t=0 being the Mad1 loss start, and **(F)** distribution of times to reach a 50% intensity ratio of initial Mad1-to-Hec1, in wild type (n=21 kinetochores) and in Hec1-9D-expressing (n=46) cells. Reducing steady-microtubule occupancy lowers Mad1 loss rates. Wild type data taken from Kuhn and Dumont 2017, JCB and acquired in a parallel experiment (*; p<0.005, 2-sided Mann-Whitney U test).

Figure 4
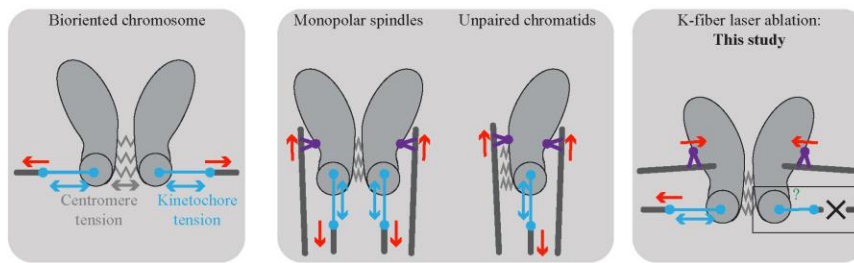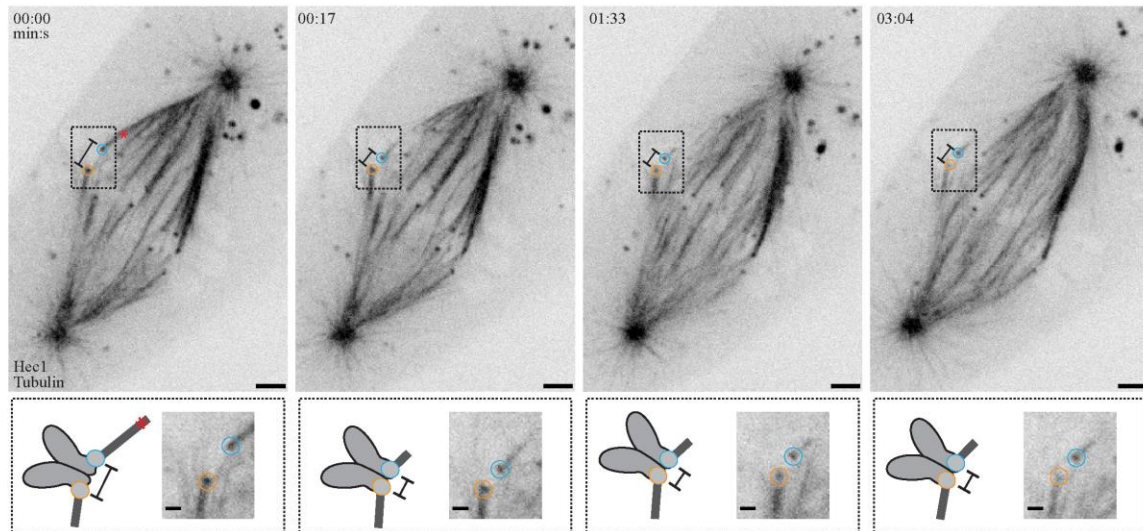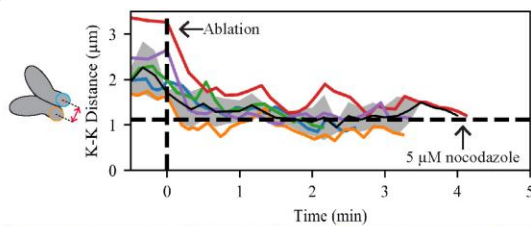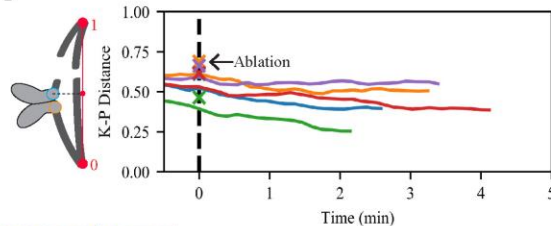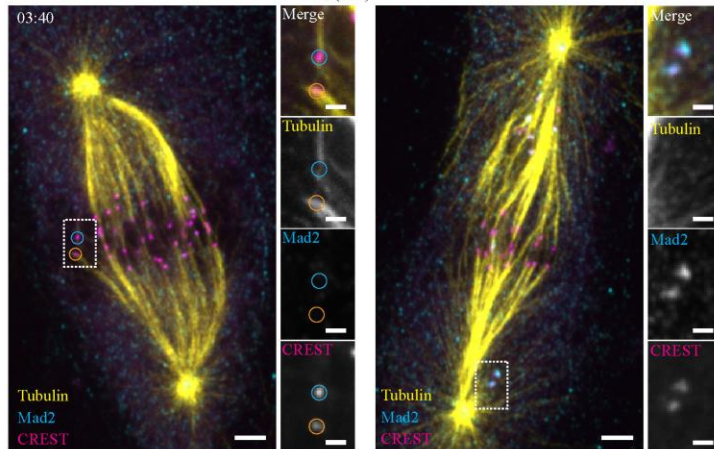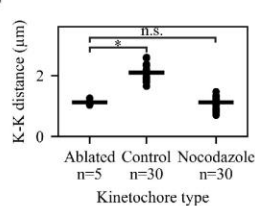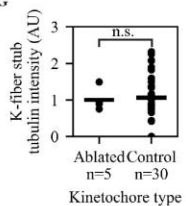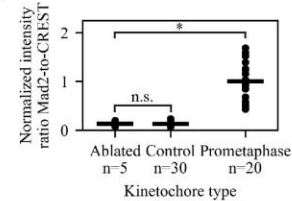
Figure 3.4: The mammalian SAC does not detect changes in spindle pulling forces at individual kinetochores.

(A) Schematic of different spatial arrangements used to probe the role of tension in the SAC. After biorientation, both centromere and kinetochore are under force (left). Preventing biorientation in monopolar or MUG spindles removes force (red) across the centromere but force (red) can still be generated across the kinetochore through polar ejection forces generated by chromokinesins (purple) (middle). By removing pulling force using laser ablation ('X'), force can in principle neither be generated across the centromere nor kinetochore.

(B) Timelapse imaging) of microtubule attachments (EGFP-tubulin) and kinetochores (Hec1-EGFP) in a metaphase PtK2 cell under Hec1 RNAi + partial NuMA RNAi during the mechanical isolation of the highlighted k-fiber (circles) using laser ablation (red X, t=0). Bottom: schematic and zoom of highlighted pair. Scale bars=3 µm (large) and 1 µm (zoom).

(C) Mean, SEM, and individual K-K distance of pairs before and after ablation (time of fixation is approximately 30 s from the end of trace). Vertical dashed line marks first ablation. Horizontal dashed line marks the average K-K distance in 5 µM nocodazole (n=30 kinetochores). Example in (B) is the purple trace.

(D) Normalized distance along the pole-to-pole axis for disconnected kinetochores before and after ablation. Dashed line marks first ablation, and X's indicate ablation position. Example in (B) is the purple trace.

(E) Immunofluorescence imaging (maximum intensity projection) of microtubule attachment (tubulin), kinetochores (CREST), and SAC activation (Mad2) at (top) the cell in (B) and (bottom) a prometaphase cell on the same dish at approximately t=3:40. Scale bars=3 µm (large) and 1 µm (zoom).

(F-H) Individual (circles) and average (lines) **(F)** K-K distance, **(G)** k-fiber intensity, and **(H)** SAC activation (Mad2/CREST, normalized to prometaphase intensity) at 'ablated' kinetochores (n=5), same-cell controls without ablation (n=30), and prometaphase cells on the same dish (n=20). There is no SAC activation and no change in attachment intensity on sister kinetochores attached to an ablated k-fiber and ablation reduces K-K distance to a value similar to that in nocodazole (p=0.40).
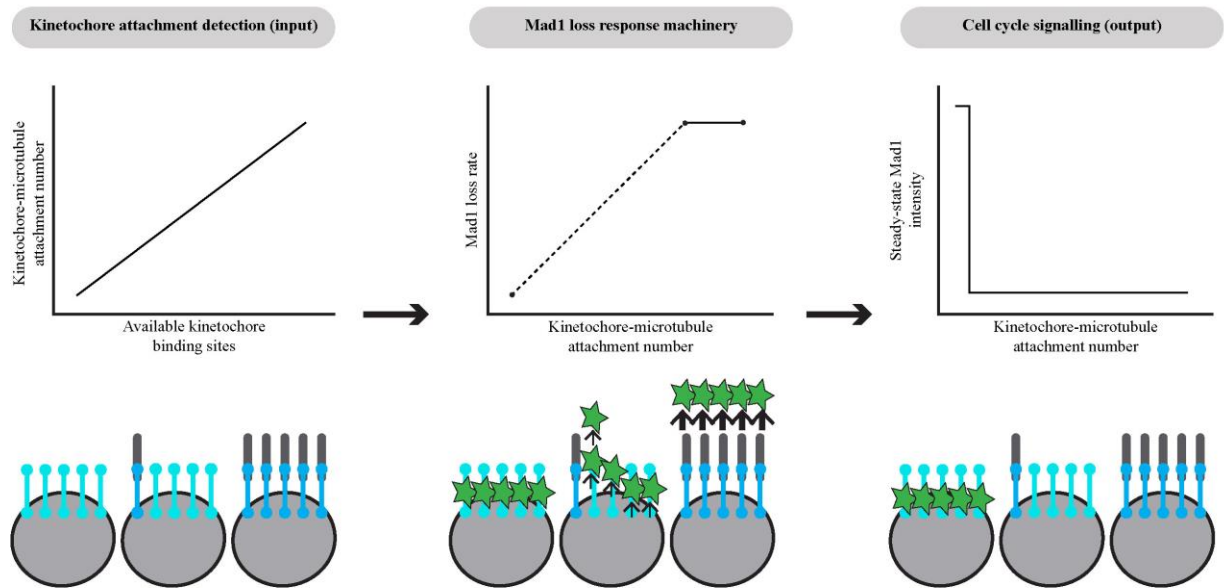
Figure 3.5: The mammalian kinetochore integrates attachment input signals in a sensitive and switch-like manner.

Microtubules bind kinetochore attachment subunits independently rather than cooperatively, leading to a wide range of kinetochore-microtubule attachment numbers (left) (Fig. 3.1). The speed of this response, the loss of Mad1, is sensitive to the number of microtubules attached (middle): Mad1 loss rates are slow at weakly attached kinetochores (Fig. 3.3), and reach a maximum at kinetochores with wild type attachment numbers (Kuhn and Dumont, 2017). However, kinetochores with very low microtubule occupancy are still capable of fully removing Mad1 (Fig. 3.2), resulting in a decision-making process that is highly sensitive and switch-like (right). The combination of switch-like decision-making and a tunable response rate is well-suited to allow cells to rapidly exit mitosis while preventing errors.

Supplemental figures and legends:
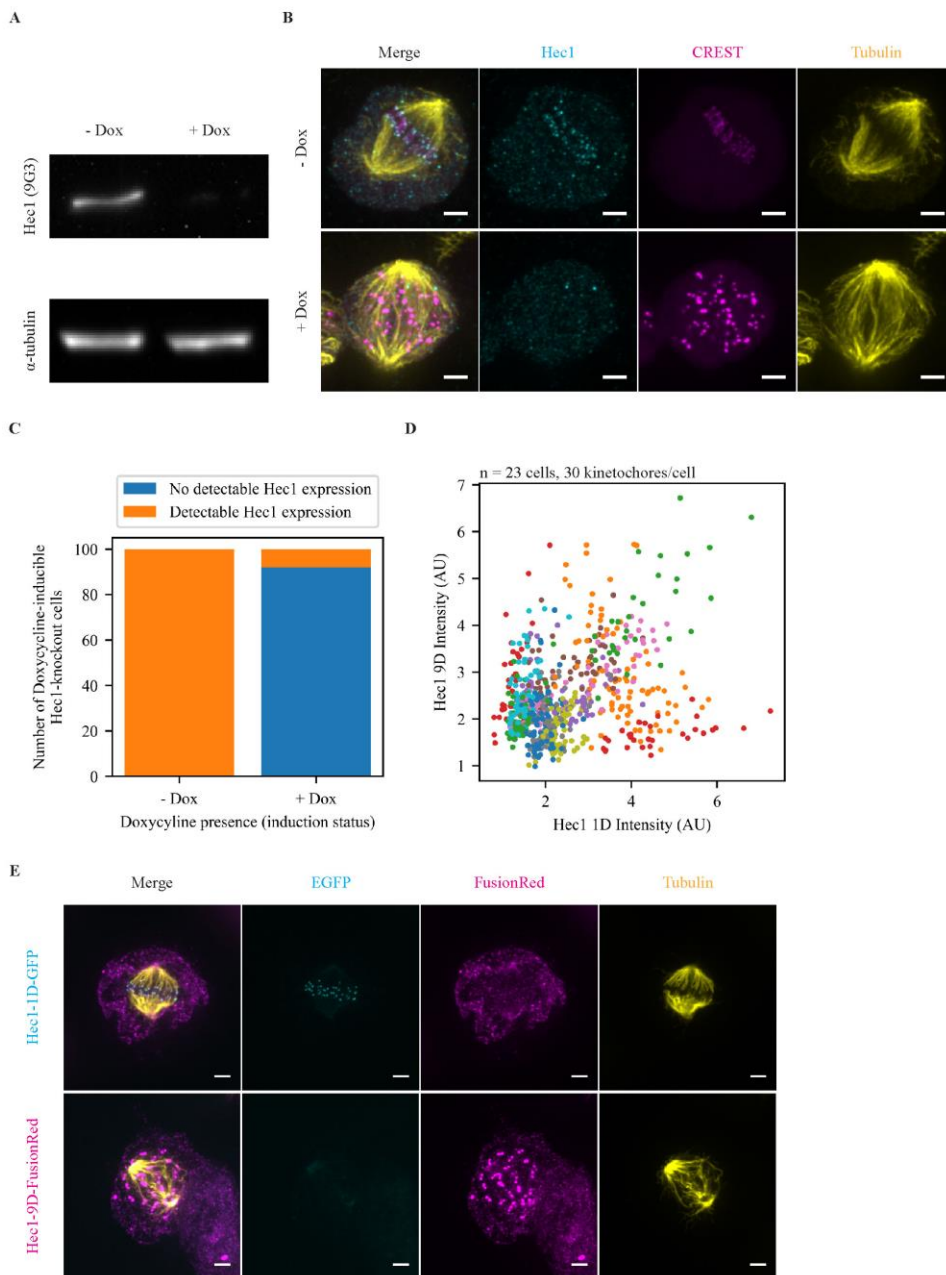
Figure S1

Figure S3.1: Hec1-1D, but not 9D, rescues spindle defects after Hec1 depletion; related to Fig. 3.1.

(A) Western blot of Hec1 and tubulin abundance in cells with a stably-expressed doxycycline-inducible Cas9 and Hec1 sgRNA (McKinley and Cheeseman, 2017).

(B) Immunofluorescence imaging (maximum intensity projection) of microtubules (tubulin), kinetochores (CREST) and Hec1 intensity in + and -dox Hec1 knockout cells. Scale bars=3 μm.

60

(C) Hec1 depletion quantified by immunofluorescence of mitotic cells with or without doxycycline fixed after 1 hour of 5 μM MG132 treatment to prevent premature anaphase onset in Hec1-depleted cells. 92/100 induced cells exhibited no detectable Hec1 kinetochore localization.

(D) Hec1-1D-EGFP and Hec1-9D-FusionRed intensity at individual kinetochores in Hec1-depleted cells expressing both mutants. Colors indicate different cells (n=23 cells, with 30 kinetochores/cell). The variation between cells is far higher that variation within cells (F = 175, p = 10^{-220} for EGFP, F = 59, p = 10^{-139} for Fusion Red, One-Way ANOVA).

(E) Immunofluorescence imaging (maximum intensity projection) of microtubule attachments (tubulin), Hec1-1D intensity (anti-EGFP), and Hec1-9D intensity (anti-mKate, binds to FusionRed) in Hec1 knockout +dox cells expressing Hec1-1D-EGFP of Hec1-9D-FusionRed. Cells were treated with 5 μM MG132 to accumulate cells at a metaphase spindle steady-state. Hec1-1D expression, but not -9D, rescues the spindle structure defects in (B).

A

	Merge	EGFP	FusionRed	Mad1	Selected planes
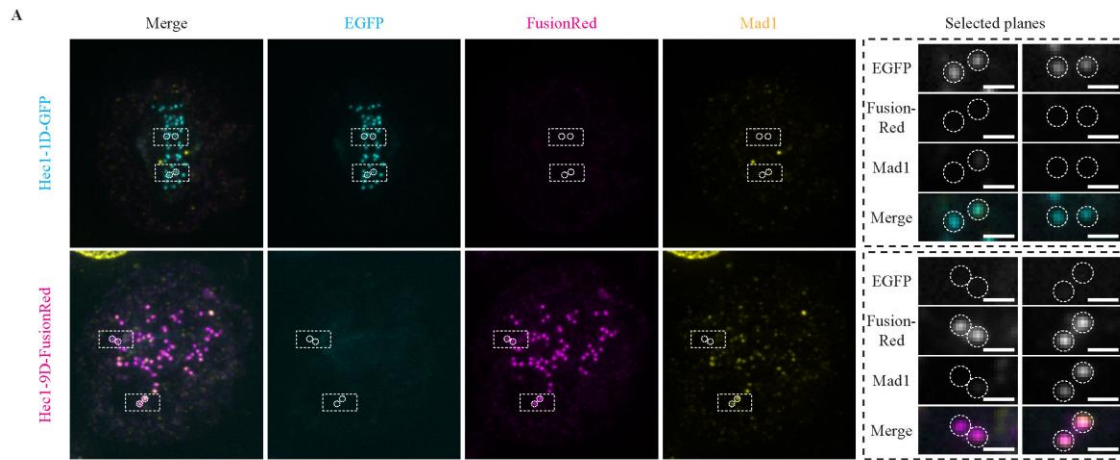
B

Method of tubulin calculation	Wild type attachment source ("high") (X in Fig. 2D)	Low attachment source ("low") (X in Fig. 2D)	% of wild type number of attached microtubules (low/high)	Number of microtubules at the weakest binding kinetochores without Mad1 (% * 17.1)
Plugging in fraction EGFP to linear fit	Fraction EGFP = 1	Fraction EGFP = lowest cellular average in Hec1-1D + Hec1-9D population, Fig. 2C	22.4%	3.84
Plugging in fraction EGFP to linear fit	Fraction EGFP = average of whole Hec1-1D population, Fig. 2C	Fraction EGFP = lowest cellular average in Hec1-1D + Hec1-9D population, Fig. 2C	24.9%	4.26
Plugging in fraction EGFP to linear fit	Fraction EGFP = average of whole Hec1-1D population, Fig. 2C	Fraction EGFP = average of whole Hec1-9D population, Fig. 2C	12.5%	2.14

Figure S3.2: Hec1-1D, but not 9D, allows for robust Mad1 loss after Hec1 depletion; related to Fig. 3.2.

(A) Immunofluorescence imaging (maximum intensity projection) of SAC activation (Mad1), Hec1-1D intensity (anti-EGFP), and Hec1-9D-FusionRed intensity (anti-mKate, binds to FusionRed) in Hec1 knockout cells expressing Hec1-1D-EGFP or Hec1-9D-FusionRed. Cells were treated with 5 µM MG132 to accumulate cells at a metaphase spindle steady-state. Hec1-1D expression, but not -9D, allows Mad1 loss to undetectable levels on most kinetochores. Some kinetochores in Hec1-9D-expressing cells are capable of losing Mad1. Scale bars=3 µm (large) and 1 µm (zoom).
(B) Table displaying different possible assumptions for choosing the parameters to estimate the number of microtubules at the weakest binding kinetochores without Mad1. Varied parameters include where the wild type ("high") and minimum ("low") attachment quantities are set. The first parameter set is identical to Fig. 3.2D. While these assumptions produce slightly different values, they are all significantly lower than previous estimates and likely represent a maximum, not a minimum, threshold value.
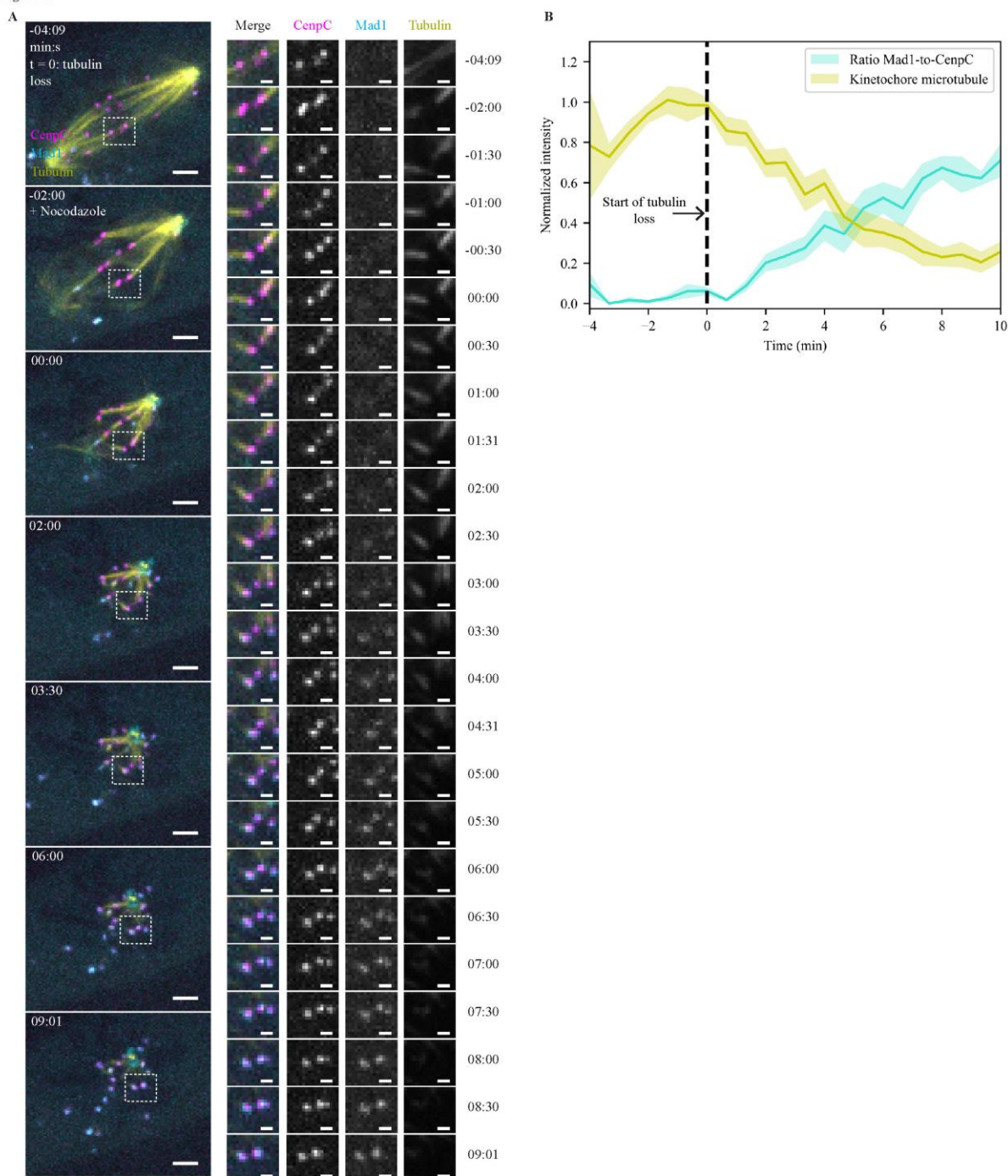
Figure S3.3: Mad1 re-recruitment is associated with microtubule loss; related to Fig. 3.4.

(A) Timelapse imaging (maximum intensity projection) of representative SAC activation kinetics (EYFP-Mad1) and microtubule attachment (SiR-Tubulin) on kinetochores (CenpC-mCherry) in PtK2 cells after treatment with 10 μM nocodazole. Nocodazole addition does not immediately depolymerize microtubule attachments. Mad1 is re-recruited on individual kinetochores rapidly only once attachments start to disappear at t=0. Scale bars=3 μm (large) and 1 μm (zoom).

(B) Mean and SEM of kinetochore-microtubule attachment intensity and Mad1-to-CenpC ratio at kinetochores in nocodazole-treated cells. Mad1 starts to re-localize to kinetochores only once tubulin depolymerizes, and it does so rapidly (<1 min) (n= 3 cells, 8 kinetochores).

Materials and methods:

Cell culture and transfection:

PtK2 EYFP-Mad1 (Shah et al., 2004) (gift from Jagesh Shah) and wild type cells were cultured in MEM (Thermo Fisher, Waltham, MA) supplemented with sodium pyruvate (11360; Thermo Fisher), nonessential amino acids (11140; Thermo Fisher), penicillin/streptomycin, and 10% heat-inactivated fetal bovine serum (FBS) (10438; Thermo Fisher). Tet-on inducible CRISPR-Cas9 HeLa cells (Hec1 knockout cells, gift from Iain Cheeseman, Whitehead Institute) were cultured in DMEM/F12 with GlutaMAX (10565018; Thermo Fisher) supplemented with penicillin/streptomycin, 5 µg/mL puromycin, and tetracycline-screened FBS (SH30070.03T; Hyclone Labs, Logan, UT). Cas9 expression was induced by the addition of 1 µM doxycycline hyclate 48 hr before fixation. Knockout was confirmed by Western Blot and the accumulation of mitotic cells after doxycycline addition. Cell lines were not STR-profiled for authentication. All cell lines tested negative for mycoplasma. Cells were maintained at 37°C and 5% CO_2. For imaging, cells were plated on 35 mm #1.5 glass-bottom dishes (poly-d-lysine coated, MatTek, Ashland, MA; Fig. 3.3, Fig. S3.3), 25 mm # 1.5 glass etched coverslips (acid cleaned and poly-L-lysine coated; G490; ProSciTech, Kirwan, AUS; Fig. 3.1), or 25 mm # 1.5 glass coverslips (acid cleaned and poly-L-lysine coated; 0117650; Marienfeld, Lauda-Königshofen, DEU; Fig. 3.1, 3.2, S3.1, S3.2). Cells were transfected with EGFP-Tubulin (Clontech, Mountain View, CA, discontinued), Hec1-WT-EGFP (gift from Jennifer DeLuca, Colorado State University), mCherry-CenpC (gift from Aaron Straight, Stanford University), Hec1-8AS8D-EGFP (1D-EGFP; gift from J. DeLuca, Colorado State University), and Hec1-9D-FusionRed (FusionRed (gift from Michael Davidson) was swapped for EGFP in Hec1-9D-EGFP (gift from Jennifer DeLuca, Colorado State University)) using ViaFect (E4981; Promega, Madison, WI) 48 hr (HeLa) or 72 hr (PtK2) before imaging. For siRNA knockdown, cells were treated with 100 nM siRNA oligos (Sigma-Aldrich, St. Louis, MO) and 4 µl oligofectamine (12252011; Thermo Fisher) either 24 hr (Fig.

65

3.3) or 6 hr (Fig. 3.4) after transfection (66 or 48 hr before imaging, respectively). The following

oligos were used: siNuMA: 5′-GCATAAAGCGGAGACUAAA-3′ (Elting et al., 2017); siHec1 5'-

AATGAGCCGAATCGTCTAATA-3' (Guimaraes et al., 2008).

Immunofluorescence:

For "ablate and fix" experiments (Fig. 3.4) and Hec1 knockout confirmation (Fig. S3.1),

cells were fixed in 95% methanol + 5 mM EGTA for 1 min on ice. Cells were then blocked at

room temperature for 1.5 hr in TBST (50 mM Tris, 150 mM NaCl, 0.05% Triton X100, pH 7.6) +

2% BSA. Primary and secondary antibody incubations were done in blocking solution for 1 hr

and 30 min, respectively. Between each step, 4-5 washes in TBST were performed. For "mixed

kinetochore" immunofluorescence (Fig. 3.1, 3.2, S3.1, S3.2), cells were pre-extracted in PHEM

(120 mM PIPES, 50 mM HEPES, 20 mM EGTA, 4 mM Magnesium Acetate, pH 7) + 1% Triton

X-100 for 20 s then fixed for 15 min in PHEM + 4% PFA (freshly dissolved from powder) at

37ºC. Cells were then permeabilized in PHEM + 0.5% IGEPAL-CA-630 for 10 min and blocked

in PHEM + 0.05% Triton X-100 + 2% BSA for 1 hr at room temperature. Both the primary and

secondary antibody incubations were done in block solution at 37º for 1 hr. Between each step

(excluding pre-extraction), 4-5 min washes in PHEM + 0.05% Triton X-100 were performed;

PFA staining protocol adapted from (Suzuki et al., 2018). For all experiments, cells were

mounted in ProLong Gold (P10144; Thermo Fisher) and stored in the dark at 4 ºC. The following

antibodies were used: mouse anti-α-tubulin DM1 (1:1,000; T6199; Sigma-Aldrich), human anti-

centromere (CREST; 1:25; discontinued; Antibodies Inc., Davis, CA), rabbit anti-rat kangaroo-

Mad2 (DeLuca et al., 2018; Kuhn and Dumont, 2017) (1:100), mouse anti-Hec1 (9G3; 1:100,

ab3613; Abcam), rabbit anti-mKate (recognizes FusionRed) (1:200; TA150072; OriGene,

Rockville, MD), mouse anti-hsMad1 (1:300; MABE867; EMD-Millipore, Burlington, MA), rabbit

anti-alpha-tubulin (1:200; ab18251; Abcam, Cambridge, UK), camel anti-EGFP conjugated to

Atto488 (1:100; added during secondary; gba-488; ChromoTek, Hauppauge, NY), anti-mouse

66

secondary antibodies (1:500) conjugated to Alexa-488 (A11001; Invitrogen, Carlsbad, CA) or Alexa-647 (A21236; Invitrogen), anti-rabbit secondary antibodies (1:500) conjugated to Alexa-488 (A11008; Invitrogen), Alexa-568 (A11011; Invitrogen) or Alexa-647 (A21244; Invitrogen), and a human secondary antibody conjugated to DyLight 405 (1:100; 109-475-098; Jackson ImmunoResearch Laboratories, West Grove, PA).

Drug and dye treatments:

To depolymerize spindle microtubules (Fig. S3.3), 5 µM nocodazole (M1404; Sigma-Aldrich) was added 10 min prior to fixation (Fig. 3.4) or 10 µM was added at the indicated time (Fig. S3.3). To prevent anaphase onset (Fig. 3.1, 3.2, S3.1, S3.2) cells were treated with 5 µM MG132 (474790; EMD-Millipore) 1 hr prior to fixation. To visualize tubulin as a third color (Fig. 3.3), 100 nM SiR-Tubulin dye (cy-sc002; Cytoskeleton, Inc., Denver, CO) was added 1 hr prior to imaging, along with 10 µM verapamil (V4629; Sigma-Aldrich) to prevent dye efflux.

Imaging:

Microscope settings: All imaging was performed on an inverted (Eclipse Ti-E; Nikon, Tokyo, JPN), spinning disk confocal (CSU-X1; Yokogawa Electric Corporation, Tokyo, JPN) microscope. Single color live imaging (Fig. 3.4) was performed with a Di01-T488-13x15x0.5 (Semrock, Lake Forest, IL) head dichroic along with a 488 nm (120 mW) diode laser, an ET500LP emission filter (Chroma, Bellows Falls, VT), and an iXon3 camera (Andor Technology, Belfast, UK; bin=1, 105 nm/pixel). For these experiments, cells were imaged in phase contrast (400 ms exposure) and fluorescence (60 ms exposure) in 3 z-planes spaced 700 nm apart every 7.5-15 s with a 100× 1.45 Ph3 oil objective through a 1.5× lens with 5x pre-amplifier gain and no EM gain (Metamorph 7.7.8.0; Molecular Devices, San Jose, CA).

Three-color live imaging (Fig 3.3, S3.3) was performed with a Di01-T405/488/568/647 head dichroic (Semrock) instead, along with 561 nm (150 mW) and 642 nm (100 mW) diode

lasers and different emission filters (ET525/50M, ET630/75M, and ET690/50M; Chroma). Cells were imaged by phase contrast (200 ms exposure) and fluorescence (40-75 ms exposure) in four z-planes spaced 350 nm apart every 13-30 s and at bin=2 (to improve imaging contrast for dim Mad1 and microtubule structures; 210 nm/pixel). All live PtK2 cells were imaged at 30 °C, 5% CO_2 in a closed, humidity-controlled Tokai Hit (Fujinomiya, JPN) PLAM chamber.

For fixed cell imaging (Fig. 3.1, 3.2, 3.4, S3.1, S3.2) a 405 nm (100 mW) laser was added along with an ET455/50M emission filter (Chroma) and two emission filters were changed to ET525/36M and ET600/50M (Chroma). Cell images were acquired in z-slices 300 nm apart with bin=1 and laser powers, exposure times, and EM Gain optimized (but not changed between cells) to fill as much of the dynamic range of the camera as possible without saturation. For mixed kinetochore experiments (Fig. 3.1, 3.2), all acquisition settings for EGFP and FusionRed were kept identical. To assess the efficiency of Hec1 knockout in Hec1 knockout cells (Fig. S3.1), we fixed cells stained for Hec1, kinetochores, and microtubules were assessed visually using these same imaging conditions.

Ablation Protocol: Laser ablation (20 3-ns pulses at 20Hz) with 551nm light was performed using the MicroPoint Laser System (Photonic Instruments, Belfast, UK). Images were acquired more slowly prior to ablation and then acquired more rapidly after ablation (typically 7.5 s prior and 15 s after). Successful k-fiber ablation was verified by loss of tension across the centromere (Fig. 3.1). To prevent k-fiber reincorporation into the spindle (Elting et al., 2014; Sikirzhytski et al., 2014), the spindle area around the k-fiber was also ablated concurrently and the minus-end of the k-fiber was re-ablated periodically prior to fixation.

Cell selection: For laser ablation (Fig. 3.4), metaphase cells with minor pole-focusing defects and wavy spindle morphology, indicative of partial NuMA knockdown, and visible Hec1-EGFP expression were chosen. In addition, Hec1 knockdown was confirmed by the lack of k-fibers and irregular motion of chromosomes in EGFP-negative cells. For imaging Mad1 loss (Fig. 3.3), prometaphase cells with moderate Mad1-EFYP expression, high Hec1-9D-FusionRed

68

expression, and low average K-K distances (to indicate lack of strong attachments) were chosen. Hec1 knockdown was confirmed by the lack of k-fibers and irregular motion of chromosomes in FusionRed-negative cells.

Data Analysis:

Tracking and feature identification: For live ablation experiments (Fig. 3.4), kinetochores (Hec1-EGFP) and poles (EGFP-tubulin) were tracked by hand using a custom-made Matlab (Mathworks, Natick, MA) GUI (available here: https://github.com/DumontLab/Image-Analysis-Gui). Pairs were then included in further analysis if they exhibited prolonged decrease in K-K distance after ablation. For nocodazole addition experiments (Fig. S3.3), kinetochores (CenpC-mCherry) and k-fibers (SiR-tubulin) were tracked by hand in a custom Matlab GUI using the plane of brightest CenpC intensity (for kinetochores) or SiR-tubulin (for k-fibers). For live imaging of Mad1 intensity (Fig. 3.2), kinetochores were tracked as previously (Kuhn and Dumont, 2017), using Matlab program SpeckleTracker (Wan et al., 2012b). For analysis of fixed images (Fig. 3.1, 3.2, 3.4, S3.1, S3.2), kinetochores were identified by hand in a custom Matlab GUI using the plane of brightest Hec1 or CREST intensity and K-fibers were identified as bundles of tubulin intensity (where applicable).

Intensity measurements: Fixed kinetochore intensities (Fig. 3.1, 3.2, 3.4, S3.1, S3.2) were measured in Matlab by summing pixel intensities in a 7x7 (0.73x0.73 µm) box centered at the indicated coordinate. To calculate the Mad2/CREST ratio (Fig. 3.4) and Mad1 kinetochore intensity (Fig. 3.2), intensities were background-corrected by dividing (Fig. 3.4) or subtracting (Fig. 3.2) the kinetochore intensity by the average of three background intensities. To calculate the fraction EGFP (Fig. 3.1, 3.2), the kinetochore EGFP intensity (background subtracted) was divided by the sum of the kinetochore EGFP and FusionRed intensity (both background subtracted). To avoid negative numbers, corrected intensities less than zero were recorded as zero. To calculate tubulin intensity on a given kinetochore, two 0.5 µm long intensity linescans

69

were taken for each kinetochore: one (Tub_{in}) perpendicular to the kinetochore-kinetochore axis 0.25 µm away from the kinetochore towards its sister, and one (Tub_{out}) perpendicular to the kinetochore-microtubule axis 0.25 µm away from the kinetochore towards the microtubule. The microtubule attachment intensity is the difference between Tub_{out} and Tub_{in}. To account for variance in staining between coverslips, all tubulin intensities were normalized to the intensity of a 7x7 pixel box centered on the spindle pole.

To determine Mad1 loss rates (Fig. 3.3), we measured EYFP-Mad1 and FusionRed-Hec1-9D intensities at each timepoint following a protocol identical to the one used to measure Mad1 loss rates previously (Kuhn and Dumont, 2017). In short, movies were thresholded by setting to zero all pixels <2 standard deviations above image background at the first frame. For each time point, the intensities of all pixels in a 5x5 pixel (1.05x1.05 µm) box around the kinetochore were summed together over all planes. We do not detect significant bleaching over the course of the movie. t=0 was set to the time for each kinetochore where Mad1 intensity started decreasing while Hec1 intensity stayed constant, and intensities were normalized to the average intensity for t=-100 to t=0 (Kuhn and Dumont, 2017). To determine the relative microtubule attachment intensity in Hec-1-9D and wild type cells, two points were placed along k-fibers and astral microtubules in these same cells using a custom Matlab GUI, and then a 1 µm intensity linescan was taken perpendicular to a line between these two points. To correct for background, a similar linescan was drawn in the cell periphery and subtracted from both values. To normalize for different cellular SiR-tubulin levels, all k-fiber intensities in a cell were normalized to an average cellular astral microtubule intensity.

To determine Mad1 accumulation timing relative to kinetochore-microtubule attachment loss after nocodazole addition (Fig. S3.3A-B), we measured EYFP-Mad1 and CenpC-mCherry at every timepoint by summing all pixel intensities across all planes in a 5x5 pixel (1.05x1.05 µm) box centered at the indicated kinetochore coordinate. To measure k-fiber intensity, an intensity linescan was taken along a 1 µm line perpendicular to a line drawn between the

70

kinetochore coordinate and its corresponding k-fiber coordinate, 1 μm away from the

kinetochore. t=0 was set to the time for each kinetochore where k-fiber intensity started

decreasing, and intensities were normalized to the average intensity for t=-100 to t=0. All code

used in intensity calculations available at https://github.com/JonAKuhn/Mitosis-intensity-

measurements and https://github.com/DumontLab/Image-Analysis-Gui.

Statistics: Data are expressed as mean ± SEM. Calculations of p-Values (Mann-Whitney U and

one-way ANOVA) and correlation coefficients (Spearman rank-order) were done using Scipy

and Numpy Python modules. To calculate the relationship between the fraction EGFP and the

number of attached microtubules, a linear regression (least-squares) was applied to the data

using Scipy. The lower limit of fraction of a metaphase attachment is calculated as the ratio

between attachment numbers at the lowest average fraction EGFP cell with Mad1-negative

kinetochores in the mixed population from Fig. 3.2 and the attachment number at fraction

EGFP=1. Alternative calculations (Fig. S3.2) instead used the average fraction EGFP in the

Hec1-1D-alone population for the denominator or the average fraction EGFP in the Hec1-9D-

alone population for the numerator. Sample sizes were determined by the number of cells that

fulfilled listed criteria out of an initial dataset (Fig. 3.3, 4) or by the number of detectably

expressing cells on a coverslip (Fig. 3.1, 3.2).

Acknowledgements:

Chapter 4: Imaging and physically probing kinetochores in live dividing cells

Abstract

The kinetochore mediates chromosome segregation at cell division. It is the macromolecular machine that links chromosomes to spindle microtubules, and is made of more than 100 protein species in mammalian cells. Molecular tools are presently revealing the biochemical interactions and regulatory mechanisms that ensure proper kinetochore function. Here, we discuss two approaches for imaging and physically probing kinetochores despite mitotic cell rounding and rapid kinetochore dynamics. First, we describe how mild spindle compression can improve kinetochore imaging, and how stronger compression can mechanically perturb the spindle and kinetochores. Second, we describe how simultaneously imaging two-colored kinetochore reporter probes at sub-pixel resolution can report on kinetochore structural dynamics under cellular forces. We hope that the experimental details we provide here will make these two approaches broadly accessible and help move forward our understanding of kinetochore function – and make these approaches adaptable to the study of other cellular structures.

Introduction:

The kinetochore:

During cell division, the two daughter cells must inherit exactly one copy of each chromosome. Errors can lead to cell death or cancer in somatic cells or developmental disorders in the germline. Chromosome segregation is mediated by the kinetochore, a 100nm-sized macromolecular machine that anchors chromosomes to microtubules in the spindle. The kinetochore regulates chromosome segregation and generates forces for chromosome movement. We now know most of the proteins that make up the kinetochore – more than 100 of them in mammalian cells (Cheeseman and Desai, 2008) – and are currently uncovering the kinetochore's underlying biochemical interactions and regulatory mechanisms. In parallel, we have begun to elucidate how kinetochores generate and respond to mechanical force.

74

Mechanical forces assemble the spindle (Karsenti and Vernos, 2001), move chromosomes within it (Nicklas, 1983), and stabilize and correct kinetochore-microtubule attachments (Nicklas and Koch, 1969). Force has also been proposed to regulate chromosome segregation (Li and Nicklas, 1995). To understand how kinetochores generate and respond to force, we need approaches for imaging kinetochore movement and structural dynamics under different forces, and externally perturbing mechanical forces. Here we focus on two such approaches that are conceptually simple and can be applied to live mammalian cells.

Mammalian cells – challenges:

While there are many powerful genetic and biochemical techniques available in mammalian cells, the fact that mammalian cells round up at mitosis and that kinetochores are located deep within the cell make imaging and mechanical perturbations based on physical contact (such as with microneedles) difficult. In addition, kinetochores move rapidly, often in and out of a chosen focal plane over time, making it difficult to follow the movement of individual kinetochores over long periods. Kinetochores can also change their tilt angles with respect to the coverslip over time, confounding attempts to image molecular-scale rearrangements within kinetochores.

Chapter overview:

In this chapter we first describe a simple approach utilizing an agarose pad and micromanipulator for compressing dividing mammalian cells and their spindles. Mild compression brings kinetochores closer to the coverslip to improve imaging, and brings the spindle and kinetochore-microtubule axis roughly parallel to the coverslip. In turn, medium compression directly flattens the spindle, confining all kinetochores to a smaller volume, bringing more kinetochores into the same focal plane, and limiting kinetochore movement in and out of focus. Even stronger compression can limit chromosome movements, externally controlling – and increasing – the cellular forces that kinetochores experience. Second, we

75

describe the use of simultaneous two-color sub-pixel imaging of kinetochore reporter probes. In combination with mild compression to help confine and align kinetochores, this allows monitoring structural kinetochore dynamics in real time under different cellular forces.

Spindle compression to image and perturb kinetochores:

Historical context:

Several mechanical approaches have been used to probe chromosome segregation in live cells: some to improve imaging, and others to mechanically perturb mitotic cells and their macromolecular machines. Examples of mechanical approaches to improve live cell imaging include: coating coverslips (e.g. with Poly-L-Lysine) to help keep dividing cells flat; confining dividing cells in PDMS devices of different heights (Le Berre et al., 2012); and laying an agar pad on top of a cell to reduce mitotic rounding and movement (Fukui et al., 1987; Pereira et al., 2009) Examples of physical perturbation approaches include microneedles to exert and measure tension on individual chromosomes and kinetochores in insect spermatocyte cells (Nicklas and Staehly, 1967; Nicklas, 1983); optical tweezers to move chromosomes inside mammalian cells (Liang et al., 1991); and laser ablation to probe kinetochore motility (Khodjakov and Rieder, 1996b), kinetochore signaling (Rieder et al., 1995) and spindle mechanics (Snyder et al., 1991). We note that outside live cells, optical tweezers have given us unprecedented access to kinetochore-microtubule attachment mechanics (Akiyoshi et al., 2010).

Motivation:

Here we describe how spindles can be compressed in live mammalian cells using a micromanipulator to controllably and reversibly press an agarose pad down on the cell (Figure 4.1). Unlike some methods of mechanical perturbation, spindle compression is compatible with

high resolution live imaging and indeed improves image quality. Furthermore, spindle compression requires little equipment besides a micromanipulator, and is fully compatible with cell health. Mild compression has been used to improve conditions for sub-pixel kinetochore imaging (Dumont et al., 2012), medium compression to study the response of spindle size to mechanical force (Dumont and Mitchison, 2009), and strong compression to exert extraordinary forces on kinetochores (Dumont et al., 2012). Below, we provide protocols for culturing cells in preparation for compression, preparing agarose pads, the experimental setup we use for compression, and details on executing and monitoring compression. We end this section with tips for troubleshooting common issues.

Methods:

Choice of cell line: Protocols in this chapter will focus on one type of mammalian cells: rat kangaroo kidney epithelial (Ptk2) cells. These already remain relatively flat at mitosis, and have a small number of chromosomes – just 13 of them (Brinkley and Humphrey, 1969) – which are large and thus easy to image and distinguish from one another. They are amenable to RNAi, transfections and other molecular techniques (Guimaraes et al., 2008; Stout et al., 2006). Based on our experience, we anticipate that compression will work in a variety of cell types, and is easiest in flatter cells.

Cell culture: We culture Ptk2 cells in MEM (Invitrogen 11095) supplemented with sodium pyruvate (Invitrogen 11360), nonessential amino acids (Invitrogen 11140), penicillin/streptomycin, and 10 % qualified and heat-inactivated fetal bovine serum (Invitrogen 10438). We plate cells on #1.5 25 mm round coverslips (HCl-cleaned, poly-L-lysine coated), and image them in Leibovitz's L-15 medium with L-glutamine without phenol red (Invitrogen 21083) with antibiotics and serum as above. When culturing Ptk2 cells, we recommend keeping cell confluency between 40 % and 90 %. When plating cells on coverslips for imaging, we typically

77

dilute them to about 60 % confluency and grow them for two days prior to imaging. Hallmarks of healthy cells include a high fraction of mitotic cells (rapidly growing population), flat cells (including mitotic ones) that establish strong junctions with neighbors and display a "football-shaped" spindle area free of mitochondria, reflecting high microtubule density.

Agarose pad preparation: Begin by mixing a solution of PBS and 2 % ultrapure agarose (Invitrogen 15510). The agarose concentration is chosen such that the pad is rigid enough to compress a large area of cells, and compliant enough for compression to be robust, easy and safe to perform. Boil this solution in the microwave until clear. Let cool for 5 min, and then use a plastic bulb pipet to fill a 60 mm plastic tissue culture dish with agarose solution around 2–3 mm deep (6–8 ml). Let the agarose solution cool until it appears "cloudy" and has solidified. Cut the agarose into 10–15 mm-wide squares, making sure to exclude any piece of agarose that touches the edge of the plate and curves up (such that the pad has uniform thickness). Store these squares in imaging media (described above) and let them sit overnight at 4 °C before using, so that they can equilibrate with the imaging media. At 4 °C, the pads will last at least one week. Before using any agarose pads on cells, warm them to the imaging temperature (we use 29–30 °C) immediately before imaging. If combining compression with pharmacological treatments (e.g. taxol), incubate the pads overnight in imaging media supplemented with the desired drug concentration. Adding a drug to, or washing a drug out from, a currently compressed cell may not be possible on a rapid timescale.

Experimental setup: We perform live imaging on a Nikon Eclipse Ti inverted microscope with 100X 1.45 Ph3 oil objective through a 1.5X lens yielding 105 nm/pixel. Before, during and after compression, we image cells by phase contrast and spinning disk confocal (Yokogawa CSU-X1) fluorescence imaging every few seconds on an Andor iXon3 camera, and keep cells in focus with the Nikon Perfect Focus System. We mount an oil hydraulic fine micromanipulator

78

(Narashige MO-202) and coarse manipulator directly to our automated stage (ASI MS-2000 XYZ) (Figure 4.2). We attach a metal rod (2 mm wide) to the fine micromanipulator to directly contact the agarose pad. We image cells at 29–30 °C in a homemade heated aluminum coverslip holder accepting 25 mm round coverslips that allows access of the micromanipulator rod to the coverslip at shallow angles. To facilitate access of the rod to the coverslip, it is easier to use a low numerical aperture (NA) condenser (we use 0.52 NA).

Before spindle compression: Mount the coverslip in its temperature-controlled holder, fill the holder with 3–4 ml of 30 °C media, and mount the holder on the microscope. Use phase contrast imaging to locate a good cell for compression and imaging, and center it in the field of view. The ideal cell to compress (Figure 4.3) and image will be as flat as possible prior to compression so that additional flattening perturbs as little as possible, have significant contact with neighboring cells but still have cell-free space around it to flatten (an area about 80 % confluent is ideal for this) and have a clear spindle region. It is critical that the cell to be compressed is away from the coverslip edges so that the agarose pad can be centered over it, and the micromanipulator rod can access it (Figure 4.2). After finding a good cell, gently deposit the agarose pad on top of the coverslip by placing it in the media. Once the pad has dropped onto the coverslip, gently nudge the side with tweezers to put the center of the pad directly above the objective. Next, position the micromanipulator rod by hand so that the rod end is directly above the objective and is touching the media but not the pad. Position the rod at as shallow an angle as possible (Figure 4.2). Take care to ensure that the micromanipulator Z-control knob is adjusted to the top of its range, so that the rod will have sufficient range to reach the pad. Then, finely adjust the position of the rod using fine micromanipulator X- and Y-control knobs to ensure it is centered above the cell (looking through the Bertrand lens is helpful).

Spindle compression: Once the rod is centered, slowly begin lowering it using the micromanipulator Z-control knob. If imaging is needed during compression, we typically send 80% of phase contrast imaging light to the camera and 20% to microscope eyepieces as these have a bigger field of view than the camera and thus allow more careful monitoring of compression progress. As the micromanipulator rod is lowered, the phase contrast image may begin to darken; if so, the condenser must be lowered as the rod is lowered to preserve Koehler illumination. Continue lowering the rod until particles in the media begin to rush (as seen through the eyepieces), reflecting first contact of the rod with the pad. From this point, only lower the rod a few microns at a time. The first sign that downward force is being exerted on the cell is that the spindle and chromosomes will spread outward. Adjustments to the focal plane are also typically necessary during compression as the position of the spindle with respect to the coverslip changes.

Choice of compression levels: We consider three compression levels, each with a different effect and purpose. Compression extent is fully under micromanipulator control, and is reversible. The extent of compression can simply be monitored by the surface area of the cell as viewed in phase contrast imaging, and can be further characterized by monitoring spindle thickness via 3D imaging (Z-stacks). While we do not know the precise amount of force that compression applies to the spindle, we estimate it to be on the order of hundreds of nanoNewtons (Dumont and Mitchison, 2009).

    i.   To achieve mild compression (Figure 4.1B), lower the rod but stop right when the cell begins to bleb. This level of compression (typically 100–150 μm of micromanipulator travel from the point of first contact of the rod and pad) flattens the cell mildly, brings the spindle and kinetochores closer to the coverslip without flattening the spindle, and aligns the spindle with the coverslip axis without affecting chromosome motion – making it

easier to follow kinetochores over time. The response of the cells to this compression level is reversible when the compression force is removed.

ii. To achieve medium compression (Figure 4.1C), continue lowering the rod for a few microns after the cell begins to bleb (after which it may or may not continue to bleb). Medium compression flattens the spindle: it widens the spindle (passively, over seconds) and lengthens it (actively, over minutes) up to 40%, and does not affect kinetochore motility dynamics or inter-kinetochore distance, a proxy for kinetochore tension (Dumont and Mitchison, 2009). Medium compression improves imaging (Figure 4.4): it confines all kinetochores to a smaller volume to image, brings more kinetochores into the same focal plane and limits kinetochore movement in and out of the focal plane. For example, in one study we found that Ptk2 spindles were about 5–7 μm in height (from top to bottom kinetochore-fibers) before and 3–4 μm in height after this level of compression (Dumont and Mitchison, 2009). As the pad is deformable, this can require 10 μm or more of micromanipulator travel beyond mild compression in our conditions. The response of the cell and spindle to this compression level is typically reversible.

iii. To achieve strong compression (Figure 4.1D), continue lowering the rod until some chromosomes can no longer move freely because cell height is not sufficient. This can require an additional 10 μm or more of micromanipulator travel beyond medium compression in our conditions. In addition to improving imaging as for milder compression, strong compression effectively pins down some of the chromosomes to the coverslip, while microtubules are still exerting pulling forces on kinetochores: strong compression can prevent one kinetochore from moving, while its sister kinetochore is free to move, yielding inter-kinetochore distances significantly above the normal range (Dumont et al., 2012). This results in extraordinary forces being exerted on kinetochores, and thus serves as a means to mechanically perturb kinetochores inside live cells. If such strong compression force is removed quickly by raising the rod rapidly, the spindle

81

response is not reversible; however, if compression is removed more slowly (over $\gg$ 10 s), the spindle responds more reversibly. For strong compression, be particularly cautious to align the rod on top of the cell and objective to avoid cracking the coverslip.

For all three compression levels, we generally lower the compression rod over 10–20 s, and keep it down in position for as long as we want to image or perturb the cell. For compression levels (i) and (ii), anaphase entry is not significantly delayed during or after compression. Monitoring the time to anaphase entry is excellent practice.

After spindle compression: After compression is no longer needed, raise the rod upward with the micromanipulator. If other cells are to be used in the area of the compressed cell, raise the micromanipulator rod slowly to encourage reversible responses to compression removal. Importantly, make sure to never move the rod or the pad in X-Y while a cell is under compression as this could shear cells off the coverslip. First raise the micromanipulator rod before moving it in the X-Y plane.

Troubleshooting tips:

i) Poor phase contrast image in compressed cells: Both the agarose pad and micromanipulator rod are in the transmitted light path and can thus affect phase contrast imaging. Koehler illumination should be maintained for good phase contrast generation, which in our experience may require bringing the condenser down during compression. Having about a 1.5 cm high pool of imaging media in the holder (several milliliters of media in our holder) is also helpful, and makes imaging more robust to media evaporation.

ii) Difficulty maintaining compression: If compression is not maintained and the cell rounds up during compression, this suggests that the area being compressed is not directly over the cell. Either the rod or pad is not directly above the objective. Slowly release compression

and correctly center the rod and pad in the X-Y plane. Cells at the edge of the coverslip may be hard to compress, either because the rod or pad center cannot reach them.

iii) Cell death upon compression: When compressing, cell bleb expansion and retraction are often observed and are expected and normal. However, excessive blebbing and lack of bleb retraction indicate compression is too strong for cell health maintenance. In particular, if the cytoplasm slowly leaks or suddenly bursts – leading to cell death – this indicates that the compression level was too strong.

iv) Coverslip cracking upon compression: If this occurs, it is most likely because the rod or pad is miscentered and not above the cell and objective. If the cell does not begin to compress shortly after the media rushes when the pad is brought down, raise the rod, re-center the rod and pad, and try again.

Imaging kinetochore dynamics at sub-pixel resolution via two-color reporter probes

Historical context:

In the previous section we described spindle compression as a method to improve kinetochore imaging under cellular forces and to externally perturb these forces. Here, we describe a method for monitoring the structural dynamics of kinetochores under force in live cells. Most of what we know about the global organization of mammalian kinetochores has come from electron microscopy, which reveals a multilayered structure (Dong et al., 2007): an inner plate at centromeric chromatin and outer plate near microtubule plus-ends. In turn, biochemical analysis has revealed information on relative positions of different kinetochore proteins between chromatin and microtubules (Cheeseman and Desai, 2008). Until a few years ago, obtaining

high resolution positional data with molecular specificity presented a major challenge: while kinetochore proteins could be tagged with fluorescent markers, the distance between chromatin-binding and microtubule-binding kinetochore proteins (about 100 nm) is below the diffraction limit of light. FRET (Förster resonance energy transfer) only informs on distances smaller than 10 nm. The application of Gaussian-fitting to find the center of diffraction-limited objects (Yildiz et al., 2003) and the distance between them (Churchman et al., 2005) now provides us with a means to use light imaging to position kinetochore proteins with respect to each other, and to measure linkage deformations under different conditions.

Motivation

Here we describe an adaptation of SHREC, single molecule high-resolution colocalization (Churchman et al., 2005), to measure the distance between two groups of differently colored reporter probes within a single kinetochore in live mammalian cells, which we refer to as "intra-kinetochore distance" (Wan et al., 2009). SHREC in fixed cells has revealed the architecture of the mammalian kinetochore-microtubule attachment site with 5 nm accuracy (Wan et al., 2009). Three key features make kinetochore live cell SHREC possible: i) the high copy number of most protein species within one kinetochore means that enough photons can be collected with genetically-encoded fluorescent proteins; ii) the natural orientation of the kinetochore-microtubule axis roughly parallel to the coverslip axis makes it possible to measure intra-kinetochore distances along this axis; iii) the cyclical nature of kinetochore movements in mammalian metaphase chromosome oscillations makes data averaging possible by providing clear synchronization points. However, challenges to live kinetochore SHREC measurements are significant: kinetochores are found deep inside round mitotic cells, move up and down – and can tilt – with respect to the imaging plane, and move fast; in addition, not all copies of the same protein may localize in a similar manner. Yet, using live kinetochore SHREC, it has been

84

possible to relate structural dynamics and different microtubule forces (Dumont et al., 2012; Joglekar et al., 2009). Below we describe cell preparation, the experimental setup, imaging, and basic data analysis guidelines for live kinetochore SHREC, and mention key questions to consider in data interpretation.

Methods

Gaussian-fitting for sub-pixel resolution: If a single fluorescent molecule is imaged, it forms a diffraction limited image of width $\lambda/(2NA)$, with λ the wavelength of light and NA the collection objective numerical aperture. If we fit the image to a 2D Gaussian, the mean corresponds to the position of the single molecule. The standard error of the mean, which reflects our ability to estimate the mean, will depend on photon noise, the effect of the detector's finite pixel size, and background noise (Thompson et al., 2002; Yildiz et al., 2003). Thus, for improved accuracy we must collect as many photons as possible and choose a camera carefully. Although Gaussian-fitting approaches were developed for single molecules, they have been applied to groups of kinetochore proteins: there are several copies of each kinetochore protein per microtubule (Johnston et al., 2010b), and multiple microtubules per mammalian kinetochore (20–25 in Ptk cells, (McEwen et al., 1997)), and thus there are a couple to a few hundred copies of some proteins at each mammalian kinetochore. As discussed below, care must be taken to understand the assumptions behind the use of a single-molecule technique for groups of molecules.

Choice of cell line and reporter probes: We focus on Ptk2 rat kangaroo kidney epithelial cells for the same reasons as for spindle compression. To measure intra-kinetochore distances via live SHREC, two reporter probes (Figure 4.5A) should be chosen such that i) the labeled

85

kinetochore proteins are expected to be sufficiently distant from each other (50 nm and above are good starting points) – based on protein distances in fixed cells (Wan et al., 2009) and related biochemical data – for live SHREC to robustly resolve this distance; ii) they are fused to fluorescent proteins with non-overlapping spectra; iii) they can be expressed at high enough levels in cells without adversely affecting function, to get high photon counts and a good estimate of the Gaussian center; iv) they are not known to bind anywhere else near kinetochores, as this could affect Gaussian-fitting (e.g. to microtubules in a kinetochore-independent manner). In addition, to aid in data interpretation on the relationship between intra-kinetochore distances and microtubule forces we recommend choosing reporter probes which take on structural (as opposed to regulatory) roles at kinetochores when possible given above constraints.

Expression of reporter probes: Two reporter probes must be expressed either using transient transfection or infection, or in stable cell lines. For example, we have recently used transient transfection to express Hec1-EGFP or EYFP-Cdc20 (outer kinetochore proteins) and CenpC-mCherry (inner kinetochore protein) in Ptk2 cells (Figure 4.5B–C): we transfect cells on a 25mm coverslip in a 6-well plate using 0.5 µg of each plasmid with 3 µl Fugene6 (Promega E2693) with 2.5 ml of media without antibiotics. Cells are either plated on coverslips 24 h before transfection, or plated and transfected together. Cells are imaged 36–48h post-transfection in imaging media as described above. Cells expressing one probe will typically also express the other, and using the above protocol we find that 30–50% of cells express both probes.

Experimental setup: We use the setup described for spindle compression, with a Yokogawa CSU-X1 spinning disk confocal with 488 nm and 561 nm diode lasers (100–150 mW lasers, used at a fraction of their power) and add a DualView (Photometrics, Chroma 565dcxr dichroic and ET525/50M and ET630/75M emission filters) module for simultaneous EGFP or EYFP and

mCherry camera acquisition (Figure 4.5B–C). We have confirmed the lack of channel crosstalk with EGFP or EYFP and mCherry (Semrock Yokogawa dichroic Di01-T405/488/561). We use an Andor iXon3 camera with 5X pre-amp gain and no EM gain: EGFP or EYFP and mCherry are simultaneously excited, and emissions collected simultaneously on each camera half. Simultaneous imaging is critical because of fast kinetochore movements at mammalian mitosis (if kinetochores move at 1 µm/min, this means 17 nm each second!).

Before live cell imaging – two-color bead registration: Before the distance between two different kinetochore protein populations can be measured with EGFP/EYFP and mCherry probes, one must map chromatic aberrations (how the same object appears in two different colors) over the field of view (Figure 4.6A). To do this, we mount scattered TetraSpeck 100 nm beads (Invitrogen T-7279) to a coverslip surface and simultaneously image the same beads in both green and red channels. We then use the 2D-Gaussian-fitted centers (lsqcurvefit, Matlab) of these beads in both channels to create a position-dependent 2D transform (we find that Matlab's cp2tform with polynomial degree 2 works well) that accounts for chromatic aberrations (Churchman et al., 2005). This transform can then be applied to other bead slides to probe its error. If performance is satisfactory, it can then be used to register (i.e. correctly align and relatively position) EGFP/EYFP and mCherry kinetochore images together and ultimately measure intra-kinetochore distances. In our experience, it is helpful to perform this bead registration every day before beginning imaging.

Sub-pixel resolution kinetochore imaging via two-color reporter probes: We use phase contrast to find metaphase cells without bleaching fluorophores, and then confocal imaging to assess whether both probes are expressed, and whether their expression level (i.e. collected photon count) is high enough for needed localization accuracy. For CenpC-mCherry and Hec1-EGFP or EYFP-Cdc20, we typically collect 4000–7000 photons/kinetochore (which we can estimate using

87

the electron-to-photon conversion factor obtained after camera calibration), and the signal-to-noise ratio (SNR) is typically 15–20 (SNR=$I_{max}/\sqrt{(I_{max}+b2)}$, with I_{max} the maximum pixel photon count and b the background photon standard deviation). Once a proper cell has been identified, we perform medium compression (as described above) to i) bring more kinetochores in the same plane, which means faster data collection; ii) limit out of plane movement, which allows us to follow a single kinetochore pair over long times as it experiences different forces; iii) help align the kinetochore-microtubule axis to the coverslip, since this is the axis along which we measure distance. We typically wait a few minutes between compression start and imaging start. At every time point, we acquire a phase contrast image to monitor cell health and associate kinetochores in pairs (a proxy for tension) by identifying chromosomes, and a simultaneous two-color confocal image to monitor the distance between the two kinetochore probes (Figure 4.6B). Images are acquired at 105 nm/pixel (bin=1), and exposure times are kept as short as possible to avoid blurring the distributions due to movement. Because we attempt to follow the same kinetochore over long times as microtubule forces change, we do not typically collect Z-stacks to avoid photobleaching, and thus only perform Gaussian fitting in 2D. If Z-stacks can be acquired, Gaussian fitting in 3D has the advantage of reporting on kinetochore tilt.

Data analysis for sub-pixel resolution kinetochore imaging: After data collection, we begin by tracking each kinetochore's position over time (SpeckleTracker, Matlab program written by Xiaohu Wan), and then determine the centroids of the Hec1-EGFP or EYFP-Cdc20 and CenpC-mCherry probes at each time point by fitting a 2D Gaussian (lsqcurvefit, Matlab) in a 10×10 pixel box (Figure 4.6C–D). Applying the two-color bead registration map to the EGFP/EYFP and mCherry images, we then find the inter-probe distance at each time (Figure 4.6E): this distance fluctuates broadly over time, and thus we pool together inter-probe distances from different times, kinetochores and cells in conditions we believe to be similar (Figure 4.6F). Metaphase

chromosome oscillations can be used as a system where averaging can be performed over well-defined periodically recurring events: for example, in recent work we found that the inter-probe distance was different by an average of 8 nm in kinetochores moving toward and away from the spindle pole (Figure 4.6E–F) (Dumont et al., 2012). To validate such conclusions, it is essential to check whether individual kinetochores behave – on average – like the means do. We calculate inter-probe distance as the mean of the Gaussian fit of the distance distribution, and note that because the inter-probe distance cannot be negative, this can overestimate the inter-probe distance – particularly for small distances (Stirling Churchman et al., 2006). In our conditions, we measure the standard deviation of the inter-probe distance distribution to be about 20 nm, and this includes contributions from centroid determination with limited photon counts (4–6 nm accuracy for our conditions (Mortensen et al., 2010)), two-color registration map estimation errors (target registration error as high as 7 nm in our tests (Churchman et al., 2005)), map application to inhomogeneous environments deep inside the cell, and biological variation (Dumont et al., 2012).

Key considerations for interpretation of inter-probe distances:

i) Meaning of the Gaussian center and of inter-probe distances

It is important to keep in mind that the Gaussian-fit center of many copies of the same kinetochore protein does not necessarily correspond to the location of all protein copies (Figure 4.7A). If protein copies are tightly clustered, mean localization will not be affected; however, if protein copies are too scattered, then assumptions behind Gaussian fitting break down (Wan et al., 2009). In an extreme example, if the protein copies were distributed in a bimodal distribution, the centroid could be in a region where few protein copies actually reside. The position of the centroid reflects the position of the center of mass of a group of proteins.

89

ii) Contributions of non-structural factors to changes in inter-probe distances

While it is tempting to interpret changes in inter-probe distance as structural changes within the kinetochore, other events may lead to inter-probe distance changes. Most notably, both kinetochore tilt with respect to the coverslip and changes in protein binding sites at the kinetochore could lead to apparent inter-probe changes. First, given that most microtubules terminate at the kinetochore within a 30 nm band along the microtubule axis (McEwen and Heagle, 1997) and that microtubule plus-ends are located in a 400 nm diameter circle in Ptk kinetochores (McDonald et al., 1992), one can estimate the amount by which tilt would be expected to widen the kinetochore probe image standard deviation (Dumont et al., 2012). While such tilt has thus far been insufficient to explain observed changes in distance between Gaussian centers, its possible effects must always be considered (Figure 4.7B). Second, dynamic changes in protein binding may always contribute to apparent inter-probe distance changes (e.g. if reporter proteins bound different sites on the kinetochore over time; Figure 4.7C), and such possibilities can be carefully evaluated by measuring changes in parameters such as protein intensities, recovery kinetics after photobleaching, and Gaussian standard deviations over time.

Conclusion and outlook

Mammalian cells round up when they divide, and many key structures that mediate division are highly dynamic. Together, these make imaging and physically probing cell division structures difficult. In this chapter, we have presented two conceptually simple methods to image and physically probe kinetochores in live dividing mammalian cells: i) spindle compression improves imaging inside round cells, and stronger compression can be used as a tool to mechanically perturb the spindle and kinetochores; ii) in turn, sub-pixel imaging of kinetochore linkages can

probe kinetochore structural dynamics under cellular forces. We hope that the experimental details we provide, as well as our open discussion of common technical and interpretation pitfalls, will make these two approaches broadly accessible – and together move forward our understanding of kinetochore function. Lastly, we note that these methods – once adapted – may help us image and physically probe other cellular structures.
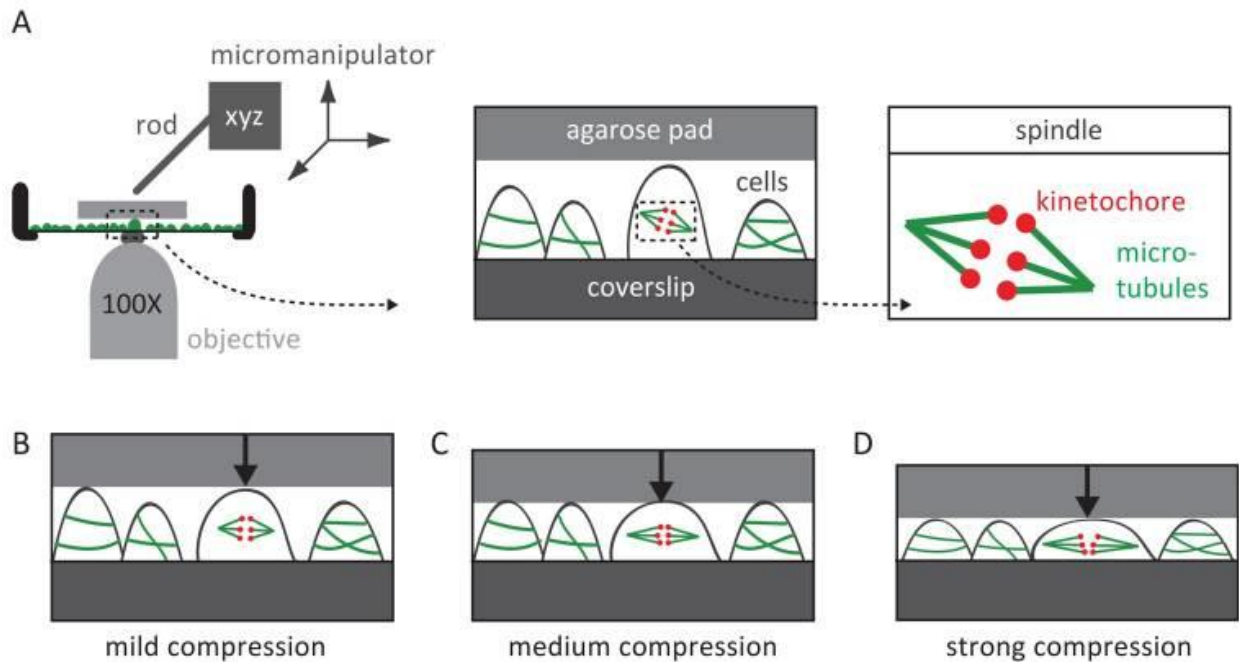
Figures and figure legends:

Figure 4.1: Spindle compression.

(A) Experimental sketch for spindle compression. A micromanipulator presses a rod down on an agarose pad to compress the cells below it.

(B) Mild compression flattens the cell, brings the spindle and kinetochores closer to the coverslip, and aligns the spindle with the coverslip axis – making it easier to follow kinetochores over time (Dumont et al., 2012).

(C) Medium compression (Dumont and Mitchison, 2009) widens and lengthens the spindle, does not affect kinetochore motion and tension, and improves imaging by bringing more kinetochores into focus and limiting their movement in and out of the focal plane.

(D) Strong compression improves imaging and pins down some of the chromosomes to the coverslip, preventing them from moving and resulting in inter-kinetochore distances significantly above the normal range (Dumont et al., 2012). Part (A) adapted from (Dumont and Mitchison, 2009).
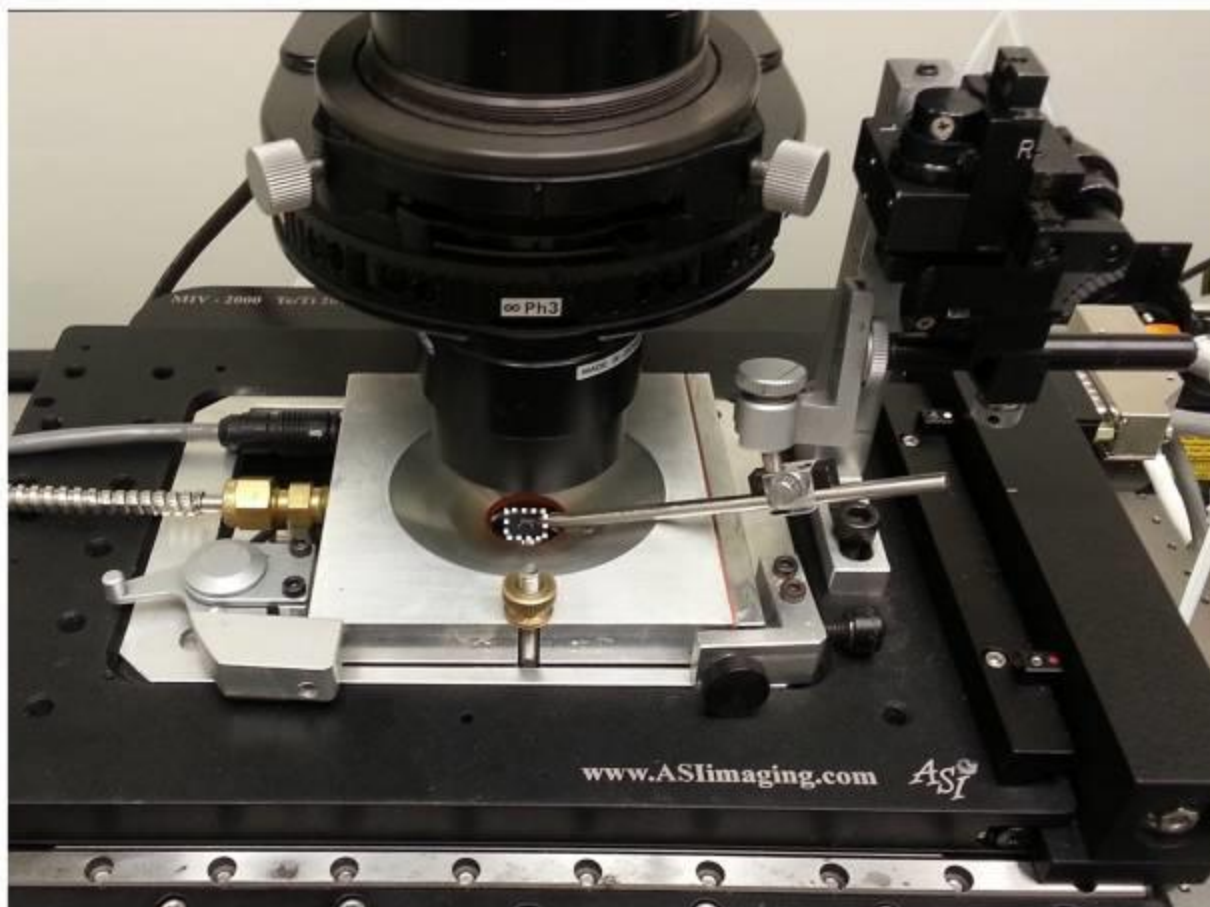
Figure 4.2: Experimental setup for spindle compression.

The shallow angle of the micromanipulator rod and coverslip holder walls allow the rod access to the agarose pad (highlighted with a white dotted rectangle). The micromanipulator is attached directly to the stage, and positioned in the center of the objective and pad.

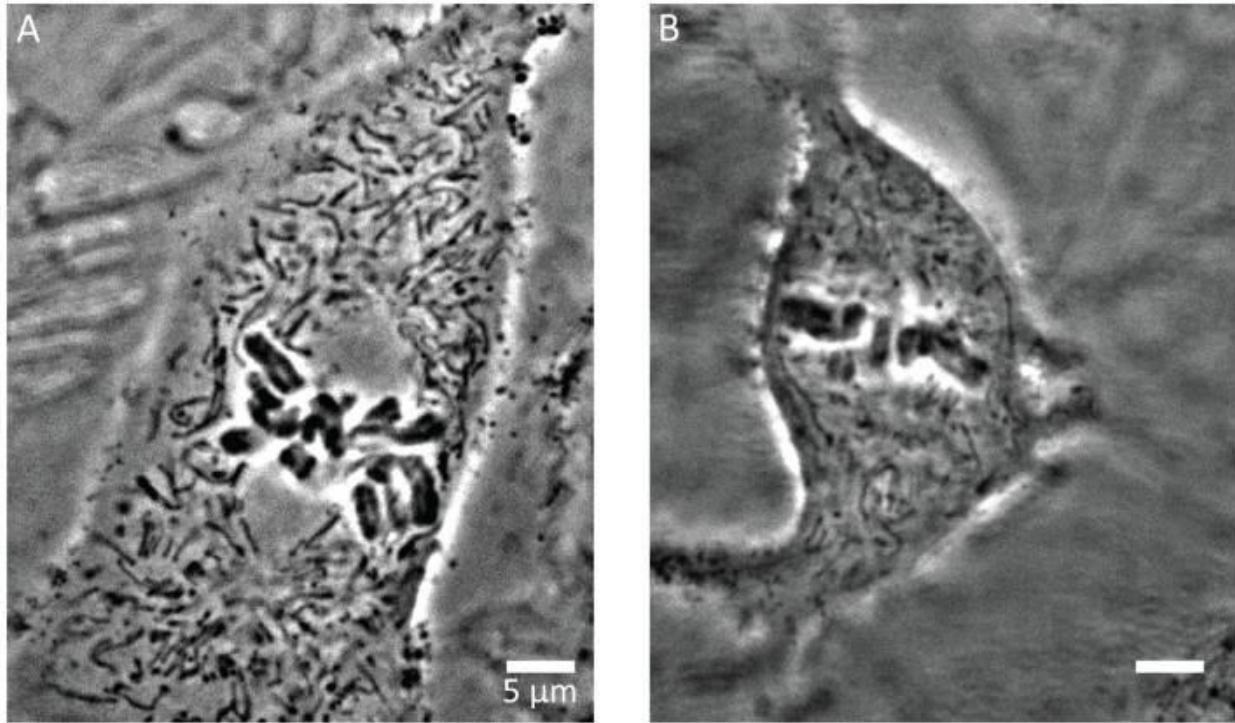**Figure 4.3: Choosing a cell for spindle compression.**

Phase contrast images of an (A) ideal and (B) non-ideal Ptk2 cell for spindle compression. An ideal cell remains flat at mitosis prior to compression, and has space available around it to increase its surface area upon compression. Note that in phase contrast imaging a healthy spindle appears as a clear "football-shaped" region around chromosomes.
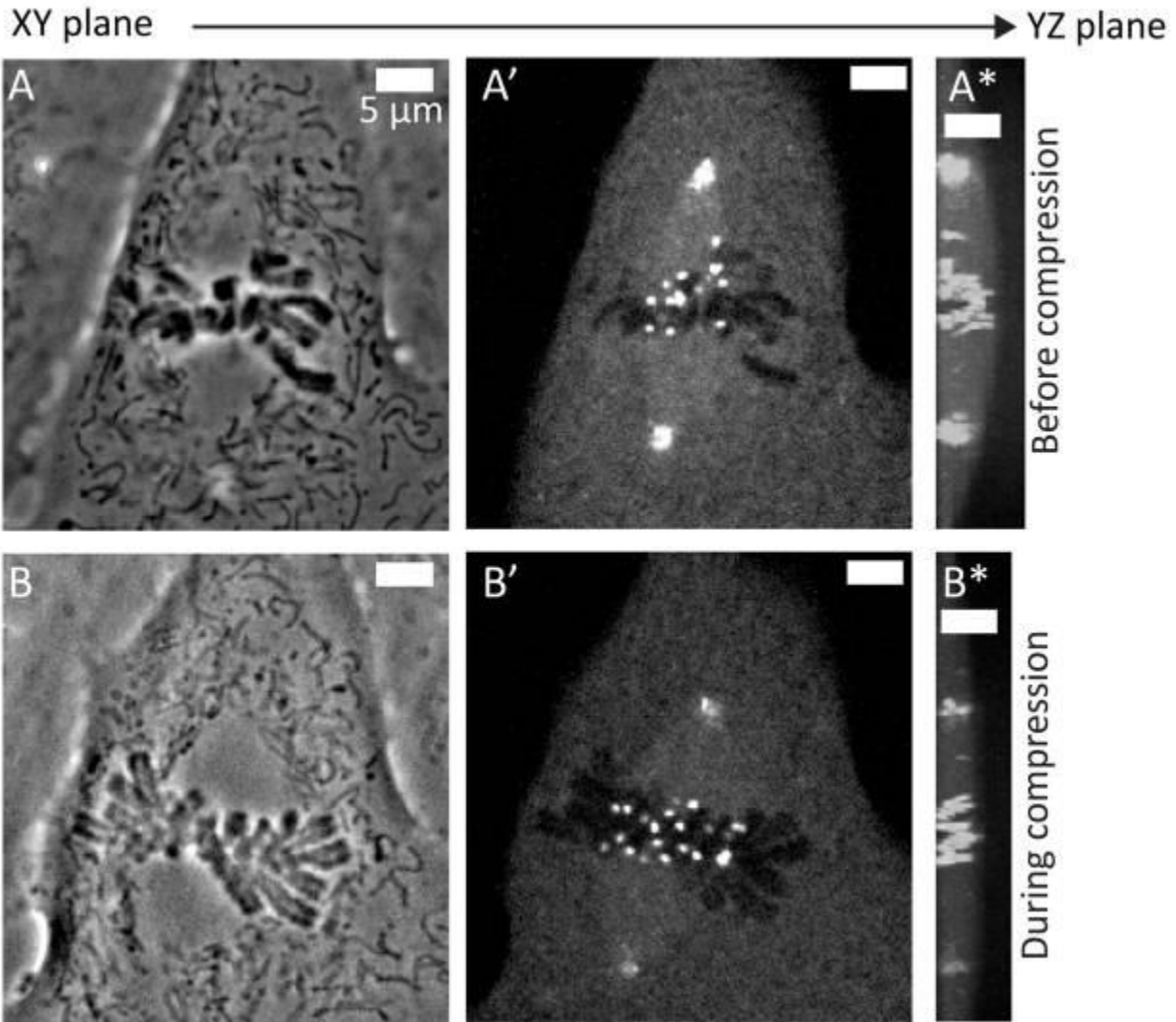
XY plane ⟶ **YZ plane**

Figure 4.4:

Images of a Ptk2 cell **(A)** before and **(B)** during medium spindle compression: phase contrast (A, B) and spinning disk confocal EYFP-Cdc20 **(A′, B′)** images. Compression increases cell area, spindle width and length, number of in-focus chromosomes and kinetochores (from about 10 to about 22). A Z-stack of confocal images was acquired (350nm between planes) and a maximum intensity projection along the Y-Z plane **(A* and B*)** confirms that kinetochores are confined to a narrower volume slice during compression. Intensities should be compared with care between images in (A) and (B) as 5 min of imaging separates them; during this time, photobleaching takes place and Cdc20 localization changes as mitosis progresses (Howell et al., 2004). Intensity display scaling was adjusted for YZ planes (to show cell shape changes as revealed by cytoplasmic EYFP-Cdc20). All XY images in this figure were acquired with 2×2 binning, yielding 210 nm/pixel.
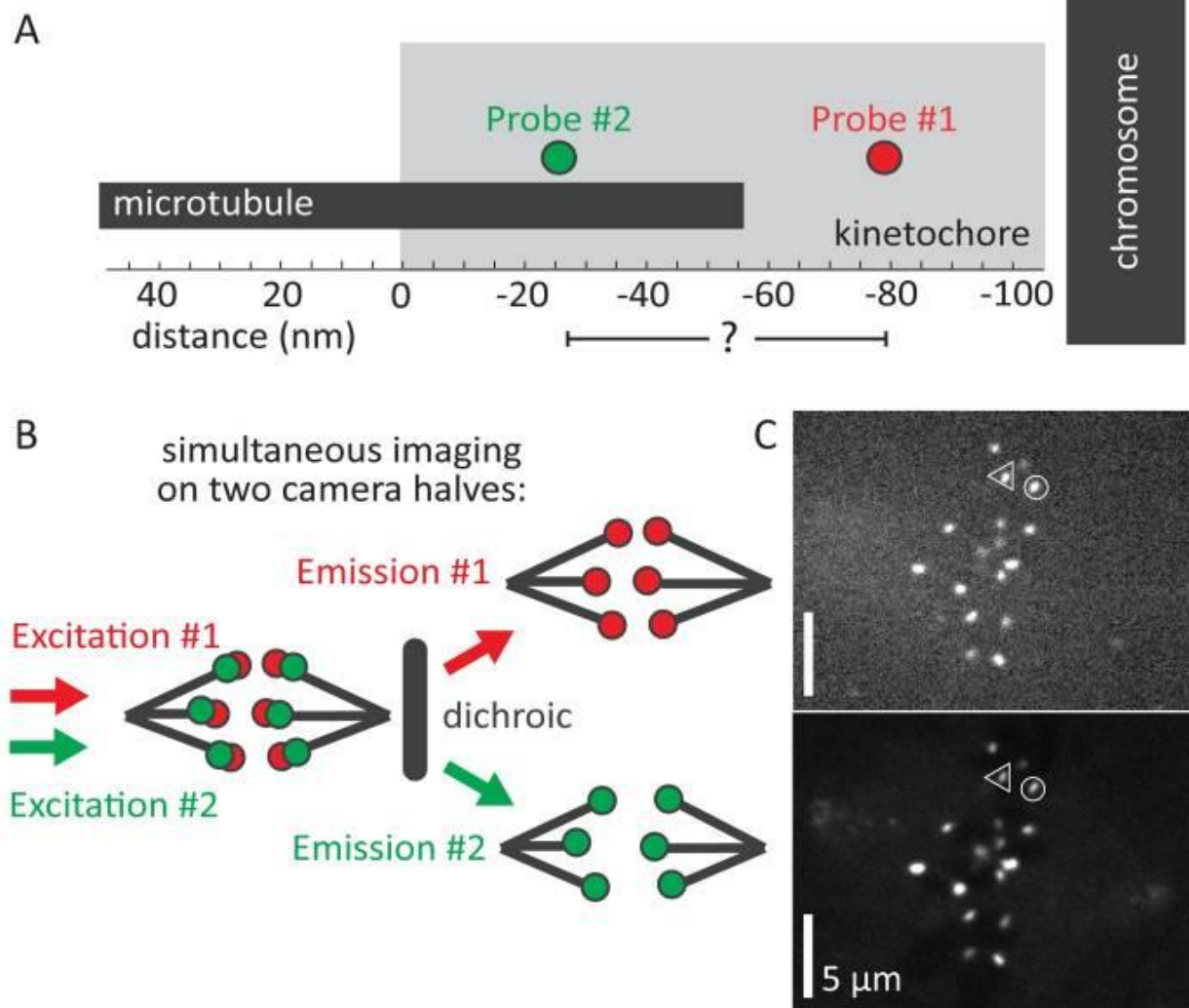
Figure 4.5: Simultaneously imaging two kinetochore reporter probes in live cells.

(A) Reporter probes must be chosen with care and here we depict the expected position (Wan et al., 2009) of two probes we have used: CenpC-mcherry (probe #1) and EYFP-Cdc20 (probe #2).

(B) To monitor kinetochore structural dynamics live, both probes are simultaneously imaged on each half of the camera by using a dichroic to separate emission photons from each probe.

(C) Simultaneous imaging of CenpC-mcherry (top, probe #1) and EYFP-Cdc20 (bottom, probe #2) on two camera halves. The identified kinetochore pair will be analyzed in Figure 4.6. Part (C) adapted from (Dumont et al., 2012).

Figure 4.6: Measuring kinetochore inter-probe distances.

(A) We image two-color beads in both green and red channels, and find the transform f(x,y) that maps Gaussian-fitted position differences in both channels.

(B) Enlarged two-color image of the kinetochore pair identified in Figure 4.5C (left = triangle, right = circle).
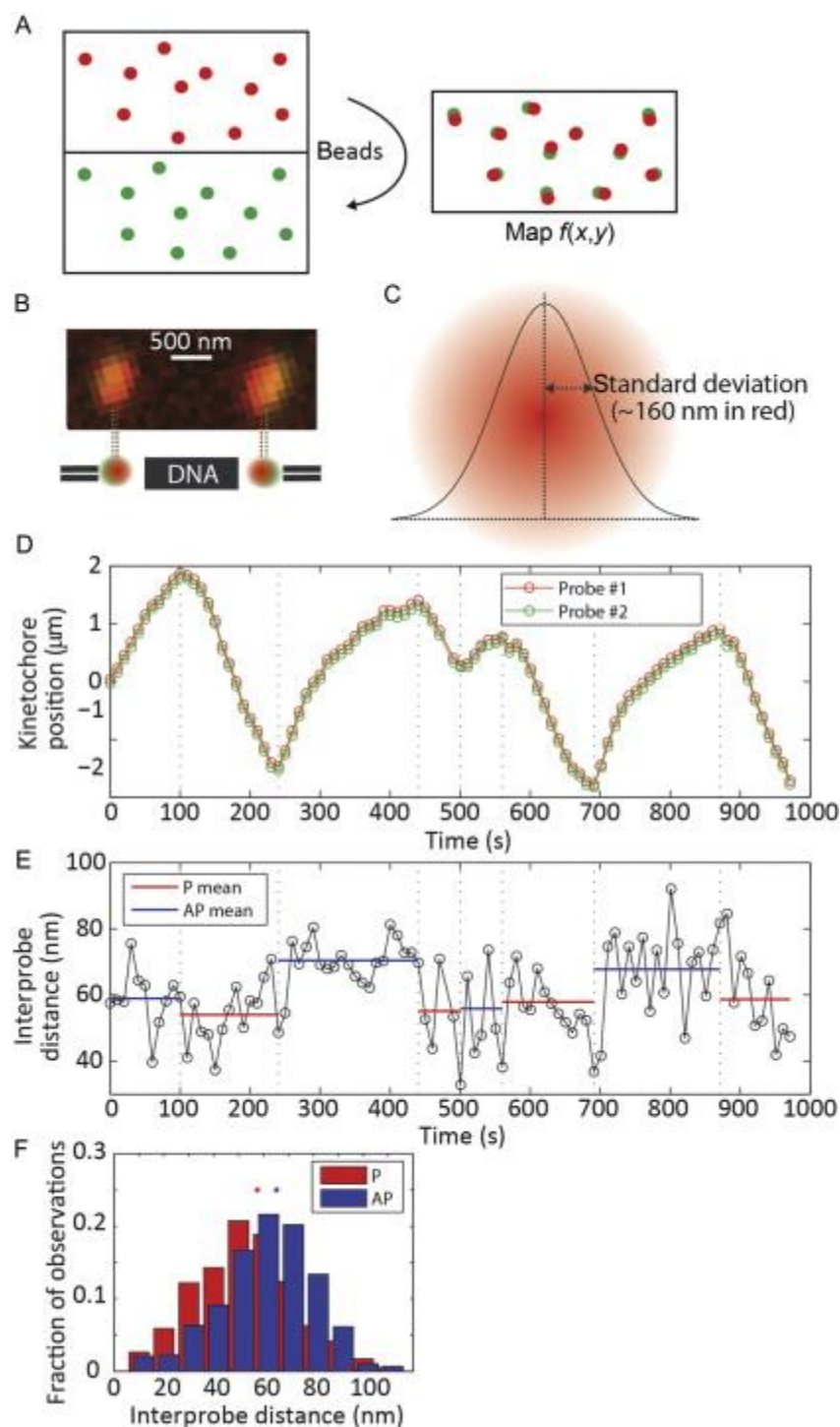
(C) Each kinetochore probe leads to an image that is fit to a 2D Gaussian (which we find has a standard deviation of about 160 nm along the microtubule axis, slightly larger than 100 nm beads (Dumont et al., 2012)).

(D) Tracks of one kinetochore's (the right one in (B)) two probes (EYFP-Cdc20 and CenpC-mCherry, as for (E) and (F)), moving during chromosome oscillations (dashed lines = reversals).

(E) Inter-probe distance versus time from the tracks in (D), highlighting poleward (P, red) and away-from-pole (AP, blue) movement.

(F) As an example measurement, we show data suggesting that kinetochores are in different structural states during poleward and away-from-pole movement. Histograms of inter-probe distances over different times, kinetochores and cells for poleward (red) and away-from-pole (blue) movement: 47±20 nm poleward (n=525) and 55±19 nm away-from-pole (n=569). Parts (B), (D–F) adapted from (Dumont et al., 2012).
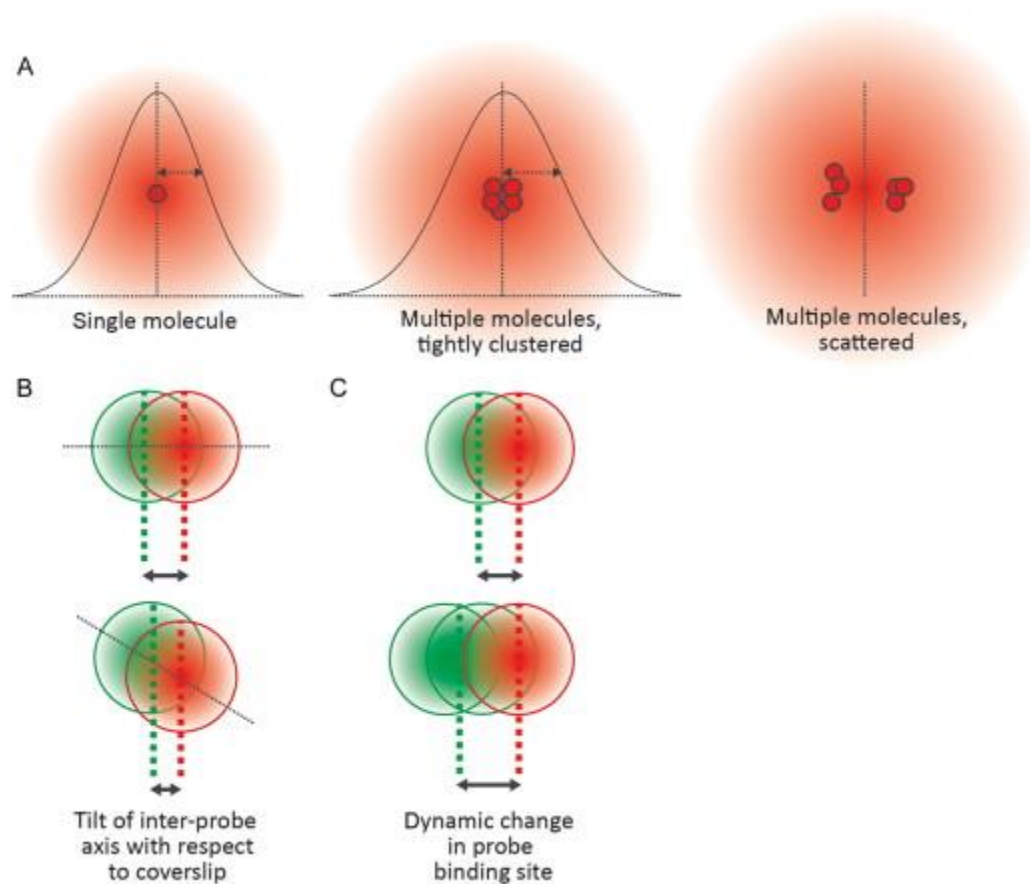
Figure 4.7: Considerations for interpreting inter-probe distances.

(A) The Gaussian-fit center of many copies of the same kinetochore protein does not necessarily correspond to the location of all protein copies. Protein copies that are tightly clustered will not affect mean localization, but if protein copies are too scattered then assumptions behind Gaussian fitting break down (Joglekar et al., 2009; Wan et al., 2009). Also, non-structural factors can lead to apparent changes in inter-probe distances, such as **(B)** tilt of the inter-probe axis with respect to the coverslip and **(C)** dynamic changes in probe binding sites (such as recruitment to a new binding site, as depicted here). In the text we provide pointers for evaluating the effects of (B–C).

Acknowledgments:

Chapter 5: Conclusions

In order to segregate chromosomes accurately, cells must coordinate the alignment and attachment of dozens of independent chromosomes over large areas. To this end, the cell uses the chromosome-microtubule attachment point as a signaling platform. In the SAC, the kinetochore acts as a subcellular computer: it accepts inputs from the environment, processes them, and produces an output controlling cell cycle progression. To understand this computer, it is critical to understand not just the inputs and outputs but also how the "hardware" (kinetochore structure) and "software" (network of biochemical interactions) interact to produce the SAC's quantitative behavior. While interest in this subject is long-standing, it is extremely difficult in practice to systematically analyze structures as complex and dynamic as the kinetochore.

In this dissertation, I asked how kinetochore detect and process attachment information. In chapter 2, I used live cell imaging to probe what inputs the kinetochore accepts. We uncovered a critical intermediate state where kinetochore pairs are under tension and one sister is Mad1-negative and end-on attached and one is Mad1-positive and laterally attached. This allowed us to demonstrate that neither kinetochore-microtubule attachment or tension are sufficient for SAC satisfaction. Instead, a specific attachment geometry – end-on attachments likely mediated through Hec1 – is needed for SAC satisfaction. Prior to this work, the fact that tension was not sufficient for Mad1 loss and that only specific attachments turned the SAC off had not been clearly demonstrated. Additionally, the actual process of Mad1 loss had not previously been captured. The kinetics of this behavior give us valuable insight into the Mad1 loss response: it is rapid, irreversible, and likely governed by one rate limiting step.

In chapter 3, I further clarify what specific inputs the kinetochore detects and analyze how the kinetochore's hardware and software tune the SAC response quantitatively. Our unique "mixed kinetochore" assay allowed us to both probe the binding behavior of individual Hec1 heads on the kinetochore and to quantify the relationship between attachment and Mad1 localization. Interestingly, individual kinetochore subunits function independently in microtubule

binding, but all coordinate a single SAC response. While there were some suggestions that the

SAC could turn off at attachment numbers below metaphase levels, the high degree of

sensitivity and switch-like behavior we show had not previously been observed. We also show

that kinetochores can modulate the rate of Mad1 loss in response to reduced attachment

numbers, a potential way for kinetochores to decrease their "false positive" rate. Finally, we

show conclusively that tension – even tension applied across Hec1 and its associated proteins –

is not needed for Mad1 loss. While this has become the increasingly favored position in the

field, the acute removal of pulling forces on kinetochores had not previously been possible.

While understanding how the kinetochore functions as a computer and the cell makes

correct decisions are exciting conceptual questions on their own, they are also urgently

important for human health. Understanding how mitotic errors can arise and how to prevent

them is critical because these errors drive both oncogenesis and tumor evolution (Giam and

Rancati, 2015). Indeed, some of the most effective cancer treatments are anti-mitotics and rely

on the SAC for their efficacy (Yamada and Gorbsky, 2006). It is only with the knowledge of what

the kinetochore detects, and how molecules in the SAC function, that we can accurately target

mitosis and treat these diseases. Much of this same logic applies to other diseases: a variety of

genetic disorders are caused by errors in meiosis (where the SAC is also functional). By

understanding the kinetochore decision-making process, it is possible in the future that we may

be able to predict or even prevent this mistakes before they happen.

Looking forward, it will be critical to better explain how the kinetochore functions

quantitatively as an ensemble. As a practical matter, our field tends to conceptually separate

kinetochore processes like error detection (the SAC), error correction, and microtubule binding

and capture. In reality, these pathways are tightly linked to one another in complex ways which

can evolve over the course of mitosis. It is only by combining finer tools to tune kinetochore

mechanics and composition with quantitative modelling of the kinetochore interaction network

that we move forward from a parts list to a deeper understanding of this macromolecular machine. A few specific outstanding questions about kinetochore and SAC function are particularly exciting: First, what molecular and/or spatial properties make the SAC so sensitive to microtubule attachments? By analyzing how the threshold number of attachments to turn off the SAC changes after mutating key structural proteins and kinases, we can ascertain how kinetochore function is set and can be modified. Second, how do other critical kinetochore processes, like error correction, respond to changes in kinetochore attachment and tension in live dividing cells? Finally, do different cell types and organisms alter their sensitivity to microtubule attachments to fit their natural environment? For example, does a 2 µm *C. elegans* kinetochore require more microtubule attachments to shut off the SAC than a 100 nm human kinetochore? Exploring these questions will help us understand the kinetochore better in a theoretical, evolutionary, and medical context.

References

Akiyoshi, B., K.K. Sarangapani, A.F. Powers, C.R. Nelson, S.L. Reichow, H. Arellano-Santoyo, T. Gonen, J.A.
Ranish, C.L. Asbury, and S. Biggins. 2010. Tension directly stabilizes reconstituted kinetochore-
microtubule attachments. *Nature*. 468:576–9. doi:10.1038/nature09594.

Alushin, G.M., V.H. Ramey, S. Pasqualato, D.A. Ball, N. Grigorieff, A. Musacchio, and E. Nogales. 2010.
The Ndc80 kinetochore complex forms oligomeric arrays along microtubules. *Nature*. 467:805–810.
doi:10.1038/nature09423.

De Antoni, A., C.G. Pearson, D. Cimini, J.C. Canman, V. Sala, L. Nezi, M. Mapelli, L. Sironi, M. Faretta, E.D.
Salmon, and A. Musacchio. 2005. The Mad1/Mad2 complex as a template for Mad2 activation in
the spindle assembly checkpoint. *Curr. Biol.* 15:214–25. doi:10.1016/j.cub.2005.01.038.

Aravamudhan, P., A.A. Goldfarb, and A.P. Joglekar. 2015. The kinetochore encodes a mechanical switch
to disrupt spindle assembly checkpoint signalling. *Nat. Cell Biol.* 17:868–879. doi:10.1038/ncb3179.

Avner, P., and E. Heard. 2001. X-chromosome inactivation: counting, choice and initiation. *Nat. Rev.
Genet.* 2:59–67. doi:10.1038/35047580.

Barisic, M., B. Sohm, P. Mikolcevic, C. Wandke, V. Rauch, T. Ringer, M. Hess, G. Bonn, and S. Geley. 2010.
Spindly/CCDC99 Is Required for Efficient Chromosome Congression and Mitotic Checkpoint
Regulation. *Mol. Biol. Cell*. 21:1968–1981. doi:10.1091/mbc.e09-04-0356.

Le Berre, M., J. Aubertin, and M. Piel. 2012. Fine control of nuclear confinement identifies a threshold
deformation leading to lamina rupture and induction of specific genes. *Integr. Biol.* 4:1406.
doi:10.1039/c2ib20056b.

Brinkley, B.R., and R.M. Humphrey. 1969. EVIDENCE FOR SUBCHROMATID ORGANIZATION IN

MARSUPIAL CHROMOSOMES: I. Light and Electron Microscopy of X-Ray-Induced Side-Arm Bridges. *J. Cell Biol.* 42:827–831. doi:10.1083/jcb.42.3.827.

Cane, S., A.A. Ye, S.J. Luks-Morgan, and T.J. Maresca. 2013. Elevated polar ejection forces stabilize kinetochore-microtubule attachments. *J. Cell Biol.* 200:203–18. doi:10.1083/jcb.201211119.

Cheeseman, I.M., J.S. Chappie, E.M. Wilson-Kubalek, and A. Desai. 2006. The conserved KMN network constitutes the core microtubule-binding site of the kinetochore. *Cell*. 127:983–97. doi:10.1016/j.cell.2006.09.039.

Cheeseman, I.M., and A. Desai. 2008. Molecular architecture of the kinetochore–microtubule interface. *Nat. Rev. Mol. Cell Biol.* 9:33–46. doi:10.1038/nrm2310.

Chen, R.H., A. Shevchenko, M. Mann, and A.W. Murray. 1998. Spindle checkpoint protein Xmad1 recruits Xmad2 to unattached kinetochores. *J. Cell Biol.* 143:283–95.

Chen, R.H., J.C. Waters, E.D. Salmon, and A.W. Murray. 1996. Association of spindle assembly checkpoint component XMAD2 with unattached kinetochores. *Science*. 274:242–6.

Churchman, L.S., Z. Okten, R.S. Rock, J.F. Dawson, and J.A. Spudich. 2005. Single molecule high-resolution colocalization of Cy3 and Cy5 attached to macromolecules measures intramolecular distances through time. *Proc. Natl. Acad. Sci.* 102:1419–1423. doi:10.1073/pnas.0409487102.

Ciferri, C., S. Pasqualato, E. Screpanti, G. Varetti, S. Santaguida, G. Dos Reis, A. Maiolica, J. Polka, J.G. De Luca, P. De Wulf, M. Salek, J. Rappsilber, C.A. Moores, E.D. Salmon, and A. Musacchio. 2008. Implications for kinetochore-microtubule attachment from the structure of an engineered Ndc80 complex. *Cell*. 133:427–39. doi:10.1016/j.cell.2008.03.020.

Collin, P., O. Nashchekina, R. Walker, and J. Pines. 2013. The spindle assembly checkpoint works like a rheostat rather than a toggle switch. *Nat. Cell Biol.* 15:1378–1385. doi:10.1038/ncb2855.

David, A.F., P. Roudot, W.R. Legant, E. Betzig, G. Danuser, and D.W. Gerlich. 2018. Augmin-mediated

amplification of long-lived spindle microtubules directs plus-ends to kinetochores. *bioRxiv*. 501445.

doi:10.1101/501445.

DeLuca, J.G., W.E. Gall, C. Ciferri, D. Cimini, A. Musacchio, and E.D. Salmon. 2006. Kinetochore

microtubule dynamics and attachment stability are regulated by Hec1. *Cell*. 127:969–82.

doi:10.1016/j.cell.2006.09.047.

DeLuca, J.G., B.J. Howell, J.C. Canman, J.M. Hickey, G. Fang, and E.D. Salmon. 2003. Nuf2 and Hec1 Are

Required for Retention of the Checkpoint Proteins Mad1 and Mad2 to Kinetochores. *Curr. Biol.*

13:2103–2109. doi:10.1016/J.CUB.2003.10.056.

DeLuca, K.F., A. Meppelink, A.J. Broad, J.E. Mick, O.B. Peersen, S. Pektas, S.M.A. Lens, and J.G. DeLuca.

2018. Aurora A kinase phosphorylates Hec1 to regulate metaphase kinetochore-microtubule

dynamics. *J. Cell Biol.* 217:163–177. doi:10.1083/jcb.201707160.

Devreotes, P.N., S. Bhattacharya, M. Edwards, P.A. Iglesias, T. Lampert, and Y. Miao. 2017. Excitable

Signal Transduction Networks in Directed Cell Migration. *Annu. Rev. Cell Dev. Biol.* 33:103–125.

doi:10.1146/annurev-cellbio-100616-060739.

Dick, A.E., and D.W. Gerlich. 2013. Kinetic framework of spindle assembly checkpoint signalling. *Nat. Cell

Biol.* 15:1370–1377. doi:10.1038/ncb2842.

Dong, Y., K.J. Vanden Beldt, X. Meng, A. Khodjakov, and B.F. McEwen. 2007. The outer plate in

vertebrate kinetochores is a flexible network with multiple microtubule interactions. *Nat. Cell Biol.*

9:516–522. doi:10.1038/ncb1576.

Drpic, D., A.J. Pereira, M. Barisic, T.J. Maresca, and H. Maiato. 2015. Polar Ejection Forces Promote the

Conversion from Lateral to End-on Kinetochore-Microtubule Attachments on Mono-oriented

Chromosomes. *Cell Rep.* 13:460–468. doi:10.1016/j.celrep.2015.08.008.

Dudka, D., A. Noatynska, C.A. Smith, N. Liaudet, A.D. McAinsh, and P. Meraldi. 2018. Complete microtubule–kinetochore occupancy favours the segregation of merotelic attachments. *Nat. Commun.* 9:2042. doi:10.1038/s41467-018-04427-x.

Dumont, S., and T.J. Mitchison. 2009. Compression Regulates Mitotic Spindle Length by a Mechanochemical Switch at the Poles. *Curr. Biol.* 19:1086–1095. doi:10.1016/j.cub.2009.05.056.

Dumont, S., E.D. Salmon, and T.J. Mitchison. 2012. Deformations Within Moving Kinetochores Reveal Different Sites of Active and Passive Force Generation. *Science (80-.).* 337:355–358. doi:10.1126/science.1221886.

Elting, M.W., C.L. Hueschen, D.B. Udy, and S. Dumont. 2014. Force on spindle microtubule minus ends moves chromosomes. *J. Cell Biol.* 206:245–56. doi:10.1083/jcb.201401091.

Elting, M.W., M. Prakash, D.B. Udy, and S. Dumont. 2017. Mapping Load-Bearing in the Mammalian Spindle Reveals Local Kinetochore Fiber Anchorage that Provides Mechanical Isolation and Redundancy. *Curr. Biol.* 27:2112-2122.e5. doi:10.1016/j.cub.2017.06.018.

Etemad, B., and G.J. Kops. 2016. Attachment issues: kinetochore transformations and spindle checkpoint silencing. *Curr. Opin. Cell Biol.* 39:101–108. doi:10.1016/J.CEB.2016.02.016.

Etemad, B., T.E.F. Kuijt, and G.J.P.L. Kops. 2015. Kinetochore–microtubule attachment is sufficient to satisfy the human spindle assembly checkpoint. *Nat. Commun.* 6:8987. doi:10.1038/ncomms9987.

Etemad, B., A. Vertesy, T.E.F. Kuijt, C. Sacristan, A. van Oudenaarden, and G.J.P.L. Kops. 2018. Spindle checkpoint silencing at kinetochores with submaximal microtubule occupancy. *bioRxiv*. 472407. doi:10.1101/472407.

Foley, E.A., and T.M. Kapoor. 2013. Microtubule attachment and spindle assembly checkpoint signalling at the kinetochore. *Nat. Rev. Mol. Cell Biol.* 14:25–37. doi:10.1038/nrm3494.

Fukui, Y., S. Yumura, and T.K. Yumura. 1987. Agar-overlay immunofluorescence: high-resolution studies of cytoskeletal components and their changes during chemotaxis. *Methods Cell Biol.* 28:347–56.

Funabiki, H., and D.J. Wynne. 2013. Making an effective switch at the kinetochore by phosphorylation and dephosphorylation. *Chromosoma*. 122:135–58. doi:10.1007/s00412-013-0401-5.

Gassmann, R., A.J. Holland, D. Varma, X. Wan, F. Civril, D.W. Cleveland, K. Oegema, E.D. Salmon, and A. Desai. 2010. Removal of Spindly from microtubule-attached kinetochores controls spindle checkpoint silencing in human cells. *Genes Dev.* 24:957–71. doi:10.1101/gad.1886810.

Giam, M., and G. Rancati. 2015. Aneuploidy and chromosomal instability in cancer: a jackpot to chaos. *Cell Div.* 10:3. doi:10.1186/s13008-015-0009-7.

Gorbsky, G.J., and W.A. Ricketts. 1993. Differential expression of a phosphoepitope at the kinetochores of moving chromosomes. *J. Cell Biol.* 122:1311–1321. doi:10.1083/jcb.122.6.1311.

Guimaraes, G.J., Y. Dong, B.F. McEwen, and J.G. Deluca. 2008. Kinetochore-microtubule attachment relies on the disordered N-terminal tail domain of Hec1. *Curr. Biol.* 18:1778–84. doi:10.1016/j.cub.2008.08.012.

Haeusser, D.P., and P.A. Levin. 2008. The great divide: coordinating cell cycle events during bacterial growth and division. *Curr. Opin. Microbiol.* 11:94–9. doi:10.1016/j.mib.2008.02.008.

Harashima, H., N. Dissmeyer, and A. Schnittger. 2013. Cell cycle control across the eukaryotic kingdom. *Trends Cell Biol.* 23:345–356. doi:10.1016/j.tcb.2013.03.002.

Heinrich, S., E.-M. Geissen, J. Kamenz, S. Trautmann, C. Widmer, P. Drewe, M. Knop, N. Radde, J.

Hasenauer, and S. Hauf. 2013. Determinants of robustness in spindle assembly checkpoint signalling. *Nat. Cell Biol.* 15:1328–1339. doi:10.1038/ncb2864.

Hengeveld, R.C.C., M.J.M. Vromans, M. Vleugel, M.A. Hadders, and S.M.A. Lens. 2017. Inner centromere localization of the CPC maintains centromere cohesion and allows mitotic checkpoint silencing. *Nat. Commun.* 8:15542. doi:10.1038/ncomms15542.

Hewitt, L., A. Tighe, S. Santaguida, A.M. White, C.D. Jones, A. Musacchio, S. Green, and S.S. Taylor. 2010. Sustained Mps1 activity is required in mitosis to recruit O-Mad2 to the Mad1–C-Mad2 core complex. *J. Cell Biol.* 190:25–34. doi:10.1083/jcb.201002133.

Hiruma, Y., C. Sacristan, S.T. Pachis, A. Adamopoulos, T. Kuijt, M. Ubbink, E. von Castelmur, A. Perrakis, and G.J.P.L. Kops. 2015. Competition between MPS1 and microtubules at kinetochores regulates spindle checkpoint signaling. *Science (80-.).* 348:1264–1267. doi:10.1126/science.aaa4055.

Howell, B.J., D.B. Hoffman, G. Fang, A.W. Murray, and E.D. Salmon. 2000. Visualization of Mad2 Dynamics at Kinetochores, along Spindle Fibers, and at Spindle Poles in Living Cells. *J. Cell Biol.* 150:1233–1250. doi:10.1083/jcb.150.6.1233.

Howell, B.J., B.F. McEwen, J.C. Canman, D.B. Hoffman, E.M. Farrar, C.L. Rieder, and E.D. Salmon. 2001. Cytoplasmic dynein/dynactin drives kinetochore protein transport to the spindle poles and has a role in mitotic spindle checkpoint inactivation. *J. Cell Biol.* 155:1159–72. doi:10.1083/jcb.200105093.

Howell, B.J., B. Moree, E.M. Farrar, S. Stewart, G. Fang, and E.D. Salmon. 2004. Spindle checkpoint protein dynamics at kinetochores in living cells. *Curr. Biol.* 14:953–64. doi:10.1016/j.cub.2004.05.053.

Hueschen, C.L., S.J. Kenny, K. Xu, and S. Dumont. 2017. NuMA recruits dynein activity to microtubule

minus-ends at mitosis. *Elife*. 6. doi:10.7554/eLife.29328.

Janssen, L.M.E., T. V. Averink, V.A. Blomen, T.R. Brummelkamp, R.H. Medema, and J.A. Raaijmakers. 2018. Loss of Kif18A Results in Spindle Assembly Checkpoint Activation at Microtubule-Attached Kinetochores. *Curr. Biol.* 28:2685-2696.e4. doi:10.1016/J.CUB.2018.06.026.

Jelluma, N., T.B. Dansen, T. Sliedrecht, N.P. Kwiatkowski, and G.J.P.L. Kops. 2010. Release of Mps1 from kinetochores is crucial for timely anaphase onset. *J. Cell Biol.* 191:281–90. doi:10.1083/jcb.201003038.

Ji, Z., H. Gao, and H. Yu. 2015. Kinetochore attachment sensed by competitive Mps1 and microtubule binding to Ndc80C. *Science (80-.).* 348:1260–1264. doi:10.1126/science.aaa4029.

Joglekar, A.P., K. Bloom, and E.D. Salmon. 2009. In Vivo Protein Architecture of the Eukaryotic Kinetochore with Nanometer Scale Accuracy. *Curr. Biol.* 19:694–699. doi:10.1016/j.cub.2009.02.056.

Johnston, K., A. Joglekar, T. Hori, A. Suzuki, T. Fukagawa, and E.D. Salmon. 2010a. Vertebrate kinetochore protein architecture: protein copy number. *J. Cell Biol.* 189:937–43. doi:10.1083/jcb.200912022.

Johnston, K., A. Joglekar, T. Hori, A. Suzuki, T. Fukagawa, and E.D. Salmon. 2010b. Vertebrate kinetochore protein architecture: protein copy number. *J. Cell Biol.* 189:937–43. doi:10.1083/jcb.200912022.

Kajtez, J., A. Solomatina, M. Novak, B. Polak, K. Vukušić, J. Rüdiger, G. Cojoc, A. Milas, I. Šumanovac Šestak, P. Risteski, F. Tavano, A.H. Klemm, E. Roscioli, J. Welburn, D. Cimini, M. Glunčić, N. Pavin, and I.M. Tolić. 2016. Overlap microtubules link sister k-fibres and balance the forces on bi-oriented kinetochores. *Nat. Commun.* 7:10298. doi:10.1038/ncomms10298.

111

Kalantzaki, M., E. Kitamura, T. Zhang, A. Mino, B. Novák, and T.U. Tanaka. 2015. Kinetochore-microtubule error correction is driven by differentially regulated interaction modes. *Nat. Cell Biol.* 17:421–33. doi:10.1038/ncb3128.

Karsenti, E., and I. Vernos. 2001. The Mitotic Spindle: A Self-Made Machine. *Science (80-.).* 294:543–547. doi:10.1126/science.1063488.

Kern, D.M., P.K. Nicholls, D.C. Page, and I.M. Cheeseman. 2016. A mitotic SKAP isoform regulates spindle positioning at astral microtubule plus ends. *J. Cell Biol.* 213:315–28. doi:10.1083/jcb.201510117.

Khodjakov, A., and J. Pines. 2010. Centromere tension: a divisive issue. *Nat. Cell Biol.* 12:919–23. doi:10.1038/ncb1010-919.

Khodjakov, A., and C.L. Rieder. 1996a. Kinetochores moving away from their associated pole do not exert a significant pushing force on the chromosome. *J. Cell Biol.* 135:315–27.

Khodjakov, A., and C.L. Rieder. 1996b. Kinetochores moving away from their associated pole do not exert a significant pushing force on the chromosome. *J. Cell Biol.* 135:315–327. doi:10.1083/jcb.135.2.315.

King, J.M., and R.B. Nicklas. 2000. Tension on chromosomes increases the number of kinetochore microtubules but only within limits. *J. Cell Sci.* 113 Pt 21:3815–23.

Kops, G.J.P.L., and J. V. Shah. 2012. Connecting up and clearing out: how kinetochore attachment silences the spindle assembly checkpoint. *Chromosoma*. 121:509–525. doi:10.1007/s00412-012-0378-5.

Koser, D.E., A.J. Thompson, S.K. Foster, A. Dwivedy, E.K. Pillai, G.K. Sheridan, H. Svoboda, M. Viana, L. da F. Costa, J. Guck, C.E. Holt, and K. Franze. 2016. Mechanosensing is critical for axon growth in the developing brain. *Nat. Neurosci.* 19:1592–1598. doi:10.1038/nn.4394.

Krefman, N.I., D.G. Drubin, and G. Barnes. 2015. Control of the spindle checkpoint by lateral kinetochore attachment and limited Mad1 recruitment. *Mol. Biol. Cell*. 26:2620–39. doi:10.1091/mbc.E15-05-0276.

Kuhn, J., and S. Dumont. 2017. Spindle assembly checkpoint satisfaction occurs via end-on but not lateral attachments under tension. *J. Cell Biol.* 216:1533–1542. doi:10.1083/jcb.201611104.

Lampson, M.A., and I.M. Cheeseman. 2011. Sensing centromere tension: Aurora B and the regulation of kinetochore function. *Trends Cell Biol.* 21:133–40. doi:10.1016/j.tcb.2010.10.007.

Levan, A. 1938. The Effect of Colchicine on Root Mitoses in Allium. *Hereditas*. 24:471–486. doi:10.1111/j.1601-5223.1938.tb03221.x.

Li, X., and R.B. Nicklas. 1995. Mitotic forces control a cell-cycle checkpoint. *Nature*. 373:630–632. doi:10.1038/373630a0.

Li, Y., and R. Benezra. 1996. Identification of a human mitotic checkpoint gene: hsMAD2. *Science*. 274:246–8. doi:10.1126/SCIENCE.274.5285.246.

Liang, H., W.H. Wright, W. He, and M.W. Berns. 1991. Micromanipulation of mitotic chromosomes in PTK2 cells using laser-induced optical forces ("optical tweezers"). *Exp. Cell Res.* 197:21–35.

Lim, W.A., C.M. Lee, and C. Tang. 2013. Design principles of regulatory networks: searching for the molecular algorithms of the cell. *Mol. Cell*. 49:202–12. doi:10.1016/j.molcel.2012.12.020.

London, N., and S. Biggins. 2014a. Mad1 kinetochore recruitment by Mps1-mediated phosphorylation of Bub1 signals the spindle checkpoint. *Genes Dev.* 28:140–152. doi:10.1101/gad.233700.113.

London, N., and S. Biggins. 2014b. Mad1 kinetochore recruitment by Mps1-mediated phosphorylation of

113

Bub1 signals the spindle checkpoint. *Genes Dev.* 28:140–52. doi:10.1101/gad.233700.113.

London, N., and S. Biggins. 2014c. Signalling dynamics in the spindle checkpoint response. *Nat. Rev. Mol. Cell Biol.* 15:736–748. doi:10.1038/nrm3888.

London, N., and S. Biggins. 2014d. Signalling dynamics in the spindle checkpoint response. *Nat. Rev. Mol. Cell Biol.* 15:736–748. doi:10.1038/nrm3888.

Long, A.F., D.B. Udy, and S. Dumont. 2017. Hec1 Tail Phosphorylation Differentially Regulates Mammalian Kinetochore Coupling to Polymerizing and Depolymerizing Microtubules. *Curr. Biol.* 27:1692-1699.e3. doi:10.1016/j.cub.2017.04.058.

Ludford, R.J. 1936. The action of toxic substances upon the division of normal and malignant cells in vitro and in vivo. *Arch. f. exp. Zellf.* 18:411–441.

Lukinavičius, G., L. Reymond, E. D'Este, A. Masharina, F. Göttfert, H. Ta, A. Güther, M. Fournier, S. Rizzo, H. Waldmann, C. Blaukopf, C. Sommer, D.W. Gerlich, H.-D. Arndt, S.W. Hell, and K. Johnsson. 2014. Fluorogenic probes for live-cell imaging of the cytoskeleton. *Nat. Methods*. 11:731–733. doi:10.1038/nmeth.2972.

Maciejowski, J., K.A. George, M.-E. Terret, C. Zhang, K.M. Shokat, and P. V. Jallepalli. 2010. Mps1 directs the assembly of Cdc20 inhibitory complexes during interphase and mitosis to control M phase timing and spindle checkpoint signaling. *J. Cell Biol.* 190:89–100. doi:10.1083/jcb.201001050.

Magidson, V., J. He, J.G. Ault, C.B. O'Connell, N. Yang, I. Tikhonenko, B.F. McEwen, H. Sui, and A. Khodjakov. 2016. Unattached kinetochores rather than intrakinetochore tension arrest mitosis in taxol-treated cells. *J. Cell Biol.* 212:307–19. doi:10.1083/jcb.201412139.

Magidson, V., C.B. O'Connell, J. Lončarek, R. Paul, A. Mogilner, and A. Khodjakov. 2011. The spatial arrangement of chromosomes during prometaphase facilitates spindle assembly. *Cell*. 146:555–67.

doi:10.1016/j.cell.2011.07.012.

Magidson, V., R. Paul, N. Yang, J.G. Ault, C.B. O'Connell, I. Tikhonenko, B.F. McEwen, A. Mogilner, and A. Khodjakov. 2015. Adaptive changes in the kinetochore architecture facilitate proper spindle assembly. *Nat. Cell Biol.* 17:1134–1144. doi:10.1038/ncb3223.

Maldonado, M., and T.M. Kapoor. 2011. Constitutive Mad1 targeting to kinetochores uncouples checkpoint signalling from chromosome biorientation. *Nat. Cell Biol.* 13:475–482. doi:10.1038/ncb2223.

Maresca, T.J., and E.D. Salmon. 2009. Intrakinetochore stretch is associated with changes in kinetochore phosphorylation and spindle assembly checkpoint activity. *J. Cell Biol.* 184:373–81. doi:10.1083/jcb.200808130.

Martin-Lluesma, S., V.M. Stucke, and E.A. Nigg. 2002. Role of Hec1 in spindle checkpoint signaling and kinetochore recruitment of Mad1/Mad2. *Science*. 297:2267–70. doi:10.1126/science.1075596.

Matson, D.R., and P.T. Stukenberg. 2014. CENP-I and Aurora B act as a molecular switch that ties RZZ/Mad1 recruitment to kinetochore attachment status. *J. Cell Biol.* 205:541–54. doi:10.1083/jcb.201307137.

McDonald, K.L., E.T. O'Toole, D.N. Mastronarde, and J.R. McIntosh. 1992. Kinetochore microtubules in PTK cells. *J. Cell Biol.* 118:369–383. doi:10.1083/jcb.118.2.369.

McEwen, B.F., and A.B. Heagle. 1997. Electron microscopic tomography: A tool for probing the structure and function of subcellular components. *Int. J. Imaging Syst. Technol.* 8:175–187. doi:10.1002/(SICI)1098-1098(1997)8:2<175::AID-IMA5>3.0.CO;2-7.

McEwen, B.F., A.B. Heagle, G.O. Cassels, K.F. Buttle, and C.L. Rieder. 1997. Kinetochore fiber maturation in PtK1 cells and its implications for the mechanisms of chromosome congression and anaphase

115

onset. *J. Cell Biol.* 137:1567–80.

McIntosh, J.R. 1991. Structural and mechanical control of mitotic progression. *Cold Spring Harb. Symp. Quant. Biol.* 56:613–9.

McKinley, K.L., and I.M. Cheeseman. 2017. Large-Scale Analysis of CRISPR/Cas9 Cell-Cycle Knockouts Reveals the Diversity of p53-Dependent Responses to Cell-Cycle Defects. *Dev. Cell*. 40:405-420.e2. doi:10.1016/j.devcel.2017.01.012.

Mortensen, K.I., L.S. Churchman, J.A. Spudich, and H. Flyvbjerg. 2010. Optimized localization analysis for single-molecule tracking and super-resolution microscopy. *Nat. Methods*. 7:377–381. doi:10.1038/nmeth.1447.

Musacchio, A., and A. Desai. 2017. A Molecular View of Kinetochore Assembly and Function. *Biology (Basel).* 6. doi:10.3390/biology6010005.

Musacchio, A., and E.D. Salmon. 2007. The spindle-assembly checkpoint in space and time. *Nat. Rev. Mol. Cell Biol.* 8:379–393. doi:10.1038/nrm2163.

Nezi, L., and A. Musacchio. 2009. Sister chromatid tension and the spindle assembly checkpoint. *Curr. Opin. Cell Biol.* 21:785–795. doi:10.1016/j.ceb.2009.09.007.

Nicklas, R.B. 1983. Measurements of the force produced by the mitotic spindle in anaphase. *J. Cell Biol.* 97:542–8. doi:10.1083/jcb.97.2.542.

Nicklas, R.B., and C.A. Koch. 1969. CHROMOSOME MICROMANIPULATION: III. Spindle Fiber Tension and the Reorientation of Mal-Oriented Chromosomes. *J. Cell Biol.* 43:40–50. doi:10.1083/jcb.43.1.40.

Nicklas, R.B., and C.A. Staehly. 1967. Chromosome micromanipulation. I. The mechanics of chromosome attachment to the spindle. *Chromosoma*. 21:1–16.

Nicklas, R.B., J.C. Waters, E.D. Salmon, and S.C. Ward. 2001. Checkpoint signals in grasshopper meiosis
are sensitive to microtubule attachment, but tension is still essential. *J. Cell Sci.* 114:4173–83.

Nijenhuis, W., G. Vallardi, A. Teixeira, G.J.P.L. Kops, and A.T. Saurin. 2014. Negative feedback at
kinetochores underlies a responsive spindle checkpoint signal. *Nat. Cell Biol.* 16:1257–1264.
doi:10.1038/ncb3065.

O'Connell, C.B., J. Loncarek, P. Hergert, A. Kourtidis, D.S. Conklin, and A. Khodjakov. 2008. The spindle
assembly checkpoint is satisfied in the absence of interkinetochore tension during mitosis with
unreplicated genomes. *J. Cell Biol.* 183:29–36. doi:10.1083/jcb.200801038.

Orth, J.D., A. Loewer, G. Lahav, and T.J. Mitchison. 2012. Prolonged mitotic arrest triggers partial
activation of apoptosis, resulting in DNA damage and p53 induction. *Mol. Biol. Cell*. 23:567–76.
doi:10.1091/mbc.E11-09-0781.

Pereira, A.J., I. Matos, M. Lince-Faria, and H. Maiato. 2009. Dissecting Mitosis with Laser Microsurgery
and RNAi in Drosophila Cells. *In* Methods in molecular biology (Clifton, N.J.). 145–164.

Peterson, J.B., and H. Ris. 1976. Electron-microscopic study of the spindle and chromosome movement
in the yeast Saccharomyces cerevisiae. *J. Cell Sci.* 22.

Pines, J., and P. Clute. 1999. Temporal and spatial control of cyclin B1 destruction in metaphase. *Nat. Cell Biol.* 1:82–87. doi:10.1038/10049.

Pinsky, B.A., and S. Biggins. 2005. The spindle checkpoint: tension versus attachment. *Trends Cell Biol.* 15:486–493. doi:10.1016/j.tcb.2005.07.005.

Pinsky, B.A., C.R. Nelson, and S. Biggins. 2009. Protein Phosphatase 1 Regulates Exit from the Spindle
Checkpoint in Budding Yeast. *Curr. Biol.* 19:1182–1187. doi:10.1016/j.cub.2009.06.043.

Rieder, C.L., R.W. Cole, A. Khodjakov, and G. Sluder. 1995. The checkpoint delaying anaphase in response to chromosome monoorientation is mediated by an inhibitory signal produced by unattached kinetochores. *J. Cell Biol.* 130:941–8.

Rieder, C.L., E.A. Davison, L.C. Jensen, L. Cassimeris, and E.D. Salmon. 1986. Oscillatory movements of monooriented chromosomes and their position relative to the spindle pole result from the ejection properties of the aster and half-spindle. *J. Cell Biol.* 103:581–91. doi:10.1083/JCB.103.2.581.

Santaguida, S., A. Tighe, A.M. D'Alise, S.S. Taylor, and A. Musacchio. 2010. Dissecting the role of MPS1 in chromosome biorientation and the spindle checkpoint through the small molecule inhibitor reversine. *J. Cell Biol.* 190:73–87. doi:10.1083/jcb.201001036.

Saotome, K., S.E. Murthy, J.M. Kefauver, T. Whitwam, A. Patapoutian, and A.B. Ward. 2018. Structure of the mechanically activated ion channel Piezo1. *Nature*. 554:481–486. doi:10.1038/nature25453.

Sarangapani, K.K., and C.L. Asbury. 2014. Catch and release: how do kinetochores hook the right microtubules during mitosis? *Trends Genet.* 30:150–159. doi:10.1016/j.tig.2014.02.004.

Saurin, A.T., M.S. van der Waal, R.H. Medema, S.M.A. Lens, and G.J.P.L. Kops. 2011. Aurora B potentiates Mps1 activation to ensure rapid checkpoint establishment at the onset of mitosis. *Nat. Commun.* 2:316. doi:10.1038/ncomms1319.

Schmidt, J.C., T. Kiyomitsu, T. Hori, C.B. Backer, T. Fukagawa, and I.M. Cheeseman. 2010. Aurora B kinase controls the targeting of the Astrin–SKAP complex to bioriented kinetochores. *J. Cell Biol.* 191:269–280. doi:10.1083/jcb.201006129.

Shah, J. V, E. Botvinick, Z. Bonday, F. Furnari, M. Berns, and D.W. Cleveland. 2004. Dynamics of centromere and kinetochore proteins; implications for checkpoint signaling and silencing. *Curr. Biol.* 14:942–52. doi:10.1016/j.cub.2004.05.046.

118

Shimogawa, M.M., M.M. Wargacki, E.G. Muller, and T.N. Davis. 2010. Laterally attached kinetochores

recruit the checkpoint protein Bub1, but satisfy the spindle checkpoint. *Cell Cycle*. 9:3619–3628.

doi:10.4161/cc.9.17.12907.

Shrestha, R.L., and V.M. Draviam. 2013. Lateral to End-on Conversion of Chromosome-Microtubule

Attachment Requires Kinesins CENP-E and MCAK. *Curr. Biol.* 23:2440–2441.

doi:10.1016/j.cub.2013.11.015.

Sikirzhytski, V., V. Magidson, J.B. Steinman, J. He, M. Le Berre, I. Tikhonenko, J.G. Ault, B.F. McEwen, J.K.

Chen, H. Sui, M. Piel, T.M. Kapoor, and A. Khodjakov. 2014. Direct kinetochore-spindle pole

connections are not required for chromosome segregation. *J. Cell Biol.* 206:231–43.

doi:10.1083/jcb.201401090.

Sikirzhytski, V., F. Renda, I. Tikhonenko, V. Magidson, B.F. McEwen, and A. Khodjakov. 2018.

Microtubules assemble near most kinetochores during early prometaphase in human cells. *J. Cell

Biol.* 217:2647–2659. doi:10.1083/jcb.201710094.

Sivakumar, S., P.Ł. Janczyk, Q. Qu, C.A. Brautigam, P.T. Stukenberg, H. Yu, and G.J. Gorbsky. 2016. The

human SKA complex drives the metaphase-anaphase cell cycle transition by recruiting protein

phosphatase 1 to kinetochores. *Elife*. 5. doi:10.7554/eLife.12902.

Smith, C.A., A.D. McAinsh, and N.J. Burroughs. 2016. Human kinetochores are swivel joints that mediate

microtubule attachments. *Elife*. 5. doi:10.7554/eLife.16159.

Snyder, J.A., L. Armstrong, O.G. Stonington, T.P. Spurck, and J.D. Pickett-Heaps. 1991. UV-microbeam

irradiations of the mitotic spindle: spindle forces and structural analysis of lesions. *Eur. J. Cell Biol.*

55:122–32.

Stirling Churchman, L., H. Flyvbjerg, and J.A. Spudich. 2006. A Non-Gaussian Distribution Quantifies

Distances Measured with Fluorescence Localization Techniques. *Biophys. J.* 90:668–671. doi:10.1529/biophysj.105.065599.

Stout, J.R., R.S. Rizk, S.L. Kline, and C.E. Walczak. 2006. Deciphering protein function during mitosis in PtK cells using RNAi. *BMC Cell Biol.* 7:26. doi:10.1186/1471-2121-7-26.

Sundin, L.J.R., G.J. Guimaraes, and J.G. Deluca. 2011. The NDC80 complex proteins Nuf2 and Hec1 make distinct contributions to kinetochore-microtubule attachment in mitosis. *Mol. Biol. Cell*. 22:759–68. doi:10.1091/mbc.E10-08-0671.

Suzuki, A., B.L. Badger, and E.D. Salmon. 2015. A quantitative description of Ndc80 complex linkage to human kinetochores. *Nat. Commun.* 6:8161. doi:10.1038/ncomms9161.

Suzuki, A., S.K. Long, and E.D. Salmon. 2018. An optimized method for 3D fluorescence co-localization applied to human kinetochore protein architecture. *Elife*. 7. doi:10.7554/eLife.32418.

Tanaka, T.U., N. Rachidi, C. Janke, G. Pereira, M. Galova, E. Schiebel, M.J.R. Stark, and K. Nasmyth. 2002. Evidence that the Ipl1-Sli15 (Aurora kinase-INCENP) complex promotes chromosome bi-orientation by altering kinetochore-spindle pole connections. *Cell*. 108:317–29.

Tauchman, E.C., F.J. Boehm, and J.G. DeLuca. 2015. Stable kinetochore–microtubule attachment is sufficient to silence the spindle assembly checkpoint in human cells. *Nat. Commun.* 6:10036. doi:10.1038/ncomms10036.

Taylor, S.S., and F. McKeon. 1997. Kinetochore localization of murine Bub1 is required for normal mitotic timing and checkpoint response to spindle damage. *Cell*. 89:727–35.

Thompson, R.E., D.R. Larson, and W.W. Webb. 2002. Precise Nanometer Localization Analysis for Individual Fluorescent Probes. *Biophys. J.* 82:2775–2783. doi:10.1016/S0006-3495(02)75618-X.

Uchida, K.S.K., K. Takagaki, K. Kumada, Y. Hirayama, T. Noda, and T. Hirota. 2009. Kinetochore stretching

inactivates the spindle assembly checkpoint. *J. Cell Biol.* 184:383–90. doi:10.1083/jcb.200811028.

Uetake, Y., and G. Sluder. 2010. Prolonged prometaphase blocks daughter cell proliferation despite

normal completion of mitosis. *Curr. Biol.* 20:1666–71. doi:10.1016/j.cub.2010.08.018.

Uhlmann, F., F. Lottspeich, and K. Nasmyth. 1999. Sister-chromatid separation at anaphase onset is

promoted by cleavage of the cohesin subunit Scc1. *Nature*. 400:37–42. doi:10.1038/21831.

Vanoosthuyse, V., and K.G. Hardwick. 2009. A Novel Protein Phosphatase 1-Dependent Spindle

Checkpoint Silencing Mechanism. *Curr. Biol.* 19:1176–1181. doi:10.1016/J.CUB.2009.05.060.

Volkov, V.A., P.J. Huis in 't Veld, M. Dogterom, and A. Musacchio. 2018. Multivalency of NDC80 in the

outer kinetochore is essential to track shortening microtubules and generate forces. *Elife*. 7.

doi:10.7554/eLife.36764.

Wan, X., D. Cimini, L.A. Cameron, and E.D. Salmon. 2012a. The coupling between sister kinetochore

directional instability and oscillations in centromere stretch in metaphase PtK1 cells. *Mol. Biol. Cell*.

23:1035–46. doi:10.1091/mbc.E11-09-0767.

Wan, X., D. Cimini, L.A. Cameron, and E.D. Salmon. 2012b. The coupling between sister kinetochore

directional instability and oscillations in centromere stretch in metaphase PtK1 cells. *Mol. Biol. Cell*.

23:1035–46. doi:10.1091/mbc.E11-09-0767.

Wan, X., R.P. O'Quinn, H.L. Pierce, A.P. Joglekar, W.E. Gall, J.G. DeLuca, C.W. Carroll, S.-T. Liu, T.J. Yen,

B.F. McEwen, P.T. Stukenberg, A. Desai, and E.D. Salmon. 2009. Protein Architecture of the Human

Kinetochore Microtubule Attachment Site. *Cell*. 137:672–684. doi:10.1016/j.cell.2009.03.035.

Waters, J.C., R.H. Chen, A.W. Murray, and E.D. Salmon. 1998. Localization of Mad2 to kinetochores

depends on microtubule attachment, not tension. *J. Cell Biol.* 141:1181–91.

doi:10.1083/JCB.141.5.1181.

Wendell, K.L., L. Wilson, and M.A. Jordan. 1993. Mitotic block in HeLa cells by vinblastine: ultrastructural changes in kinetochore-microtubule attachment and in centrosomes. *J. Cell Sci.* 104 (Pt 2):261–74.

Wojcik, E., R. Basto, M. Serr, F. Scaërou, R. Karess, and T. Hays. 2001. Kinetochore dynein: its dynamics and role in the transport of the Rough deal checkpoint protein. *Nat. Cell Biol.* 3:1001–1007. doi:10.1038/ncb1101-1001.

Wood, K.W., L. Lad, L. Luo, X. Qian, S.D. Knight, N. Nevins, K. Brejc, D. Sutton, A.G. Gilmartin, P.R. Chua, R. Desai, S.P. Schauer, D.E. McNulty, R.S. Annan, L.D. Belmont, C. Garcia, Y. Lee, M.A. Diamond, L.F. Faucette, M. Giardiniere, S. Zhang, C.-M. Sun, J.D. Vidal, S. Lichtsteiner, W.D. Cornwell, J.D. Greshock, R.F. Wooster, J.T. Finer, R.A. Copeland, P.S. Huang, D.J. Morgans, D. Dhanak, G. Bergnes, R. Sakowicz, J.R. Jackson, and J.R. Jackson. 2010. Antitumor activity of an allosteric inhibitor of centromere-associated protein-E. *Proc. Natl. Acad. Sci. U. S. A.* 107:5839–44. doi:10.1073/pnas.0915068107.

Yamada, H.Y., and G.J. Gorbsky. 2006. Spindle checkpoint function and cellular sensitivity to antimitotic drugs. *Mol. Cancer Ther.* 5:2963–9. doi:10.1158/1535-7163.MCT-06-0319.

Yildiz, A., J.N. Forkey, S.A. McKinney, T. Ha, Y.E. Goldman, and P.R. Selvin. 2003. Myosin V Walks Hand-Over-Hand: Single Fluorophore Imaging with 1.5-nm Localization. *Science (80-.).* 300:2061–2065. doi:10.1126/science.1084398.

Yoo, T.Y., J.-M. Choi, W. Conway, C.-H. Yu, R. V Pappu, and D.J. Needleman. 2018. Measuring NDC80 binding reveals the molecular basis of tension-dependent kinetochore-microtubule attachments. *Elife*. 7. doi:10.7554/eLife.36392.

Zaytsev, A. V, J.E. Mick, E. Maslennikov, B. Nikashin, J.G. DeLuca, and E.L. Grishchuk. 2015. Multisite

phosphorylation of the NDC80 complex gradually tunes its microtubule-binding affinity. *Mol. Biol. Cell*. 26:1829–44. doi:10.1091/mbc.E14-11-1539.

Zaytsev, A. V, L.J.R. Sundin, K.F. DeLuca, E.L. Grishchuk, and J.G. DeLuca. 2014. Accurate phosphoregulation of kinetochore-microtubule affinity requires unconstrained molecular interactions. *J. Cell Biol.* 206:45–59. doi:10.1083/jcb.201312107.

Zhao, Q., H. Zhou, S. Chi, Y. Wang, J. Wang, J. Geng, K. Wu, W. Liu, T. Zhang, M.-Q. Dong, J. Wang, X. Li, and B. Xiao. 2018. Structure and mechanogating mechanism of the Piezo1 channel. *Nature*. 554:487–492. doi:10.1038/nature25743.
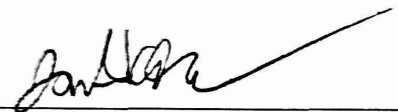
Zirkle, R.E. 1970. Ultraviolet-microbeam irradiation of newt-cell cytoplasm: spindle destruction, false anaphase, and delay of true anaphase. *Radiat. Res.* 41:516–37.

Publishing Agreement

It is the policy of the University to encourage the distribution of all theses, dissertations, and manuscripts. Copies of all UCSF theses, dissertations, and manuscripts will be routed to the library via the Graduate Division. The library will make all theses, dissertations, and manuscripts accessible to the public and will preserve these to the best of their abilities, in perpetuity.

Please sign the following statement:

I hereby grant permission to the Graduate Division of the University of California, San Francisco to release copies of my thesis, dissertation, or manuscript to the Campus Library to provide access and preservation, in whole or in part, in perpetuity.

_____   06/06/2019
Author Signature   Date